MULTI-PORT POWER ELECTRONIC INTERFACE FOR RENEWABLE ENERGY SOURCES

by

WEI JIANG

Presented to the Faculty of the Graduate School of
The University of Texas at Arlington in Partial Fulfillment
of the Requirements
for the Degree of

DOCTOR OF PHILOSOPHY

THE UNIVERSITY OF TEXAS AT ARLINGTON

December 2009

ACKNOWLEDGEMENTS

It is my great pleasure to acknowledge the help and support I have received during my graduate study at UTA. First and foremost, I would like to express my greatest gratitude to my supervisor Professor Babak Fahimi. This work would not have been possible without the guidance and support from Dr. Fahimi. I am very indebted to his advice and encouragement throughout my Master and Ph.D. study. It is Dr. Fahimi who led me into a wide spectrum of research in energy conversion. I especially appreciate and recognize all he time he spent on advising me with this project and my academic work. He guided me to the discovery of the path to new ideas and new concepts, which is very invaluable to me. He made available his support in numerous ways, providing me with abundant research funding to carry out my project from concept to prototype, supporting my attendance of professional conferences, and involving me in various research and teaching activities which I found interesting and rewarding. Dr. Fahimi is a very considerate and compassionate professor. The intellectual talk with him is always pleasant, inspiring and convincing. Study under him proved to be very enjoyable and fruitful. One simply could not wish for an even better or friendlier supervisor.

I owe my great gratitude to all my committee members. Dr. Wei-Jen Lee taught me courses on PLC and Renewable Energy in which I had access to the frontier know-how in engineering field and green energy. It is an honor for me to have Dr. Lee as my committee member both in my master thesis and Ph.D. dissertation defense. I took Dr. Daniel W. Engels' RFID course, which broadened my horizon in the interdisciplinary dimension of information technology and milliwatt energy

conversion. I am very grateful and honored that Dr. Raymond R. Shoults and Dr. William E. Dillon join in the committee, my graduate study would not have been successful without their support.

I would also like to thank sincerely Dr. Stephen Gibbs, Dr. Kai-Shing Yeung, Dr. Rasool Kenarangui, Dr. Nikolai Stelmakh, Dr. Mehrdad Ehsani and Dr. Mehdi Moallem for their advice and support. I would like to thank Dean Carroll especially for his tolerance of the noises from the wind turbine, which is right above the Dean's office.

Another great thanks goes out to all my lab colleagues. Our friendship brightened every day of my research and kept me in a very upbeat mood. I also offer my gratitude to the friends I made during my graduate study, with whom I shared laughers, had hearty conversations, and created precious memories.

I also want to express my gratitude to the Department staff, librarians and physical plant engineers who are respectfully helpful, professional and kind.

I can not end this acknowledgment without thanking my beloved wife Su Xie, whose love have accompanied my through all the toughness and offered me enormous strength to make today's achievement. I deeply appreciate all the endeavors and sacrifices Su has made for me and our daughter Isabelle for recently years. I also own a big thanks to my parents and parents-in-law, from whom the guidance and support are cherished.

September 1, 2009

ABSTRACT

MULTI-PORT POWER ELECTRONIC INTERFACE FOR RENEWABLE ENERGY SOURCES

WEI JIANG, Ph.D.

The University of Texas at Arlington, 2009

Supervising Professor: Babak Fahimi

Energy intensive products and services are penetrating people's daily life as well as different sectors of industry during recent decades. Further effort to improve efficiency, reduce green house gas and hazardous particle emission lead to the emergence of the "more electric" concept in several industries including transportation. This trend, however, burdens the aging power system and existing local power networks. To offer a remedy to the problem and a smooth transition to a more reliable, more diverse, and more efficient power grid of the future, the concept of Multi-port Power Electronic Interface (MPEI) for localized power processing is introduced in this dissertation, which interfaces and manages various sources, loads and storages. Different means of integrating multiple sources and storages into the existing power system are studied and evaluated; the six phase-leg structure is chosen to interface five sources/loads: fuel cell, wind turbine, solar cell, battery and utility grid. Partitioning of source-interface and load-interface on a system level as well as analysis and modeling on small signal level are performed. A novel control structure for source-

interface is proposed in the design, which forms Controlled Quasi Current Source (CQCS) during the load sharing operation and offers several salient advantages:

- Inherent average current-mode control.
- Easy share of steady state current/power.
- Share of load dynamics for better source protection.

Local control loops for various input ports are designed based on linearized system model; controller performance is tuned to accommodate the characteristics of different sources. To maintain a sustainable operation, different modes of operation are defined for MPEI; detailed state-transition with associated events are also defined in each operation mode. Prototype of MPEI is built and control system is implemented digitally in a digital signal processor; steady state and transient performance of MPEI is tested under variety of meaningful conditions, which proves the feasibility of the proposed design. The concepts, analysis and design of MPEI conducted in this dissertation pave the way for designing of intelligent power electronic infrastructure for future sustainable energy systems.

TABLE OF CONTENTS

Appendix

LIST OF FIGURES

LIST OF TABLES

CHAPTER 1

INTRODUCTION

1.1 Sustainable Energy System - the Challenges

Over the past decades, different sectors of society has been undergoing fast development, which induced enormous energy demand. Since the major resources consumed to produce energy product are non-renewable fossil fuels, excessive usage results in increasing production of carbon dioxide and particles, which are the main contributors to global warming. The latest data [1] of international energy consumption indicated in Figure 1.1 by US Energy Information Administration (EIA) has shown an undeniable truth that the consumption of fossil based fuels is dominating the world energy composition and is still projected to increase in the upcoming 20 years. Carbon dioxide emission is one of the conspicuous consequences of burning

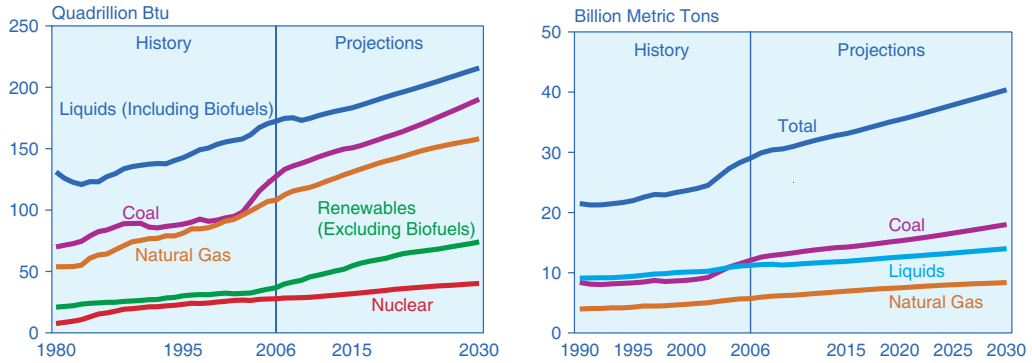

Figure 1.1. Energy data: (a) world energy consumption, (b) world carbon dioxide emission.

fossil fuels. Figure 1.1(b) indicates an obvious increasing rate of CO_2 emission due to excessive usage of coal, especially in recent five years. The message delivered by the figure can be simply translated into one problem: energy sustainability. The definition of sustainable energy system was brought out in [2]

> **Sustainable Energy**: *a dynamic harmony between the equitable availability of energy-intensive goods and services to all people and the preservation of the earth for future generations.*

Since fossil fuel is non-renewable and the tremendous environmental impact caused by the consumption of fossil fuel can only be reduced by even more usage of energy, the traditional manner of energy flow from fossil fuel to energy product is hence considered as unsustainable.

In the sense of engineering, usage of fossil fuels is inevitable in the short run; therefore, the imperative task is to how to harvest "free energy" and to use the energy efficiently. "More electric" is the idea firstly introduced and implemented in aerospace and vehicular engineering since electric components and infrastructures possess less weight and more efficiency. In fact, electric components are being considered and are gradually replacing the bulky and inefficient hydraulic, pneumatic and combustive counterparts in varies of applications. In spite of a variety of advantages, wide application of "more electric" concept eventually leads to heavy burdens on electric power system. Being the two most important sectors in energy consumption, transportation (vehicular system) and electric power system are facing many challenges toward future sustainability. The energy chain of conventional electric power system involves three major important elements: generation, transmission and distribution. Current electric power system is built on the assumption that all electricity would be generated at very large central plants [3][4][5]. Therefore, the energy flow is one-way from central power plants via transmission and distribution systems to

end users. However, deliverable power by electric power system is bounded by the capacity of the transmission infrastructures hence impose obstacles upon distributed energy resource interconnection. Due to large inertia of central generation units, the system is incapable of adjusting to changing demand patterns. During system contingency, complex and time-consuming control algorithms must be applied to coordinate between transmission and distribution system to void loss of load[6]. Also in conventional electric power systems, the consumers are uniformed and non-interactive with the power systems, either in healthy or contingency state.

On the other hand, the advent of flex-fuel and hybrid vehicles alleviates the consumption of fossil fuels by incorporating renewable fuels and energy storages, which, however, introduce more complex hybrid power system. Therefore, investigation of hybrid power structures and power management are crucial tasks in vehicle power system design in order to achieve optimal balance among efficiency, performance and durability of system components [7].

Figure 1.2. Power grid for the future [3].

Smart Grid [8] and its associated technologies is one of the most promising solutions to future sustainable energy system. By introducing localized power electronics-based renewable energy harvester, power conditioner and energy storages with intelligent management, the bottleneck of transmission capability will be eventually relaxed, and better local compensation and power conditioning can be achieved. With seamless integration of local energy storage systems (ESS), smart grid solution can provide resilience to contingency and involve the consumers actively in power system demand response. As the prospective super energy storages, personal hybrid vehicles can also be integrated into smart electric networks, where the vehicle power management system can make sound judgment to modes of operation given the access to states and pricing of power grid. A conceptual drawing of smart grids is presented in Figure 1.2 [8].

Smart grids demand complex and integrated technologies to become a reality. Power electronics and its control is one of the most fundamental and enabling technologies in the development process toward smart energy systems. However, only under the prerequisites of stable operation and flexible power management of local generators can smart grid deliver optimized, efficient and clean power to the end customers.

Renewable energy sources are getting more attention in a broad range of applications. With "more electric" components in stationary and mobile applications, the demand from electric grid has been increasing over the years. A collection of renewable sources are good additions to conventional electric power system for enhanced power capability. Typical integration of renewable energy resorts to distributed generation(DG), where centralized power plants and renewable energy plants share the ac distribution bus, as indicated by Figure 1.3. However,transmission capacity still persists as the bottleneck since most centralized plants are located at remote regions.

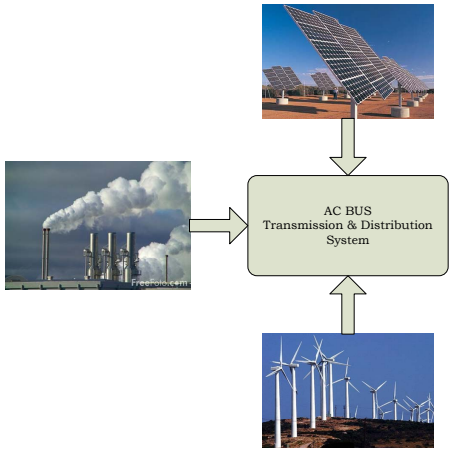

Figure 1.3. Distributed generation by centralized renewable energy plant.

As it is moving toward the age of smart grid, localized generation tends to become the new generation pattern and lead to a further reduction in transmission infrastructure cost. Therefore, the local organization and coordination of distributed generation merges as the concept of Microgrid [4][9].

1.2 Overview of Previous Work

Applications of multiple converter based distributed power systems have been reported in the literatures to deal with multi-source input. One of the most adopted system configurations is based on localized converters with communication capabilities or agent-based decision making mechanism[5][10][11][6], which share power on either ac bus or dc bus. The system configuration for such a system is illustrated in Figure 1.4. Nevertheless, if power sources are locally available for low to medium power range applications (such as micro-grid and critical industrial zones), such solutions allow room for improvement since the load sharing among different power modules are entirely based on communication channel, which inevitably introduces increased failure rate, degradation in load regulation, complex implementation and

high manufacturing and maintenance cost. Multi-converter system with integrated controller, which has been used extensively in spacecraft power systems, telecommunication systems and battery charger systems [12][13][14][15][16], possesses excellent load regulation and load sharing capabilities. However, such system are monospecifically designed to certain tasks and are not suitable for versatile performance in smart energy systems.

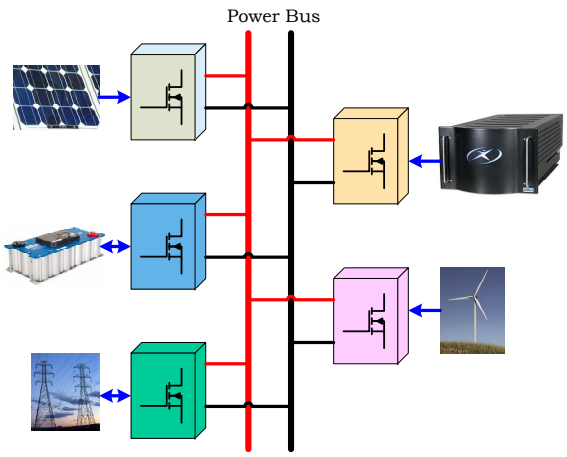

Figure 1.4. Local distributed power system based on multiple converters.

Multiple-input converter is one of the best candidates for smart grid infrastructures since it can harvest and process the power from different sources and energy storages as a "lumped" unit. Unified multiple-input topology has the advantages of low cost, high power density and ease of management. There have been extensive researches on multiple-input converter in recent ten years which resulted in wide spectrum of topologies. Generally, multiple-input converter can be classified into two categories: magnetically coupled converter (MCC) and electrically coupled converter (ECC).

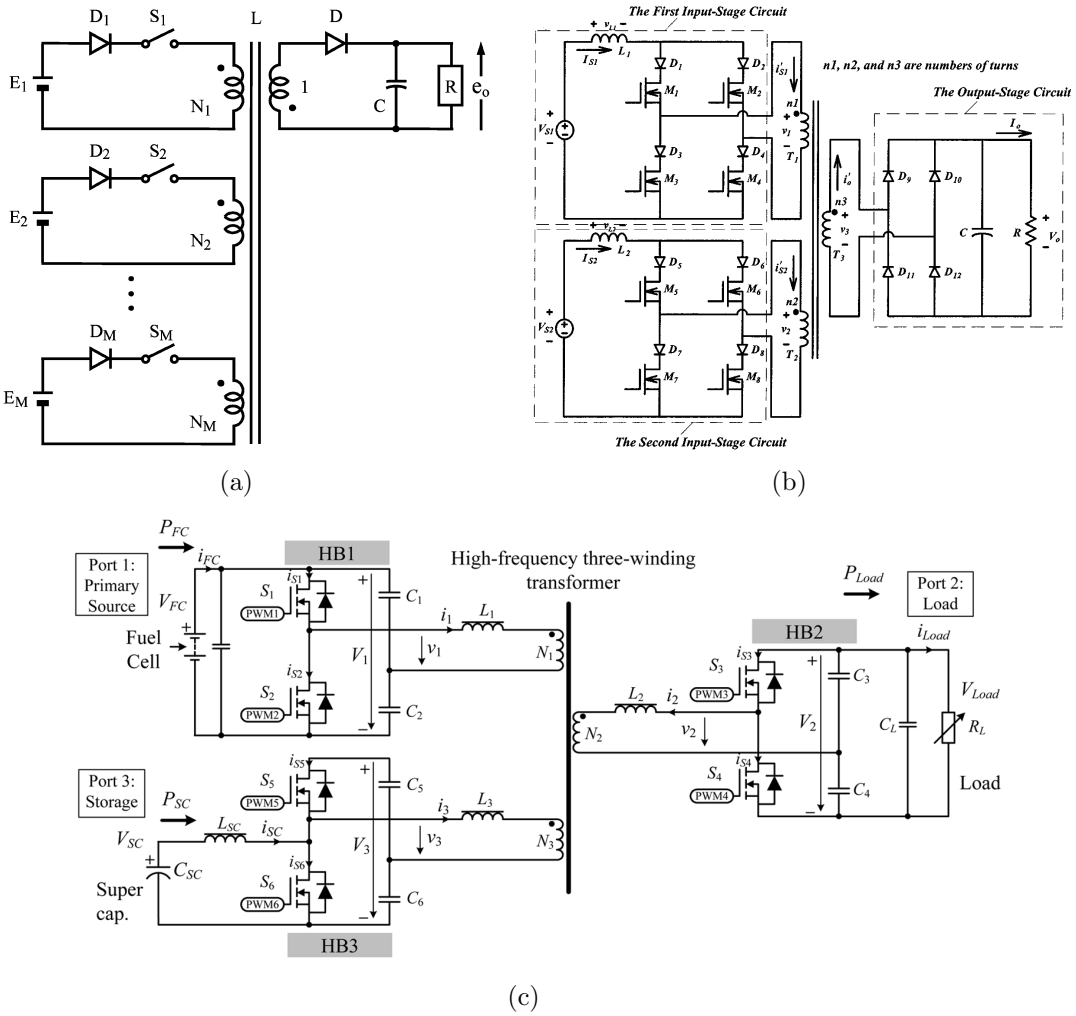

Figure 1.5. Magnetic-coupled Converters: (a) time domain multiplexing[17], (b) flux addition[18], (c) power flow control[19].

Based on the converter topology, flux addition, time domain multiplexing and magnetic energy transfer methods are applied in MCC to transfer energy from primary side of the converter to the secondary. [17] [20] was one of the earliest version of MCC using time domain multiplexing method, in which author proposed flyback/forward based multiple-input topology to couple energy to the secondary side as in Figure 1.5(a). Time domain multiplexing in MCC is easy to implement and renders discontinuous current mode of operation in each channel which is easy

to control; however, power density of such topologies is limited due to the nature of flyback/forward topology and dissected energy transfer time frame. [18][21][22] proposes multiple-input MCC based on flux addition principle; energy from different sources is transferred to the secondary by adding total flux in magnetic core from each conversion channel. Nonetheless, flux addition operation requires current sourced inverter on each input/output, which, in most cases, is uni-directional and not suitable for applications with energy storage elements; Figure 1.5(b) presents a current-source full bridge based multiple-input converter where power only transfers from left to right hand side. Magnetic energy transfer method is based on power flow analysis, where series reactance X_L and voltage phase-shift angle δ dominate the power flow as indicated in Equation (1.1), such multiple-input topologies are full/half bridge based and transformer leakage inductance is used for power transfer; [23] is the first literature which proposes the concept in a single input single output topology, and [24][25][26][27][28][19][29] augment the idea by applying to other topologies and multiple-input versions; Figure 1.5(c) illustrates the tri-port converter where variety of topologies are used. However, one has to note that magnetic energy transfer method is circuit parameter based, therefore, is subject to potential inaccurate performances; capability of current shaping is another fact to consider when interfacing with renewable sources such as fuel cell. However, energy transfer method is not focused on current regulation but mainly power flow control. MCC offers high power density and more flexible output voltage level since high frequency transformer and soft switching techniques can be applied; however, peripheral circuit for MCC is very complex and the implementation of load sharing among different sources and energy storage elements is complicated (although time multiplexing controlled MCC is straight forward). Additioinally, due to the limitations of magnetic design, MCC is popular below $10kW$.

$$P = \frac{V^2}{X_L} sin\delta \tag{1.1}$$

Electrically coupled converters (ECC) are usually implemented with nonisolated converter topologies, such as buck, boost and buck-boost. The power flow control of ECC is relatively straight forward and peripheral circuit for ECC is usually simple. Although ECC has less flexibility for voltage output, the modular structure and lower cost make ECC more favorable in a variety of applications such as automotive and communication power systems. Figure 1.6 presents several typical implementation of multiple-input topologies. [30][31][32] implement the multiple-input interface by stacking different sources to achieve high output voltage, and switching pattern of such multiple-input channels is either time domain multiplexed or mix of multiplexing and simultaneous switching; Figure 1.6(a) presents a boost cell based topology with stacked input. [33] proposes buck-boost topology based multiple-input ECC and operates with time multiplexed switching pattern as in Figure 1.6(b). In [34] author considered sources with different input levels and proposes the topology with mix boost and buck-boost switching cells as front-end converter for microgrid application; as indicated in Figure 1.6(c), two buck and two buck-boost switching cells have been integrated to share the power, stack of sources are also implemented due to negative output of buck-boost switching cells. [35] uses the mixed switch-mode and charge-pump topology to create multiple-input ECC, in which all subsystems have common ground and power flow is bidirectional due to inductor coupling. [36] couples buck cells to feed inverter load. [37][38][39][40][41] adopt uniform boost cells to form a multiple-input converter system for both stationary and mobile applications, and switching cells can provide power simultaneously to the load as indicated in Figure 1.6(d). Literature [42] reports the Tri-modal topology using isolated topology; although magnetically isolated, the load sharing takes place on the primary side

of Tri-modal converter by switching a half bridge asymmetrically, therefore, is still categorized as ECC. The simple structure and reliable implementation of ECC make it popular in both low power applications (such as LED driver) and high power applications (hybrid vehicle power system); more than $100kW$ implementation of ECC has been reported in hybrid vehicles.

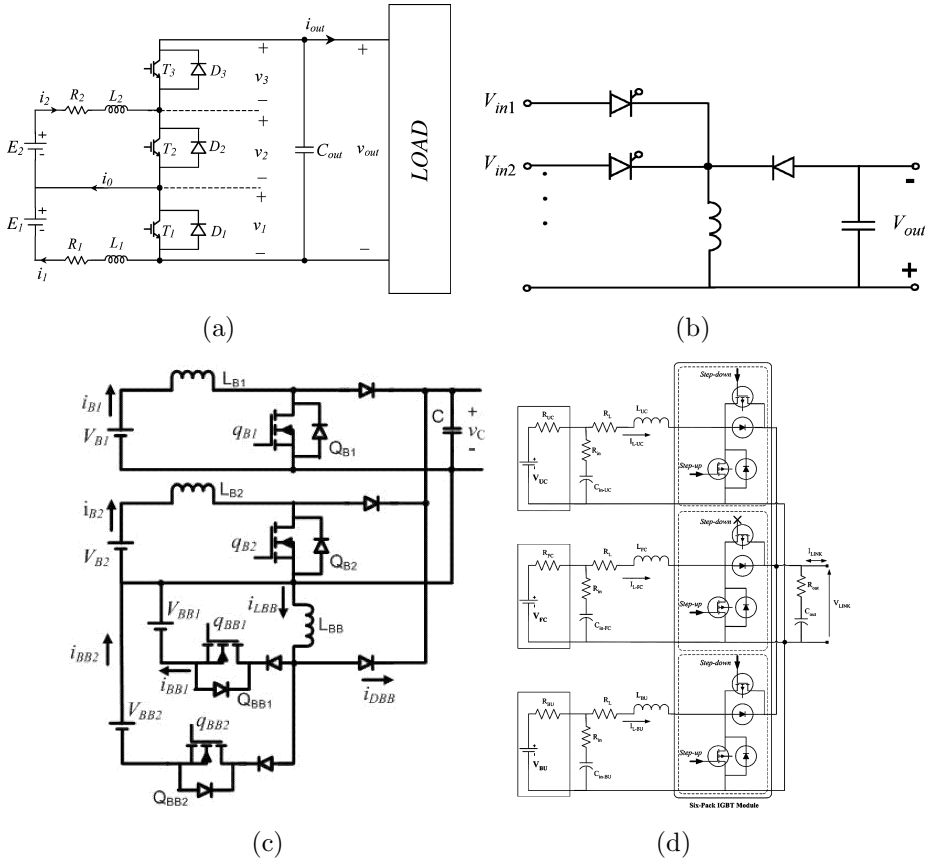

Figure 1.6. Electric-coupled Converters: (a) stack/multi-level[31], (b) multi-channel multiplexing[33], (c) switching cell combination[34], (d) uniform switching cell[38].

1.3 Research Motivation and Objectives

Based on a comprehensive review of past literatures, there are several microscopic level as well as system level technical aspects which demand improvement.

1. Past literatures mainly focus on multiple-input converter topology derivation and circuit operation, Nonetheless, without focus on a sustainable mode of operation at a system level, the proposed converter with multiple sources has to accommodate critical load demand as well as energy source/storage protection. Sustainable mode of operation is one of the most desirable features of local generation unit in smart grid, and local generator plays different roles of generator, compensator, conditioner and backup source.
2. The fact that different renewable sources have their own dynamic range and supply of "fuel", characteristics of renewable sources also must taken into account during the system design. The proposed converter is desired to accommodate the source characteristics with minimum component count and simple operation.
3. Research performed in cited literatures only cover dc-dc conversion part. In fact, most of the cited multiple-input dc-dc converters are not stand-alone system since output dc voltage is not directly utilizable, downstream dc-dc converter or dc-ac converter has to be incorporated into the system.

To provide a remedy to the disadvantages of the DG and current multiple-input converter systems, the concept of Multi-port Power Electronic Interface (MPEI) will be introduced in this dissertation. Term "interface" is adopted here due to the fact that both ac and dc power can be processed by the system and dispatched quantitatively to desired port while the past literatures all focuse on dc-dc power conversion. The objectives of this dissertation is listed as follows:

- To define the concept of Multi-port Power Electronic Interface (MPEI), targeting at a versatile performance power processing system which is able to harvest, condition and dispatch power optimally.
- To evaluate hybrid power system with different structures and choose a practical and cost effective solution to MPEI implementation.
- To define the modes of operation in order to achieve optimal harvest of versatile renewable energy, optimal power management and optimal grid interactions.
- To develop a mathematical model for MPEI in large signal and small signal.
- To propose and design a local control system for source-interface of MPEI to achieve power sharing in both dynamic and steady states; and verify the design with experiments..

1.4 Dissertation Outline

The dissertation will be arranged as follows,

- **Chapter 1** In this chapter, the challenges in contemporary electric power and vehicle power systems are identified; literature review on multiple-input converter system for local power processing is conducted; different topologies are categorized and evaluated. The goals of dissertation is defined.
- **Chapter 2** The concept of Multi-port Power Electronic Interface (MPEI) is defined; different methods/structure to integrate hybrid power system are compared and analyzed. With the presence of multiple sources, storages and loads, the modes of operation are defined for various scenarios.
- **Chapter 3** A five-port MPEI circuit topology which interfaces with four dc sources and one ac source is proposed; system level of analysis is performed to reduce the complexity of analysis; averaging technique is applied in following step to obtain large signal as well as small signal model the system.

- **Chapter 4** This chapter is to propose an integrated local control system and global power management control system for a five-port power electronic interface under study. Detailed control loop design is performed at each energy conversion port.
- **Chapter 5** The hardware design is presented and experiments are conducted under different operation modes; both transient and steady state tests are performed.
- **Chapter 6** The final chapter concludes on the proposed idea and performance of the system andpropose the future work on the system and its applications.

CHAPTER 2

MULTI-PORT POWER ELECTRONIC INTERFACE (MPEI)

2.1 MPEI - the Conceptual Development

2.1.1 Duality Between Signal Processing and Power Processing

As indicated by the literature review, previous work dealing with multiple input converter focus on dc-dc conversion design, which, in most cases, only forms the front-end interface to renewable energy sources or storages. Being proposed as a power processing interface, MPEI is defined to harvest and process energy into usable forms. Taking a close inspection into MPEI's counterpart in communication signal processing area, dualities can be found between signal processing and power processing [43]. As illustrated in Figure 2.1, a signal processing system can interface with digital and analog signals and perform a variety of tasks such as amplification, encoding, decoding, analog-to-digital conversion and digital-to-analog conversion, etc. The task of a signal processing system is to maintain the signal and information integrity, yet, the power consumption is incidental. A general definition of signal processing is given in (2.1), where "power" is not included in the operation.

Similar to signal processing system, a power processing system processes the available power from the input and shapes the output voltage or current into certain usable form by certain signal modulation. Power processing can take different forms, which include rectification, inversion, dc-dc conversion and cycloconversion etc. In smart grid and vehicular applications, it is desirable that energy flow be controlled in different scenarios and the voltage or current waveform on each interface is shaped to desired usable waveform. The generic expression for power processing is also given

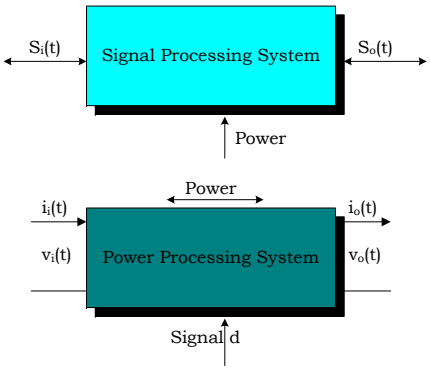

Figure 2.1. Duality between power and signal processing.

as in (2.2). Since power is load dependent (different load level demands different power, different load type also render different power), the processing is described by terminal quantities: voltage and current. As indicated in (2.2), the voltage and current generated by a power processing system might depend on input voltage or current or both or none, however, must have a relationship with modulation signal d. Based on the analogy, the MPEI concept is proposed here in this dissertation.

$$S_o(t) = \psi(S_i(t)) \tag{2.1}$$

$$\begin{cases} v_o(t) = f(v_i(t), i_i(t), d) \\ i_o(t) = g(v_i(t), i_i(t), d) \end{cases} \tag{2.2}$$

2.1.2 Definition of MPEI

The concept of Multi-port Power Electronic Interface (MPEI) is introduced here [44]

MPEI: *A Multi-port Power Electronic Interface (MPEI) is a self-sustainable multiple input and output static power electronic converter which is capable of interfacing with different sources, storages and loads. The integrated control system of MPEI enables both excellent system dynamic and steady state performance which renders optimal*

renewable energy harvesting, optimal energy management and optimal and economical utility grid interactions in a deregulated power market.

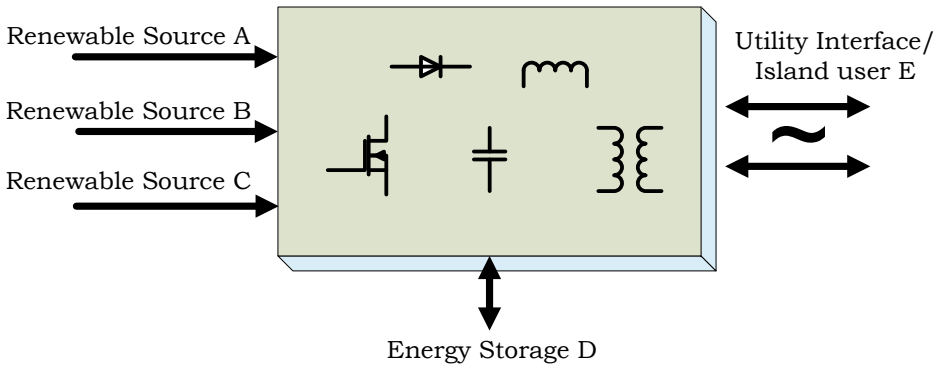

Figure 2.2. MPEI conceptual diagram.

Figure 2.2 presents a conceptual block diagram of MPEI. Different source/load and storages are connected to the ports of MPEI in forms of dc or ac power; as indicated in the figure, in certain ports (such as port A, B and C), the power flow is unidirectional since MPEI performs energy harvesting from external sources; the port which interfaces energy storage devices is bidirectional, is part of the salient features of multi-port system for optimal storage and dispatch; the ac port can either interface island user (feeding a standalone load) or utility grid which can source or sink power from/to MPEI. With access to a variety of renewable sources, energy storage and grid, MPEI possesses more degrees of freedom in power management than a conventional distributed generator unit: in some regions where wind generation take a considerable percentage of total power generation, certain generation margin is reserved for voltage regulation purpose since energy storage for wind farm demands enormous capital investment and infrastructures; however, for localized generation, incorporation of energy storage system for medium power capacity is far more affordable and much less

complex to implement. With flexible energy management system, MPEI will initiate a revolutionary change of relationship between end user and electric grid system: from a uniformed role of consumer to an informed, involved and active partner in power system demand response.

For generality of the study, five sources/sinks with different characteristics have been selected for the study, including Proton Exchange Membrane Fuel Cell (PEMFC), battery, wind generator, solar cell and utility grid. Fuel cell has its own fuel supply, hence it can provide power on a continuous basis. However, the chemical reaction demands certain pressure and temperature in chamber, and supply of fuel (hydrogen) relies on large inertia mechanical system [45][46][47][48]; therefore, start-up and load transient become the challenges for PEMFC interface circuit design. With certain ambient input, a maximum power output exists for solar cell and wind generator, a power tracking mechanism is desirable to harvest maximum power from ambient. Battery is so far one of the cost-effective and durable energy storage devices, and it is used as the main/secondary source in various applications. State Of Charge (SOC) of battery has to be maintained above or recovered to certain a percentage for longer battery life time and more cycle time, and a well designed battery management system can achieve this goal. Grid is considered as a infinite power source and power sink where phase control and frequency matching are crucial for power electronic interface. The key issues in interfacing with selected elements are summarized as follows,

- Cold start-up of fuel cell system.
- Management of slow dynamics of fuel cell system.
- Maximum power point tracking (MPPT) of solar power and wind power.
- Battery management and power dispatching.
- Phase and frequency control of grid-tie interface for desired power factor.

2.1.3 MPEI in Smart Grid

Due to the technology development and economical issue, current means of energy storage have limited capacity to medium and low power range. The advent of MPEI can fully utilized and incorporate current energy storage technology into localized power processing system. Figure 2.3 illustrates the concept of Home-to-Grid (H2G) for future smart grid system. As the power supplying unit at household, MPEI is managed by Intelligent Energy Management System (IEMS), which processes historical and current energy consumption data as well as real-time price of energy to issue commands to MPEI. Based on the commands from IEMS, MPEI performs harvest, generation, and storage so that an efficient and economical energy flow is achieved.

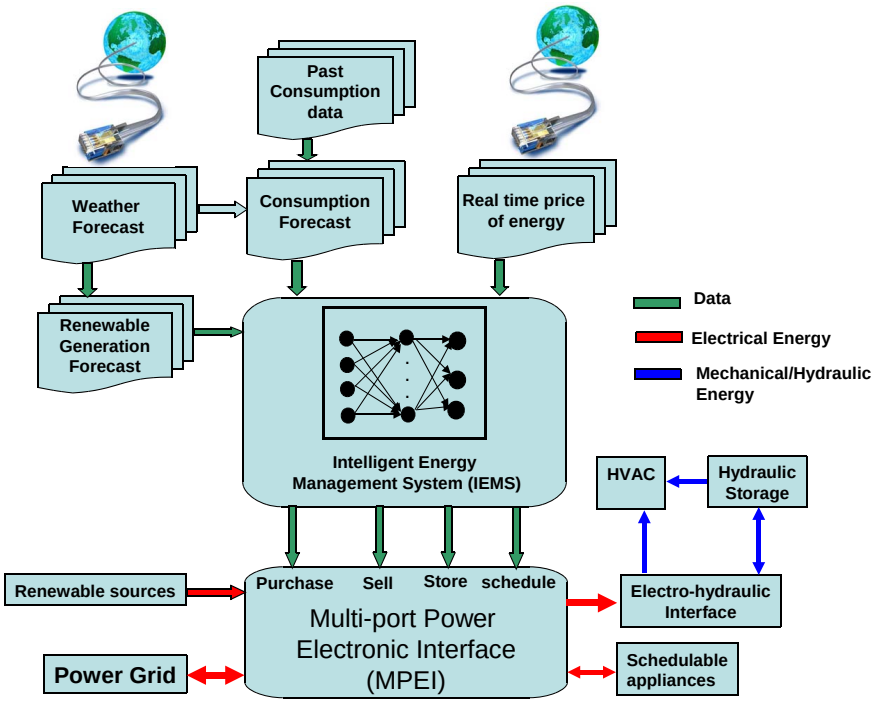

Figure 2.3. MPEI based Home-to-Grid system.

2.2 Integration of Energy Storage into Hybrid Power Systems

As stated in the previous section, some features of selected renewable sources are undesirable in system design. For example, the availability of solar/wind input and the slow dynamics of fuel cell system. Therefore, with varying input power and load demand, adding an energy/power buffer is one of the most effective and popular solutions [7][49][50]. Battery is chosen in this dissertation to form hybrid power system along with the other renewable sources. Given an open port for energy storage as shown in Figure 2.2, there are different ways to integrate the battery into MEPI. This section will investigate the hybrid power system structures for MPEI topology selection.

Several system structures have been proposed for the hybrid power system in the past literatures [37][51][52][53][54][55]. To simplify the analysis, fuel cell and battery are chosen as two sources in the hybrid power system under study, which interfaces two dc sources and one ac source. Figure 2.4 shows four most popular system structures which have been proposed recently. In structure A, battery is directly connected to low voltage power bus, paralleling with fuel cell; in structure B, battery is placed at high voltage dc-link bus; in structure C and D, battery is connected to a dc-dc converter, in structure C, battery voltage is step up/down to the same voltage level as fuel cell; while in structure D, battery voltage is stepped up to supply the high voltage bus.

There exist advantages and disadvantages regarding the above structures in terms of system dynamics, component selection and system cost etc. Structure A is the most common solution to fuel cell dynamics. The battery pack is working as the energy buffer to take care of the load transient as well as part of steady state load, and fuel cell shares the steady state load in an uncontrolled manner with battery pack and charges the battery whenever battery terminal voltage is lower than fuel

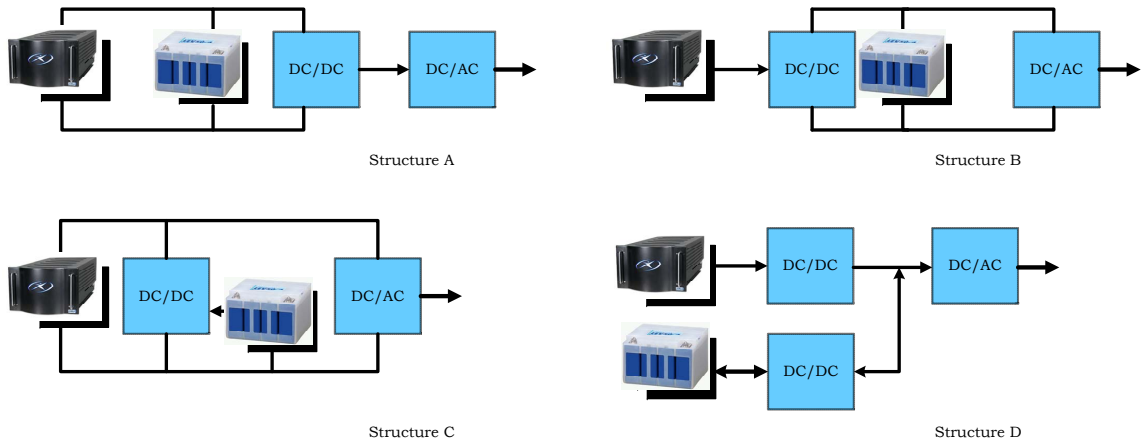

Figure 2.4. Hybrid Power System Structures.

cell voltage. In this case, dc-dc converter processes all the power from the source side, which will lead to a current intensive design. Structure B has battery pack after the front-end dc-dc converter. As indicated in the figure, high voltage battery pack is needed to match dc-link voltage. With this configuration, less noisy dc-link voltage is expected, and battery pack is working as energy buffer with uncontrolled charging and discharging. The common feature of structure A and B is that battery is directly connected to the voltage bus and can react to load transient at the first time; however, in both cases, charging and discharging of battery are taking place in an uncontrolled manner. Overcharging or overdischarging of the batteries might happen in certain situation which can lead to a short battery life time. System parameter matching (battery voltage) is also a problem in structure A and B. Therefore, there is less flexibility in choosing the system components which might render a higher system cost. Structure C offers a managed battery charging/discharging mechanism and is good for fuel cell current ripple elimination, but dc-link voltage is as low as fuel cell output. In order to use this configuration in high voltage applications (120VAC output for example), another stage of dc-dc conversion is needed to step up dc-link voltage level,

which results in an improved version of structure A. Structure D presents a dual converter solution. In this case battery is used as the secondary source to make a hybrid power system with independent power conversion channel. The power output of each source channel can be properly controlled; the unnecessary interactions between fuel cell and battery can be eliminated; charging and discharging of battery can be fully controlled to ensure a healthy status of battery and an extended life time. Without a direct link between battery and voltage bus, the dynamic response will degrade to a certain extent. However, by proper controller design, satisfactory dynamic response can be achieved. A spider chart is created to evaluate the four structures discussed above qualitatively, as shown in Figure 2.5. One can observe that although structure D renders higher system cost and more complex system implementation, it is more flexible in selection of system components and have superior performance than other system structures in terms of fuel cell protection, battery management and load peaking capability. Therefore, structure D is chosen as the power structure in this design.

2.3 Sustainable Modes of Operation

As an important infrastructure in future "smart" energy systems, MPEI is designed to achieve sustainability on three levels, which are addressed below in details,

- Electric power system level: MPEI takes the role of distributed generator to provide active and reactive power in demand, and provide uninterruptible power for system contingency.
- MPEI system level: ability of continuous operation and optimal harvest, storage and dispatch.
- Component level: excellent power management for a longer system component life time.

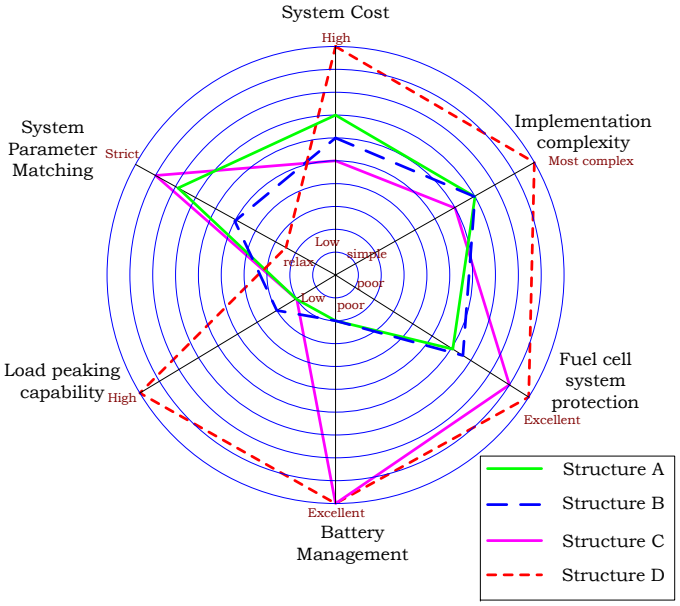

Figure 2.5. Spider plot for evaluation of different hybrid structures.

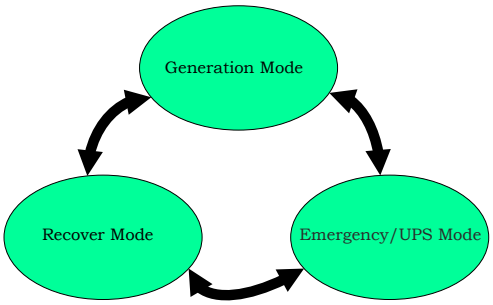

Figure 2.6. Modes of system operation.

In this prospective, three modes of operation are proposed in this dissertation which include generation mode, emergency mode and recover mode as shown in Figure 2.6.

Generation mode interacts with utility grid. As show in in Figure 2.7, two states have been defined in generation mode. With sufficient ambient input and sufficient battery SOC in State I, maximum power is harvested from solar cell and wind turbine; and battery is used as the energy buffer, compensating the disturbance

from renewable energy input. In case of no ambient input as State II, battery will be providing power to grid if generation is economical at the moment.

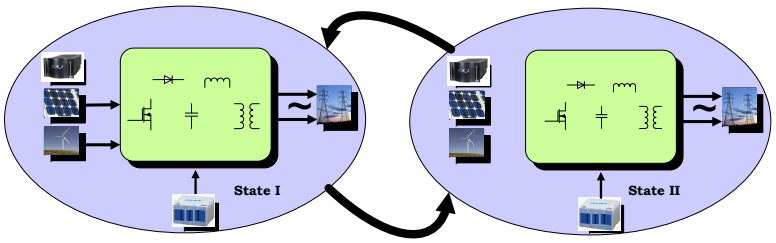

Figure 2.7. Mode A: generation mode.

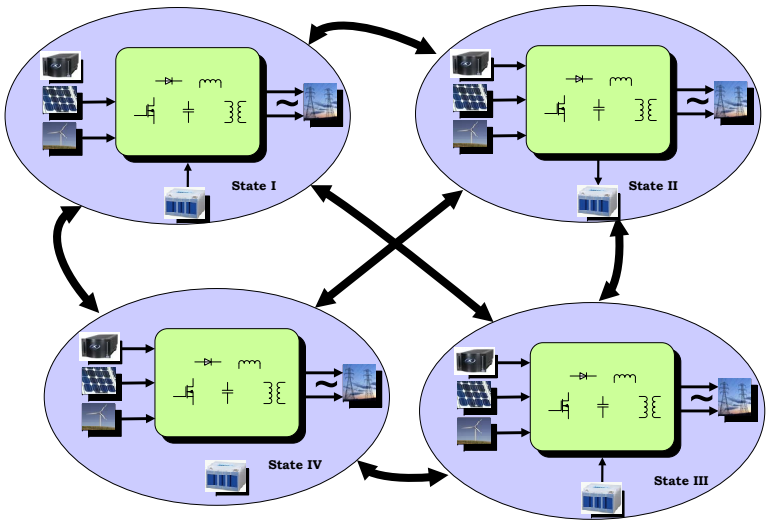

Figure 2.8. Mode B: emergency mode.

In case of line voltage collapse, MPEI runs in the emergency mode where MPEI works as a standalone generator to provide uninterruptible power to the end-user. For optimal harvesting, power tracking mechanism is always applied to solar and wind energy conversion. In the mean time, optimal dispatch can be achieved by properly controlling the power out of fuel cell and battery. Nonetheless, PEM fuel cell and

battery have their own limitations: Fuel cell has long start-up period (for Hydrogenics HyPM-XR 4.5kW module under test, a warm up period of 15 minutes is required) and slow dynamics to dynamic load; SOC of battery is a critical factor to monitor during system operation. Based on practical considerations, four states of operation have been proposed in the emergency mode, which is addressed in Figure 2.8. State I is the starting phase in which solar, wind and battery supply the load and fuel cell in warming up process. States II, III and VI are triggered by corresponding events and not necessarily in sequence. If the demand from customer-end is increasing and fuel cell is ready to generate, MPEI transitions into State II where fuel cell, battery, solar and wind power are supplying the load with properly controlled power from each source; if the load demand is dropped below the capacity of fuel cell and SOC of battery is low, fuel cell, solar and wind supply the load as in State III; if power capacity of fuel cell plus solar and wind has controllable surplus, MPEI transits into State VI: the bidirectional port of battery will charge the battery to recover SOC. Due to the uncertainty of solar and wind input, those two conversion channel can only works as the addition/bonus to system to alleviate stress on fuel cell and battery, hence design of MPEI in emergency mode mainly depends on fuel cell and battery power. Table 2.1 lists the status of system components (fuel cell and battery) to system states. The status bit "0" and "1" for each item is defined as follows,

Fuel Cell

0 Fuel cell system not ready (cold start)

1 Fuel cell system ready

Battery

0 Battery low SOC

1 Battery high SOC

System Load

0 System light load

1 System heavy load

Table 2.1. Component status and system states

Fuel Cell	Battery	System Load	System State
0	1	0	I
0	1	1	I
1	0	0	IV
1	0	1	III
1	1	0	I
1	1	1	II

Due to continuous operation of MPEI, either fuel cell or battery can be in service during the operation; therefore, simultaneous "0" states for both fuel cell and battery is not discussed in Table 2.1.

Mode C aims at battery SOC recovery. State I presents a fast charging scenario when all available sources are used to recover the charges in the battery. State I is only necessary when a heavy discharge of battery is scheduled within a short period of time. If the battery SOC is recovered to a sufficient value, fuel cell and grid are disconnected from the port, and only wind and solar power the charging process.

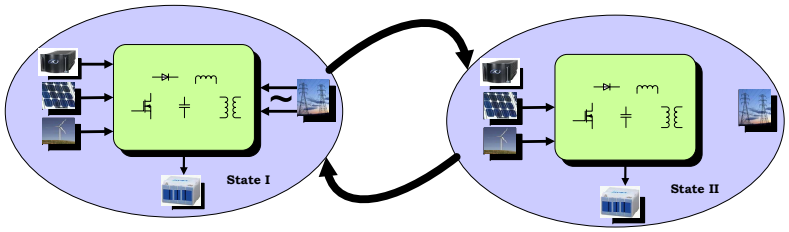

Figure 2.9. Mode C: recover mode.

Proposed mode/state transitions demand system component acting multiple roles in the system. For example, in Mode B State I, battery is the main source of power since there is no guarantee of sufficient solar and wind input; in State IV, fuel cell is the main source of power which feeds ac load as well as charges battery. Different from conventional hybrid power system where the roles of primary and secondary source are fixed, MPEI proposed in this dissertation assigns roles of sources in response to external events and component status, which render a more flexible power processing system.

CHAPTER 3

MPEI CIRCUIT, SYSTEM, AND MODELING

3.1 Switching Cells for MPEI

As indicated by literature review in section 1.2 and structure evaluation in section 2.2, ECC based topology is preferred due to simplicity and reliability of system implementation. There are several switching cell candidates for MPEI topology: buck, boost, and buck-boost. The criterion of selecting switching cell for MPEI is based

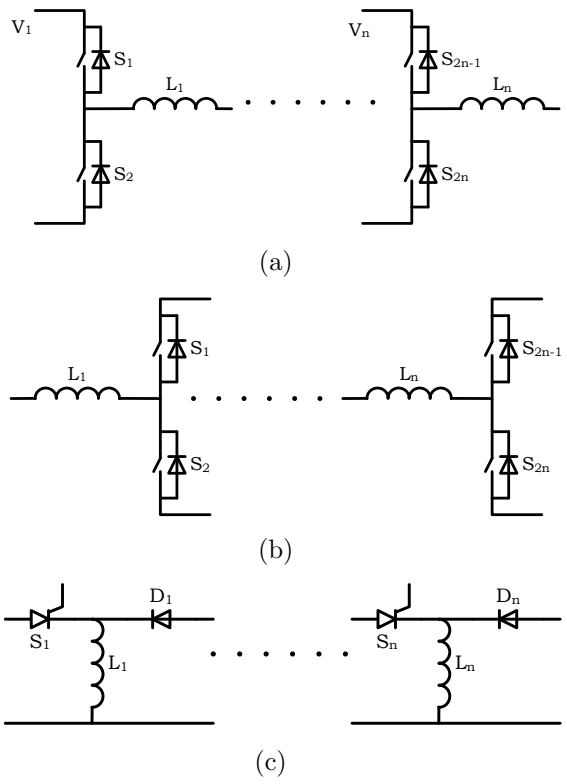

Figure 3.1. Three switching cells: (a) Buck cell, (b) Boost cell, (c) Buck-boost cell.

on following factors,

- Flexibility of voltage output
- Port characteristics
- Simultaneous power delivery

For all three listed switching cell candidates, the power from port element can be simultaneously processed. As indicated in Table 3.1, for buck switching cell, the output voltage can only be lower than input and input current is discontinuous. Therefore, extra filtering elements are required to interface with fuel cell; boost switching cell takes continuous input current from the port which is desirable in fuel cell and machine interface. It is also a fact that low voltage version of renewable sources/storage discussed in this dissertation are commercially available in the market. Buck-boost switching cell can deliver flexible voltage output for the system, but it shares the similar input current waveform like buck switching cell. The negative output for buck-boost cell also renders potential higher implementation cost for the entire system. Therefore, boost cell is preferred to synthesize MPEI topology.

Table 3.1. Three switching cell comparison

	Voltage gain	Input current	Input filtering
Buck Cell	D	Discontinuous	Required
Boost Cell	$\frac{1}{1-D}$	Continuous	Not required
Buck-boost Cell	$-\frac{D}{1-D}$	Discontinuous	Required

3.2 Circuit Topology and System Organization of MPEI

The circuit topology is presented in Figure 3.2 where uniform phase-leg modules are used. Different sources/sinks are interfaced to MPEI through boost switching cells. Phase-leg structure enables bidirectional power flow at the energy storage and

grid port. The switching cell connected to battery will operate in boost mode if there is load demand from battery, in buck mode if battery SOC needs recovery. On the grid side, the single-phase bridge can either work in inverter mode for generation or in rectifier mode for storage. For other sources used in the dissertation (fuel cell, solar cell and wind turbine), the corresponding switching cell will operate in unidirectional mode, and only harvesting is performed in those processing channels.

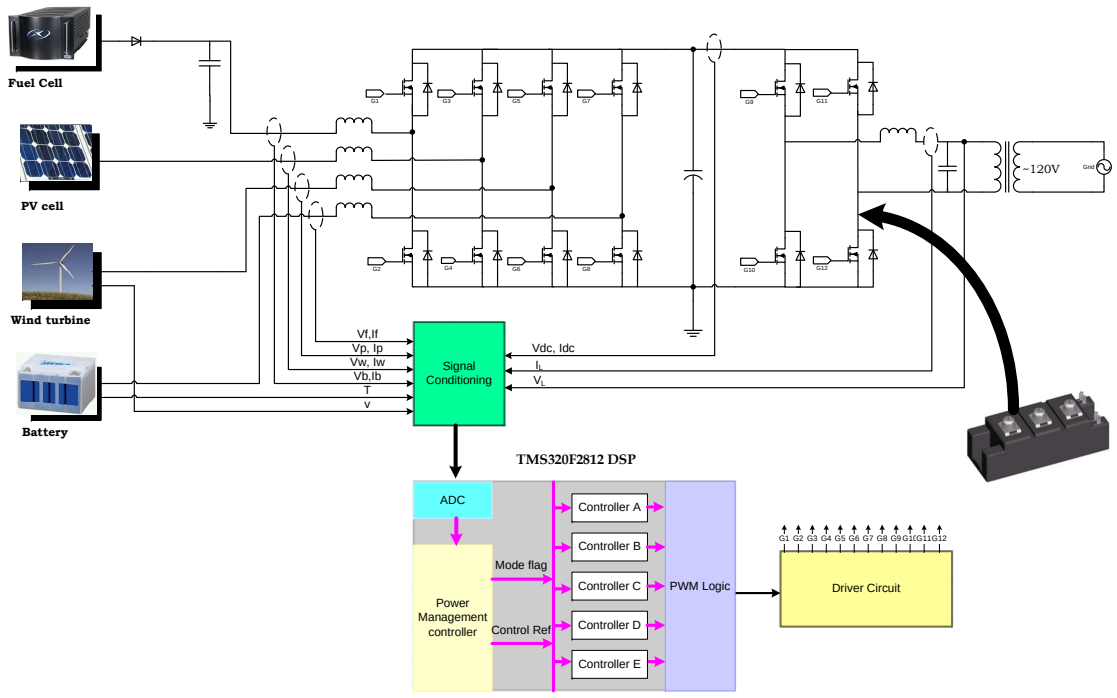

Figure 3.2. MPEI circuit implementation.

Expandability is another attractive feature of phase-leg based topology. Although only DC elements are connected to port of MPEI in this study, the structure can accommodate different type of inputs/outputs. For example, multiple phase-legs can be configured as multiphase converter for high current dc-dc conversion; three phase (multiphase) wind turbine can also connected to the port of MPEI and phase-

leg will operate as rectifier; in this study single phase utility interface is used, although three phase interface is also easily achievable.

In the prospective of engineering cost, commercially available phase-leg module can be used to construct the power stage, which is manufacturing and maintenance friendly. The system will be implemented in a digital controller which requires minimum peripheral circuit for port quantity sensing.

3.3 MPEI System Model

In this section, the large signal and small signal model of MPEI will be derived for control system design. For a multiple port system, the state space representation for the system can be expressed as in Equation 3.1.

$$\begin{cases} \dot{\underline{X}}(t) = f[\underline{X}(t), \underline{d}(t), \underline{u}(t)] \\ y(t) = \psi[\underline{X}(t), \underline{d}(t), \underline{u}(t)] \end{cases} \tag{3.1}$$

where $\underline{X}(t)$ is the state vector, $\underline{d}(t)$ is the control vector and $\underline{u}(t)$ is the port vector. However, as illustrated in the system circuit topology, MPEI as a whole is not a single stage power converter; hence, regulation of system internal states is required. System dynamics of MPEI therefore, can not studied by black-box approach as in [56], but a deep insight system model is required.

3.3.1 Zonal Analysis of MPEI

As a power interface, MPEI does not store energy. Energy from external sources are harvested, shaped into usable form or stored into energy storage. It has to be understood that MPEI is not a single stage power processing since port can interface with either dc or ac power. Therefore, from a functionality perspective, power processing in MPEI have two stages: front-end conditioning and load conditioning.

An intermediate goal exists in MPEI for frond-end interface to provide a solid voltage or current link to supply downstream load interfaces; hence, introduce numbers of internal state for the system. For high performance regulation, port variable as well as internal state have to be used inside the control loop: considering a two-port MPEI with a single buck stage, in order to perform regulation, output voltage as well as output inductor current which is essentially an internal state, have to be used in the control loop; for the five-port MPEI in this study, a stable dc-link voltage is the object for front-end switching cells, which is also an internal state. Therefore, the diversity power processing with multiple stage processing port states are insufficient to present the entire system dynamics, and internal states should be considered in the modeling process.

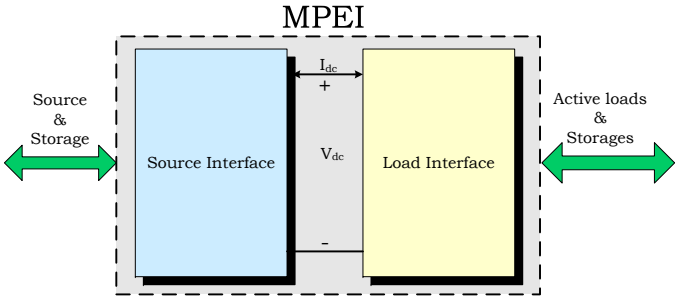

Figure 3.3. Zonal analysis of MPEI.

Zonal analysis is the method proposed in this research by grouping power processing blocks which are of common interests. Combination of four boost switching cells is treated as source interface while single phase inverter which supplies ac load is treated as load interface, as shown in Figure 3.3.

The source and load interface system are modeled separately and designed to meet stability and dynamic performance. The interface system stability can be determined by Middlebrook's criterion [57]. Figure 3.4 shows a voltage-link interconnected

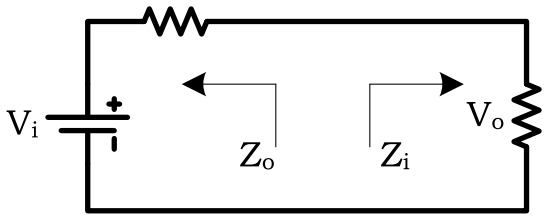

Figure 3.4. Middlebrook's criterion.

system, where the output impedance of source interface is founded as $Z_o(s)$ while the input impedance of load interface is $Z_i(s)$. Middlebrook's criterion indicates that the system is stable if poles of transfer function $H(s)$ in Equation 3.2 are located on the left half plane of imaginary axis.

$$H(s) = \frac{V_o}{V_i} = \frac{Z_i(s)}{Z_i(s) + Z_o(s)} \tag{3.2}$$

3.3.2 Average Model for Single Switching Cell

Averaging method is one of the best effective tools to approach time varying switching-mode system. If the long term system dynamics are the objective of study, the switching function, which is of faster dynamics, can be averaged over small period of time interval without altering the essential nature of system response [58]. Therefore, the averaging method will be valid such that the response time of state variables is much longer than the switching period T. The averaging operation can be defined as in Equation 3.3.

$$< d > (t) = \frac{1}{T} \int_{t-T}^{t} d(x)dx \tag{3.3}$$

During the last thirty years, several modeling methods have been proposed for power electronic converters. Circuit averaging technique was proposed in [58]

and a canonical equivalent circuit model for switch-mode power supply was brought up; state space averaging was proposed in [59][60], which mainly considered the dc components of state variables; generalized averaging method was proposed in [61] and elaborated in [62], which included high order harmonics to reflect converter dynamics in a closer manner; injected-absorbed current current method was discussed in [63]; Vorperian invented the concept of average switch modeling method in [64] which enabled fast transfer function derivation; switching frequency dependent modeling was discussed in detail in [65].

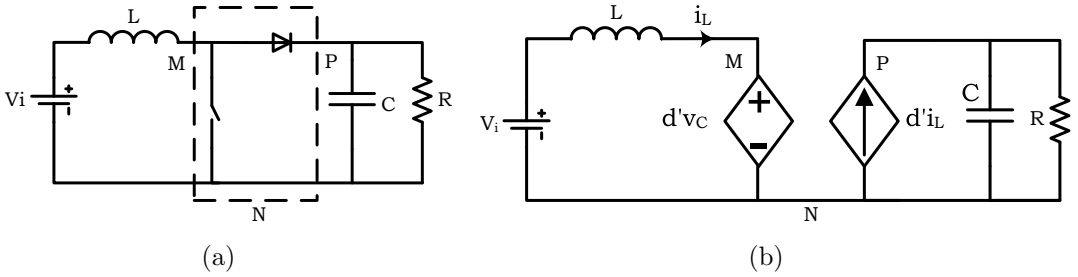

Figure 3.5. Boost converter model: (a) boost converter, (b) average model of boost converter.

Average switch method models the behavior of three-terminal switching network, and hence transfers a nonlinear switch-mode system into a simple circuit problem which allows fast computation. Figure 3.5(a) presents a boost converter as the switching cell of MPEI. The switch-diode combination is indicated in the dashed box. Sharing a common ground the electrical behavior of three terminal switching network is modeled for input and output port respectively. As shown in Figure 3.5(b), the input port is modeled by a voltage controlled voltage source $v_{MN} = D'v_C$ where $D' = 1 - D$ is the complementary of switching duty cycle, and v_C is output voltage; the output port is characterized by a current controlled current source $i_{PN} = D'i_L$, and i_L is the input inductor current. Linearization can be performed by introduc-

ing small signal perturbation into state variables and control variable [66][67], as in Equation 3.4.

$$\begin{cases} D' = 1 - (D + \tilde{d}) \\ v_C = V_C + \tilde{v_C} \\ i_L = I_L + \tilde{i_L} \end{cases} \tag{3.4}$$

The reassembling of equivalent circuit with the presence of small signal perturbation is relatively straight forward. Figure 3.6 presents the circuit model of boost converter without considering the parasitic parameters. The small signal can be derived by solving KCL and KVL equations.

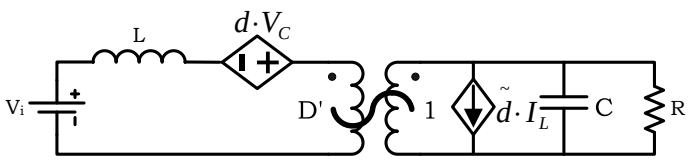

Figure 3.6. Boost converter model with small signal perturbations.

3.3.3 Large and Small Signal Model of MPEI

Using average switch method, large signal model of MPEI is derived as shown in Figure 3.7. As explained in previous section, MPEI system is partitioned into two processing stages. Since energy harvesting and dispatch features are all managed by the source/front-end interface, modeling of source interface is investigated in this dissertation. To simplify the analysis of the source interface, the load interface is modeled by a resistor as indicated in Figure 3.7.

In order to verify the proposed large signal model, simulation is conducted. However, one needs to note that limitation still apply to average switch model since

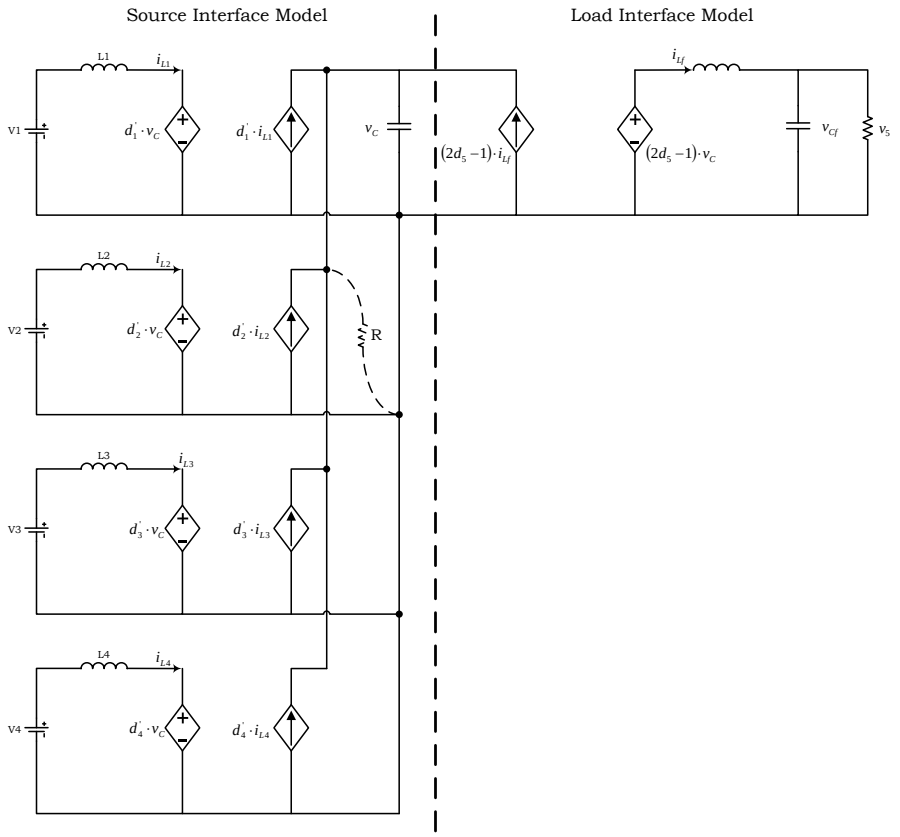

Figure 3.7. Large signal model of MPEI.

constraint of unidirectional current in diode is not modeled by three-terminal behavior model. Therefore, oscillation which leads to negative flow of inductor current can be observed in open loop simulations; further, in parallel connected boost switching cell case, open loop simulation demands strict parameter matching in order to prevent unrealistic simulation results. Based on those facts, close-loop simulation is conducted by controlling two boost switching cells to share even current in Figure 3.8.

As indicated in Figure 3.9, The terminal behavior is validated by inspecting voltages and currents. Figure 3.9(a) illustrates that the summation of output port current from each switching cell is equal to load current ($i_{PN1} + i_{PN2} - i_C = i_{load}$). Figure 3.9(b) indicates the measured input port voltage of three-terminal network

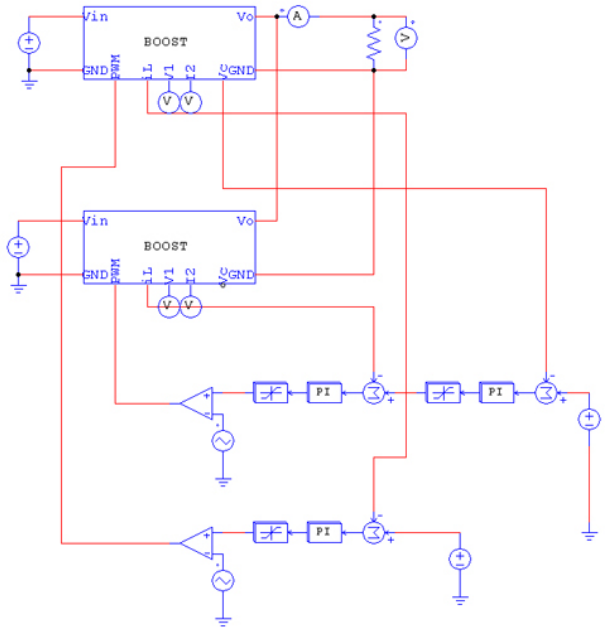

Figure 3.8. Even current sharing control simulation using average model.

and modeled port voltage ($v_{MN} = D' \cdot v_C$). The simulation results indicate validity of averaged model in a multi-port system.

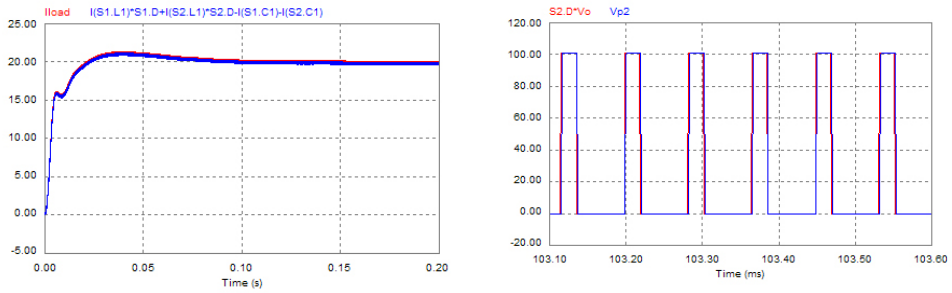

(a) (b)

Figure 3.9. Average model validation: (a) output port validation, (b) input port validation.

With a similar approach, small signal perturbations are added to MPEI large signal model as implemented in Equation 3.5, in which subscript i indicates a dif-

ferent switching cell. Given a much higher desired control bandwidth, input source disturbance is ignored in the analysis, therefore, no $V_i + \tilde{v_i}$ term is introduced.

$$\begin{cases} D_i' = 1 - (D_i + \tilde{d_i}) \\ v_C = V_C + \tilde{v_C} \\ i_{Li} = I_{Li} + \tilde{i_{Li}} \end{cases} \tag{3.5}$$

This renders three-terminal network input voltage and output current as described in Equation 3.6. V_{MNi} describes the terminal voltage of individual boost switching cell, and I_P is the current flowing out of the common node of boost switching cells.

$$\begin{cases} V_{MNi} = D_i' \cdot V_C + D_i' \cdot \tilde{v_C} - \tilde{d_i} \cdot V_C \\ I_P = \sum_{i=1}^{4} D_i' \cdot I_{Li} + \sum_{i=1}^{4} D_i' \cdot \tilde{i_{Li}} - \sum_{i=1}^{4} \tilde{d_i} \cdot I_{Li} \end{cases} \tag{3.6}$$

MPEI model with small signal perturbation is derived in Figure 3.10; ideal dc transformer is used in the model which enables simultaneous transfer dc power from primary of the circuit to the secondary.

Further simplification of the perturbed average model of MPEI renders small signal model in s-domain. KVL is applied to each switching cell as shown in Figure 3.10. The equation set is presented in Equation 3.7.

$$\begin{cases} \tilde{d_1} \cdot V_C - (\tilde{v_o} \frac{1}{R \| \frac{1}{Cs}} + \sum_{i=1}^{4} \tilde{d_i} \cdot I_{Li}) \cdot \frac{1}{D_1'} \cdot L_1 s = \tilde{v_o} \cdot D_1' \\ \tilde{d_2} \cdot V_C - (\tilde{v_o} \frac{1}{R \| \frac{1}{Cs}} + \sum_{i=1}^{4} \tilde{d_i} \cdot I_{Li}) \cdot \frac{1}{D_2'} \cdot L_2 s = \tilde{v_o} \cdot D_2' \\ \tilde{d_3} \cdot V_C - (\tilde{v_o} \frac{1}{R \| \frac{1}{Cs}} + \sum_{i=1}^{4} \tilde{d_i} \cdot I_{Li}) \cdot \frac{1}{D_3'} \cdot L_1 s = \tilde{v_o} \cdot D_3' \\ \tilde{d_4} \cdot V_C - (\tilde{v_o} \frac{1}{R \| \frac{1}{Cs}} + \sum_{i=1}^{4} \tilde{d_i} \cdot I_{Li}) \cdot \frac{1}{D_4'} \cdot L_1 s = \tilde{v_o} \cdot D_4' \end{cases} \tag{3.7}$$

Reorganization of the equation set into a matrix form results in Equation 3.8.

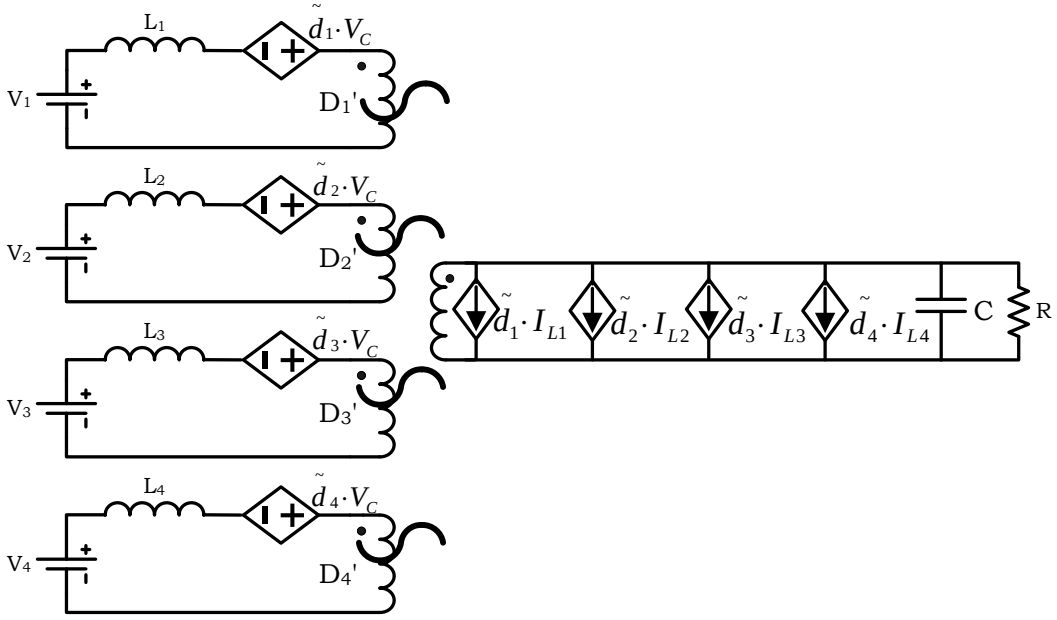

Figure 3.10. MPEI model with small signal perturbation.

$$\begin{bmatrix} \psi_{11} & \phi_{12} & \phi_{13} & \phi_{14} \\ \phi_{21} & \psi_{22} & \phi_{23} & \phi_{24} \\ \phi_{31} & \phi_{32} & \psi_{33} & \phi_{34} \\ \phi_{41} & \phi_{42} & \phi_{43} & \psi_{44} \end{bmatrix} \cdot \begin{bmatrix} \tilde{d}_1 \\ \tilde{d}_2 \\ \tilde{d}_3 \\ \tilde{d}_4 \end{bmatrix} = \begin{bmatrix} \alpha_1 \\ \alpha_2 \\ \alpha_3 \\ \alpha_4 \end{bmatrix} \cdot \tilde{v_C} \tag{3.8}$$

where

$$\psi_{ii} = V_C - \frac{I_{Li} L_i s}{D_i'};\ \phi_{ij} = -\frac{I_{Lj} L_i s}{D_i}, i \neq j;\ \alpha_i = D_i' + \frac{L_i s(RCs+1)}{RD_i'},\ i,j = 1,2,3,4$$

For a four switching cell front-end interface, the control-to-output voltage transfer function takes the form of 4×4 matrix. Reduction of the number of ports leads to reduction of matrix order; for a single input system, the control-to-output transfer function eventually reduces to a linear form, which matches the transfer function of conventional dc-dc boost converter. Different from conventional single stage power

conversion, source interface of MPEI takes the superposed form instead of single linear form. The i^{th} row of Equation 3.8 reflects the effort of i^{th} control variable to stabilize output voltage. However, cross terms exist in i^{th} control-to-output transfer function, which indeed is the disturbance injected from other switching cell operations. The control-to-output transfer function is plotted for the first row of Equation 3.8. In this case, channel 1 mainly contributes to voltage control of MPEI dc-link. Figure 3.11 demonstrates the frequency response of transfer function of interest: control-to-output transfer function of battery is given as G_{vbattd} and disturbances from solar, fuel cell and wind conversion channel is represented as $G_{vsd},\ G_{vfcd},\ G_{vwd}$ respectively. As indicated in the figure, though limited, the disturbances from other conversion channel contributes to a slight change in control-to-output transfer function response at high frequencies (above resonant frequency).

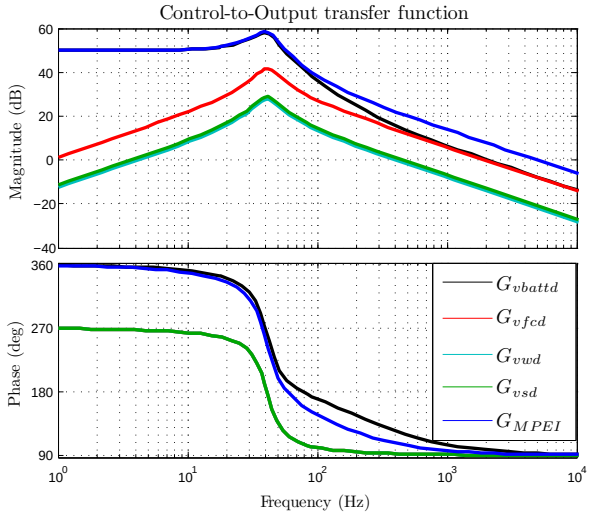

Figure 3.11. MPEI control-to-output transfer function.

If the output voltage is to be controlled by $\tilde{d_1}$, the disturbance introduced by $\tilde{v_o}/\tilde{d_2},\ \tilde{v_o}/\tilde{d_3},\ \tilde{v_o}/\tilde{d_4}$ has to be considered in the control system design and disturbance

has to be compensated, which is indicated in Figure 3.12. Similar situations also apply to voltage control of other switching cells.

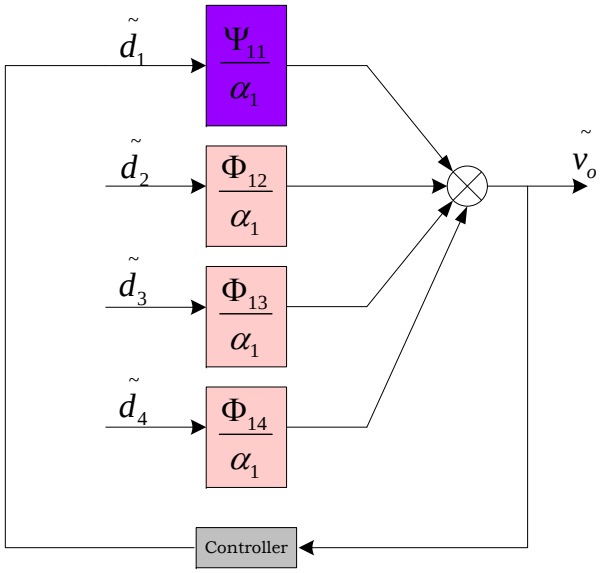

Figure 3.12. Disturbance injection during voltage regulation.

CHAPTER 4

CONTROL SYSTEM DESIGN OF MPEI

4.1 Local Control System Structure

For a "lumped" system structure, integrated control system has advantages over distributed control structure since the unnecessary communication channel can be eliminated and control reference and internal states can be directly passed to individual control loops within the control program. Typical implementation of control system takes the form of analog [18][21] and digital [38]. Analog controller has the advantages of simple implementation and high reliability, but not adaptive to variable control references. [38] implements the control system in a single DSP controller; however, local controllers are organized in a discrete manner and designed independently.

As defined in the previous chapter, MPEI operates in different dynamic modes up on system/ambient events, which is associated with reorganizing and modifying local controllers. Two features are desirable for the proposed control system:

- An easy interface to upper level controller.
- Capability of steady state load and dynamics sharing.

Integrated local controller is able to pass intermediate control variable or reference inside control loop, therefore has the potential to achieve faster response, better steady state performance and easier management.

4.1.1 Average Current-mode Control

The current-mode control was proposed in late 70s and has been widely used in nowadays high performance switch-mode power converters. Different methods of current-mode control have been proposed in the past. Peak current-mode is one of the earliest implementations, where peak value of the inductor current is sensed and compared with current-programmed signal; this feature allows easy current sensing, however, introduces excessive noise inside control loop and instability issue [68][69][67], which requires extra slope compensation. Peak current-mode control is widely used in low cost switch-mode power supply and a variety of commercial controller chips are available such as UC3842/3 from Texas Instrument.

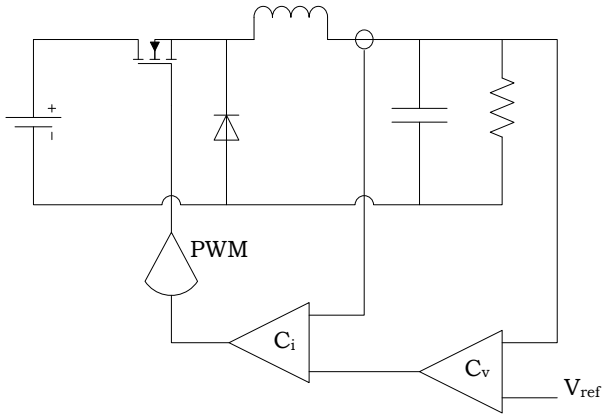

Figure 4.1. Average current mode control of a buck converter.

In average current-mode (ACM) control, actual value of current is measured and compared with programmed reference from outer voltage loop; high gain current controller is used to amplify current error and eliminate high frequency noise. Figure 4.1 is the block digram of ACM controlled buck converter; the output voltage of buck converter is sensed and the voltage error is amplified by voltage controller as the programmed current reference for current controller; the current error is obtained by

comparing the current reference with actual inductor current and later amplified by current controller for PWM generation. Following the signal follow, one can see that output capacitor voltage is indirectly controlled by direct control of inductor current. ACM can provide better dynamic regulation and source disturbance rejection than voltage regulation due to direct control of fast dynamic states. With compensation network, steady state error can be eliminated and accurate current share can be achieved.

4.1.2 MPEI Controller Structure and Controlled Quasi Current Source (CQCS) Technique

The local control system for MPEI source interface is presented in Figure 4.2, where $x = 1, 2, 3, 4$ and description of transfer function blocks are listed in Table 4.1

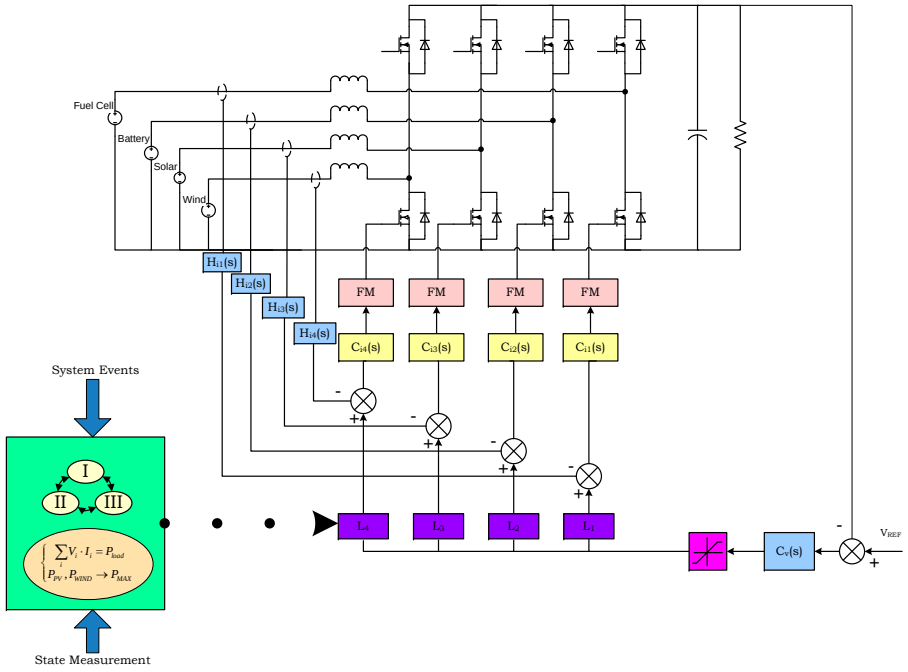

Figure 4.2. Integrated local control system for MPEI.

Table 4.1. Description of transfer function blocks

$H_{ix}(s)$	current transducer gain
$H_{vx}(s)$	voltage transducer gain
$C_{ix}(s)$	current controller
$C_v(s)$	voltage controller
L_x	control vector element
F_M	PWM modulation gain

A parallel-cascaded control structure is proposed in this dissertation. As shown in Figure 4.2, for each energy conversion channel, the voltage controller generates the programmed current reference for the paralleled internal current loops of individual source; each boost switching cell is configured as average current-mode (ACM) control [59][66][70][14] instead of single voltage loop control as presented in Figure 3.12. ACM is one of the best candidates for MPEI for several particular reasons:

1. Direct control of output voltage of a boost switching cell is unstable in the sense of Lyapunov while current control of boost switching cell is stable.
2. As justified in section 3.3.1, MPEI is not a single stage processing, therefore, regulation of the internal state is required. ACM provides a reliable and high-performance way for the dc-link voltage control.
3. The cascaded control structure with paralleled internal control loops will enable a current sharing capability.
4. With an integrated structure, current references are passed along the inside control loop, therefore, immune to external noises due to the signal transmission.

Since the common target of switching cells in source interface is to keep the dc-link voltage at a constant value, output voltage (dc-link) voltage is sensed and compared with the reference voltage. The voltage error is fed into the voltage controller

of the system and the current controller reference is generated. The programmed current reference signal is scaled by adjusting block L_x and used as the modified reference for individual current controller respectively. Since current reference for each controller can be made different, the current in each inductor can be controlled for power dispatching purposes.

Control vector $\vec{\boldsymbol{L}} = [L_1\ L_2\ L_3\ L_4]$ can be used to dispatch power from/to different port. The element L_x value is chosen within interval $\in [0, 1]$. Since the internal current loops share the same current reference, in case of control vector bypass ($L_x = 1$), each interface is under ACM control and total current is split evenly among different ports; the current of each channel in even current sharing is expressed by Equation 4.1, where P is the total power input from all ports.

$$I_E = \frac{P}{V_{Wind} + V_{PV} + V_{Battery} + V_{FuelCell}} \tag{4.1}$$

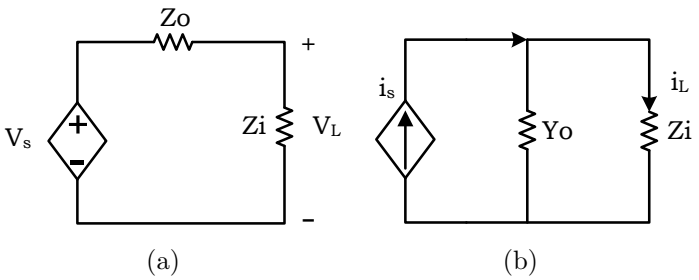

Figure 4.3. Close-loop controlled converter (a) voltage control, (b) current control.

To deliver power from input port to the load, two methods can be used: controlled current source and controlled voltage source. Figure 4.3 shows the equivalent circuit for a generic switch-mode circuit, and $V_s = d \cdot G_{vd}$, $I_s = d \cdot G_{id}$ under close loop control. In the presence of multiple sources, a combination of controlled current and voltage is used [40]. With four sources engaged in power dispatching, two major

combinations is proposed as in Figure 4.4. In Figure 4.4(a), fuel cell and battery interface share the same amount of current; solar and wind interface inject power into MPEI in the form of current sources; in this case, voltage and main load dynamics are controlled by fuel cell and battery switching cells. Figure 4.4(b) presents a single voltage source three current source (1V3C) combination: fuel cell or battery is used to stabilize dc-link voltage and the other power sources provide base power to the system in the form of current source.

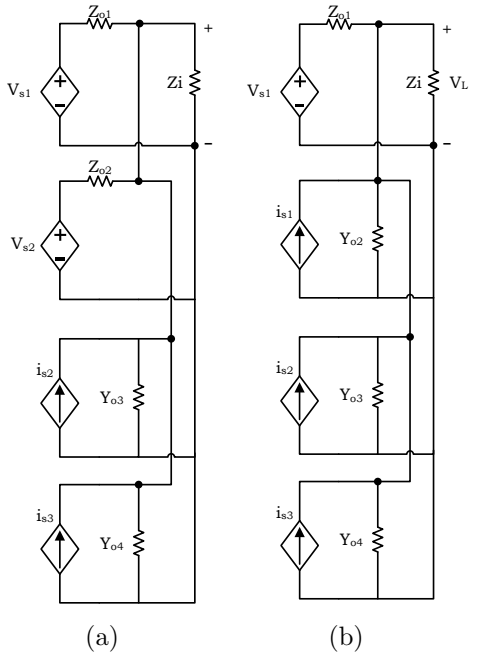

Figure 4.4. Power sharing equivalent circuit: (a) Two voltage sources and two current sources, (b) One voltage sources and three current sources.

In the case of multiple interfaces and given power level, $\vec{\boldsymbol{L}} = [L_1\ L_2\ L_3\ L_4]$ can be reconfigured for power dispatching, as explained, at least one element in $\vec{\boldsymbol{L}}$ is bypassed to support a stable dc-link voltage, the other elements are configured to interval $(0, 1)$ to program the proper reference values for direct current control. In

fact, enforcing update of L_x element will vanish, however not completely, the effort of outer voltage control loop and shape the inductor current into desired value. Equation (4.2) gives the relationship among voltage control output I^*_{Ref}, control vector element L_x and total input current I_{IN} for a four-port source interface; $|H_{ix}(s)|$ refers to dc gain of current transducer.

$$\sum_{x=1}^{4} \frac{I^*_{Ref} \cdot L_x}{|H_{ix}(s)|} = I_{IN} \tag{4.2}$$

Given the same current transducer gain for all port current measurement, the current in each conversion channel can be simplified as,

$$I_x = \frac{L_x}{\sum_{x=1}^{4} L_x} \cdot I_{IN} \tag{4.3}$$

which is indeed a weighted current distribution based on element L_x. In fact, there is no constraint in choosing L_x value as indicated in Equation (4.3), and in theory $L_x \in [0, \infty]$; however, considering practical implementation in digital system, only the interval $[0, 1]$ is chosen in this research.

In the current sharing process, the inner current loop references are enforced to desired values, hence forming Controlled Quasi-Current-Sources (CQCS) for the hybrid power system. During the steady state operation, the current draw from each power source/storage is programmed for current sharing, which reflects as independently controlled current source. Since the current reference is still generated by the voltage controller, during the load transient, the output from the voltage controller will vary to request more or less current draw from input; subsequently, the scaled current references also change proportionally to control vector $\vec{\boldsymbol{L}}$. Therefore, comparing with independent current control of each conversion channel in [38] where all load

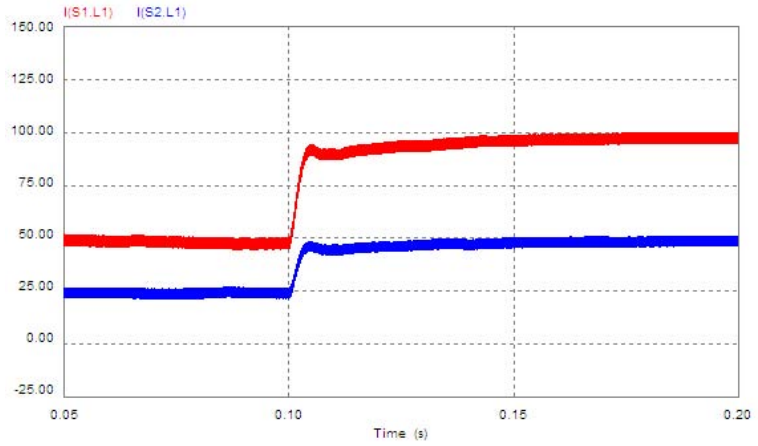

Figure 4.5. Dynamic current sharing in load step transient.

transients are taken by voltage controlled ultra-capacitor channel, load transients in MPEI with CQCS techniques will shared by all power sources. Figure 4.5 presents the simulation result of three-port MPEI with load step transient; the control vector is configured as $[1, \frac{1}{2}]$, which indicates voltage control in one channel and quasi current control in the other channel. As can be interpreted from the figure, the effort of control vector redistributes the load dynamics between two conversion channels, and the channel with less steady state current share (with smaller L_x) will contribute less to load dynamics. This feature is desirable in real operation: the conversion channels with less current sharing usually work with constraints: for example, battery with low SOC or fuel cell in cold start-up process. Therefore, scaled/suppressed dynamics will further help to maintain the efficient and health operation of those sources while at the mean time relieve the current stress on voltage controlled conversion channel.

4.1.3 Control Loop Design

The proposed control structure is applied to small signal circuit model of MPEI in Figure 3.6, which yields the close-loop system in Figure 4.6. The small signal

control variable d_x generated by the current loop regulates system states in the dashed block in the figure, while the rest of the function blocks keep the same notation as described in Table 4.1.

For control system design purpose, Figure 4.7 is presented in forms of transfer function blocks. Considering the uncertainties in sun irradiation and wind resource, control of solar cell and wind turbine output current by changing control vector $\vec{\boldsymbol{L}}$ value will introduce unnecessary computation and inaccuracy; therefore, solar and wind energy conversion is directly current controlled: modification will be applied to the control loops for solar cell and wind turbine channel in the system implementation; the current reference value is directly fed by the MPPT routine. However, in order to maintain the generality of the study, control system will be designed based on the model in Figure 4.7. G_{idx} denotes the control-to-current small signal transfer function, and control to output voltage relationship is presented by the transfer function matrix in Equation 3.8.

With a direct inspection into MPEI system model presented in Figure 3.10, the control-to-current transfer function will still end up with a multiple-input version. However, averaging method does not have constraint of inductor current direction (in fact, there does exist a constraint of current current direction introduced by the main diode); due to unidirectional feature of inductor current, there is one-to-one mapping between duty cycle and current in each switching cell; therefore, the transfer function can be obtained by solving small signal equivalent circuit of a single switching cell. KVL ad KCL are applied to ac equivalent circuit of Figure 3.6, which renders

$$\begin{cases} \tilde{d} \cdot I_L + \frac{\tilde{v_C}}{R \| \frac{1}{Cs}} = \tilde{i_L} \cdot D' \\ Ls \cdot \tilde{i_L}(s) + \tilde{v_C}(s) \cdot D' = \tilde{d}(s) \cdot V_C \end{cases} \tag{4.4}$$

And the control-to-current and control-to-voltage transfer function can be found as

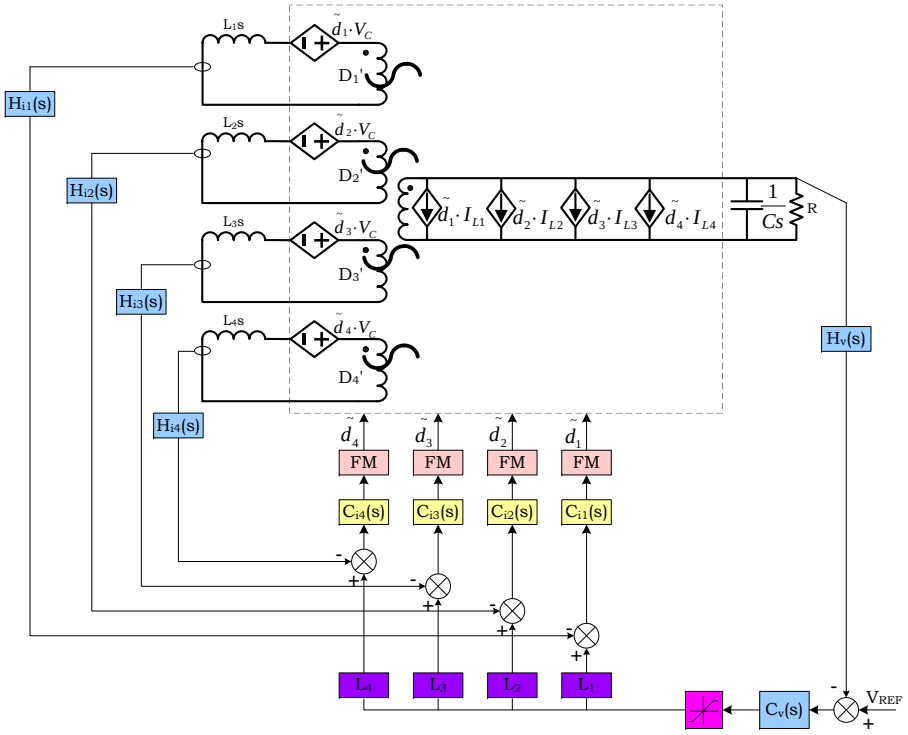

Figure 4.6. Close-loop controlled small signal MPEI circuit.

$$G_{id}(s) = \frac{i_L\tilde{(s)}}{d\tilde{(s)}} = \frac{V_C RCs + V_C + RI_L(1-D)}{RLCs^2 + Ls + R(1-D)^2} \tag{4.5}$$

$$G_{vd}(s) = \frac{v_C\tilde{(s)}}{d\tilde{(s)}} = \frac{RV_C(1-D) - RLI_L s}{RLCs^2 + Ls + R(1-D)^2} \tag{4.6}$$

where the resonant frequency is obtained as,

$$\omega_r = \omega_n \cdot \sqrt{1-2\zeta^2} = \frac{1}{\sqrt{L \cdot C}} \cdot D' \cdot \sqrt{1 - \frac{L}{2R^2 C D'^2}} \tag{4.7}$$

PI controller is used as the current controller, which is of form

$$C_i(s) = k_i \frac{1 + \frac{s}{\omega_c}}{s} \tag{4.8}$$

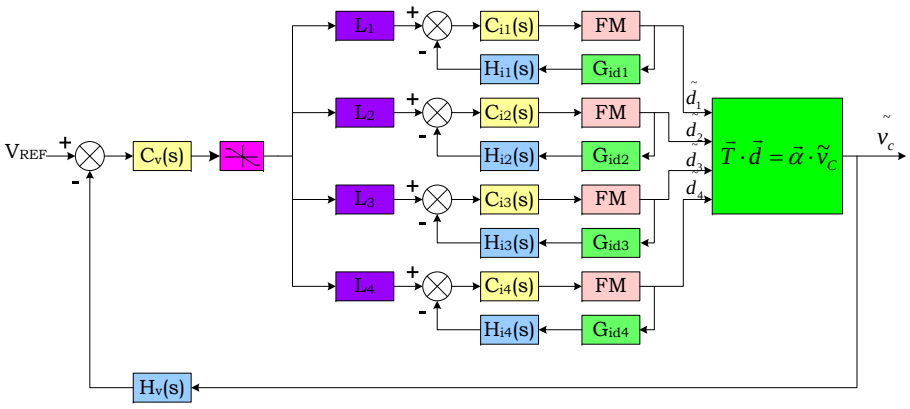

Figure 4.7. MPEI close-loop transfer function blocks.

and PI controller zero is chosen at or below system resonant frequency for oscillation damping, and gain k_i is chosen for proper phase and gain margin. The close-loop system is shown in Figure 4.8; zero-order-hold (ZOH) is used due to implementation of digital control system. The loop transfer function $T(s)$ is found as,

$$T_i(s) = C_i(s) \cdot FM \cdot G_{id}(s) \cdot H_i(s) \cdot ZOH \tag{4.9}$$

$$ZOH = \frac{1 - s\frac{T}{4}}{1 + s\frac{T}{4}} \tag{4.10}$$

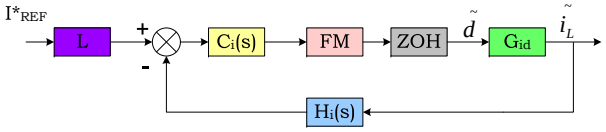

Figure 4.8. Close loop system for input current.

MPEI system is designed for 3kW of load. The detailed power distribution is given in the Table 4.2, and system component parameters are selected as shown in Table 4.3. The DC-link voltage is chosen as $100V$ based on safe voltage step-up ratio

of boost switching cells. Detailed current and voltage loop design for MPEI will be presented in the following discussion..

Table 4.2. MPEI power distribution

Fuel cell	Battery	Wind Turbine	Solar
$1kW$	$1.2kW$	$400W$	$400W$

Table 4.3. MPEI passive components

Fuel cell inductor	$L_{FC} = 595\mu H$
Battery inductor	$L_{Battery} = 534\mu H$
Solar inductor	$L_{PV} = 845\mu H$
Wind inductor	$L_{Wind} = 1000\mu H$
dc-link capacitor	$C_{DC-link} = 2900\mu F$

Since fuel cell system dynamic response is dominated by the fuel delivery system and chemical reaction, both of which are systems with large time constant comparing to that of the switching power converter systems [45][48][71][72][73]. Therefore, fuel cell could not react to fast load dynamics. With CQCS control, fuel cell current is the direct controlled system quantity, the bandwidth of fuel cell current loop should be as low as possible to relieve the current stress of fuel cell membrane as well as balance-of-plant of fuel cell system. In dc load applications, the bandwidth of fuel cell current loop can be selected as low as possible with half a decade separation from voltage control loop. However, more constraints apply to MPEI case, since the source interface is meant to supply the inverter load, which can be simply addressed by Expression 4.11 where $v(t),\ i(t)$ is the inverter output voltage and current respectively,

$$\begin{aligned} v(t) \cdot i(t) &= V_M sin(\omega t) \cdot I_M sin(\omega t) \\ &= \frac{V_M I_M}{2}(1 - cos(2\omega t)) \end{aligned} \tag{4.11}$$

It is obvious that the power flow on dc-link contains $120Hz$ ac components due to power balance. The dc-link capacitor will consume part of $120Hz$ current ripple, and rest of the ripple will propagate to dc source side if control loops are not well designed. However, given a ripple-free dc source current, the dc-link capacitor will be enforced to consume the ac power, which is the guide line for the control loop design. In dual loop design proposed in this dissertation, at least half a decade separation of bandwidth is required on either side of $120Hz$ frequency to avoid interaction between the controllers. The inner current loops are designed first for each switching cell.

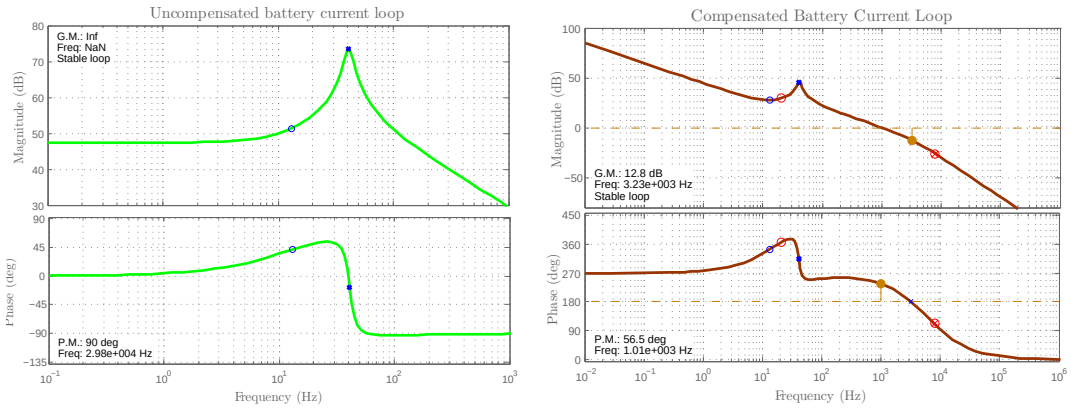

(a) (b)

Figure 4.9. Battery current loop design: (a) open-loop transfer function G_{id}, (b) compensated loop gain.

Given sufficient SOC, battery is the most reliable source for steady state power and dynamics. The current loop for battery is expected to have a high bandwidth for load dynamics. The control-to-current transfer function G_{id} is obtained from Equation (4.5) and PI controller parameter is obtained by placing the zero at half of power stage resonant frequency which is $255rad/s$; k_i is selected as 600 to have a cross-over frequency of $1kHz$ to offer a separation of more than half a decade from $120Hz$. The bode plot for open loop transfer function G_{id} and compensated loop

gain are plotted in Figure 4.9. Original resonant peak is attenuated and cross-over frequency is adjusted to $1kHz$ for desired speed of regulation and noise immunity, the design current loop has a phase margin of 56.5° and gain margin of $12.8dB$.

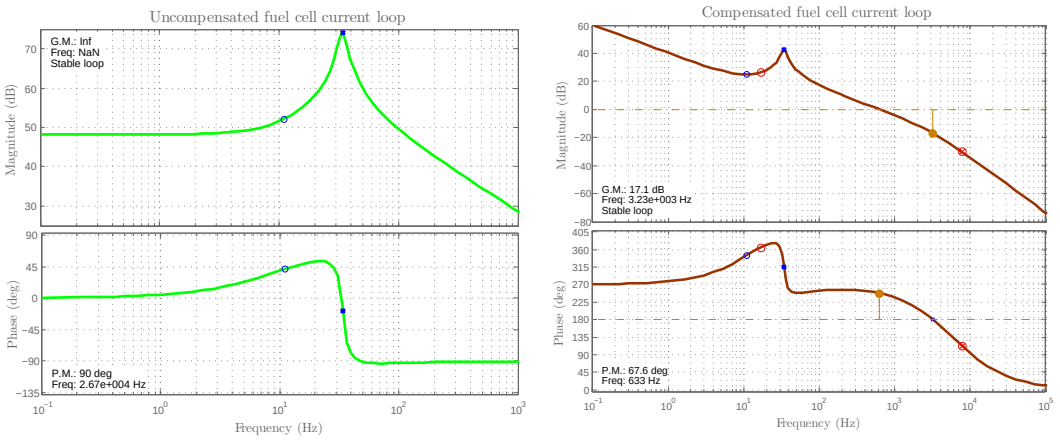

(a) (b)

Figure 4.10. Fuel cell current loop design: (a) open-loop transfer function G_{id}, (b) close-loop gain.

Since fuel cell has poor transient response, current loop cross-over frequency is design lower than than battery current loop, however, still half a decade above $120Hz$ ripple frequency. The PI controller zero is selected at half of fuel cell switching cell resonant frequency to attenuate resonant peak from $75dB$ to $40dB$; k_i is chosen as 280, the designed cross-over is $633Hz$. The frequency response of open-loop transfer function and close-loop gain are given in Figure 4.10.

Solar and wind source are under current control. There are two reasons for current control: first, both sources behave like current source in wide power region; second, perturbation in source renders large deviation of output voltage, which is suitable for maximum power tracking control based on perturbation and observation. The current loop of solar source is designed as high as battery current loop. As

reflected in Figure 4.11, the cross-over frequency is designed at $1.07kHz$ with gain margin and phase margin of $12.2dB$ and $55.1°$. The gain margin of $11.5dB$ and phase margin of $52.7dB$ for wind current loop are obtained by placing PI controller zero at $\frac{1}{4}$ of system resonant frequency and k_i gain of 600.

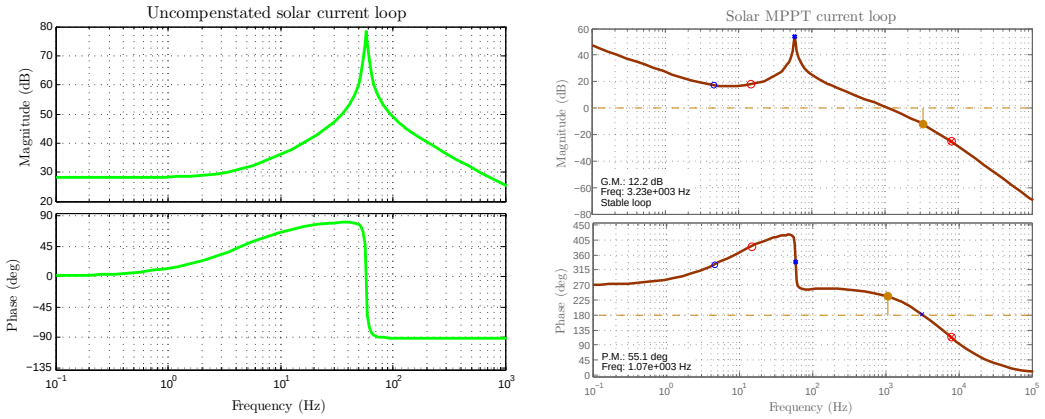

(a) (b)

Figure 4.11. Solar current loop design: (a) open-loop transfer function G_{id}, (b) close-loop gain.

The MPEI source-interface is designed with the assumption of CCM operation. Therefore, at low ambient input, solar panel and wind turbine could not offer sufficient voltage/current, and MPEI will inevitablely falls into discontinuous current mode of operation. To avoid this scenario, the minimum solar current ($1.5A$) and minimum wind turbine cut-in voltage ($40V$) is set for CCM mode of operation.

At least one switching cell is responsible to support dc-link. As explained in section 2.3, the role of primary and secondary source is not fixed. As a high inertia system, fuel cell can not respond to load dynamics well; therefore, the role of primary source is suitable for fuel cell, providing base power to the load. Battery, as an excellent candidate for the secondary source, can react to fast dynamics and

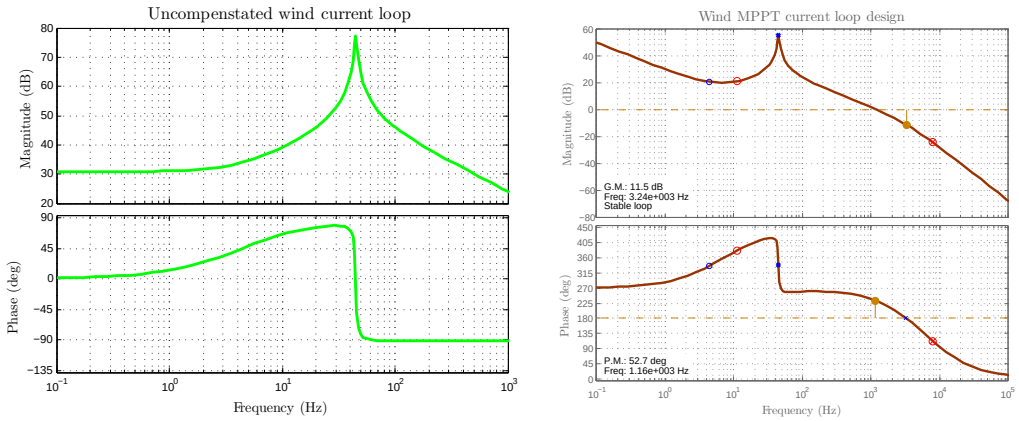

(a) (b)

Figure 4.12. Wind current loop design: (a) open-loop transfer function G_{id}, (b) close-loop gain.

contribute to load peaking. However, battery can only store finite amount of energy and SOC has to be recovered above certain level for extended battery life. Therefore, in MPEI, the role of primary source and secondary power source should not be fixed, a more flexible configuration has to be proposed to accommodate a variety of system component states and different load scenarios.

The simplest mode of operation for MPEI is the single supply case, where only one source works under ACM control to supply the load. Fuel cell and battery are considered as the best candidates for the single source mode operation since solar and wind input is incidental.

With the inner current loop under close-loop control, the open loop transfer function for voltage loop can be derived from Figure 4.13 and expressed as in (4.12), where $T_i(s)$ is indicated in Equation 4.9.

$$G_v(s) = L \cdot \frac{C_i(s) \cdot ZOH \cdot FM}{1 + T_i(s)} \cdot G_{vd} \tag{4.12}$$

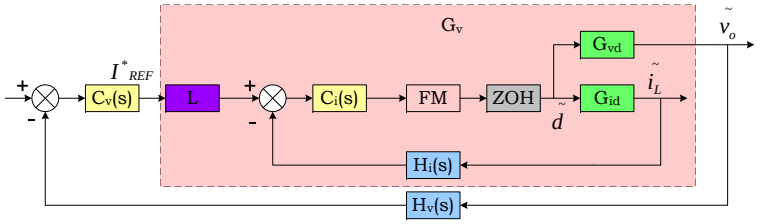

Figure 4.13. Single voltage loop control diagram.

The bode plots G_v and G_{id} for battery and fuel cell conversion channel are shown in Figure 4.14 with $L = 1$. As indicated in the plot, both transfer functions for battery and fuel cell are not stable. With inner current close-loop control, although still unstable, the gain margin of open loop system has been increased noticeably and the resonant peak is eliminated. The PI controller is designed to satisfy the stability and system response. The close loop gain for voltage loop is given in Equation 4.13

$$T_v(s) = C_v(s) \cdot G_v(s) \cdot H_v(s) \tag{4.13}$$

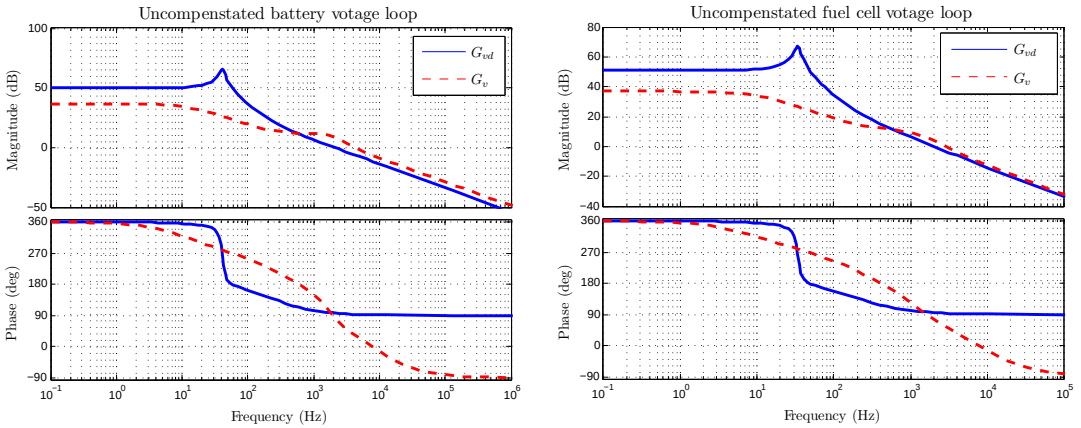

(a) (b)

Figure 4.14. Voltage open loop bode plot: (a) battery voltage open loop, (b) fuel cell voltage open loop.

The resonant frequency can be located numerically and compensated by PI controller zero. The zero for fuel cell voltage loop is picked at 135 rad/s and $k_i = 30$; the cross-over frequency of compensated system is set at $5.7Hz$, and 74° of phase margin and $35.5dB$ of gain margin can be achieved. Similarly, battery voltage controller is designed with zero at 157 rad/s and $k_i = 50$, which offers cross-over frequency of $8Hz$, phase margin of 73.5° and gain margin of $32.5dB$, which is indicated in Figure 4.15.

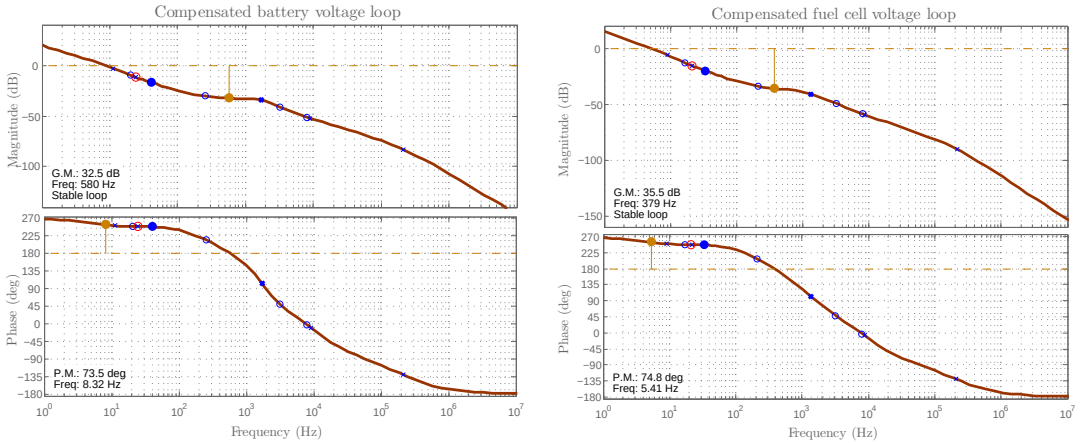

(a) (b)

Figure 4.15. Voltage loop design: (a) battery voltage loop, (b) fuel cell voltage loop.

In the case of multiple-source operation, MPEI is organized as a cascade-parallel structure as shown in Figure 4.7. Since only one voltage controller is proposed in the entire control structure, the duty cycle perturbations ($\tilde{d}_i$) generated by different current loops must be evaluated and compensated for dc-link voltage stabilization. According to Figure 4.7, the current reference to duty cycle transfer function under close-loop control can be found as in Equation 4.14, where $C_{ix}(s)$ and $T_{ix}(s)$ is the current controller and current loop gain for i^{th} port respectively.

$$G_{Ix} = \frac{C_{ix}(s) \cdot ZOH \cdot FM}{1 + T_{ix}(s)}, \ x = 1, 2, 3, 4 \tag{4.14}$$

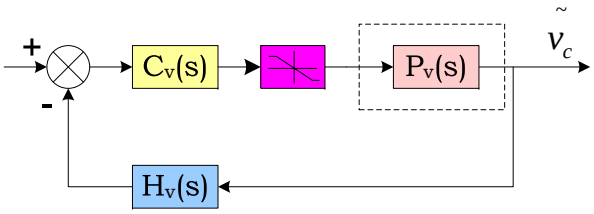

Figure 4.16. MPEI control system with equivalent voltage-control plant.

Four paralleled current loops and duty-cycle-to-output transfer function matrix in Equation 3.8 can be further simplified into an equivalent voltage-control plant $P_v(s)$ as in Figure 4.16. If port 1 is chosen as work under ACM control and current from the other sources are actively controlled by vector $\vec{\boldsymbol{L}}$. The resulted equivalent voltage control object (voltage controller $C_v(s)$ output to $\tilde{v_C}$ transfer function) and voltage loop gain $T_v(s)$ can be expressed in (4.15) and (4.16) respectively. For a designed power level, the control vector $\vec{\boldsymbol{L}}$ can be obtained by normalize the current from the rest of the sources to the current of the ACM controlled source.

$$P_v(s) = \frac{L_1 \cdot G_{I1} \cdot \psi_{11} + L_2 \cdot G_{I2} \cdot \phi_{12} + L_3 \cdot G_{I3} \cdot \phi_{13} + L_4 \cdot G_{I4} \cdot \phi_{14}}{\alpha_1} \tag{4.15}$$

$$T_v(s) = C_v(s) \cdot P_v(s) \cdot H_v(s) \tag{4.16}$$

Figure 4.17 presents the bode plot of simplified voltage control object $P_v(s)$ and its cross terms in a multiple-input scenario. With a similar pattern to the open loop control-to-output transfer function in Figure 3.11, within low frequency range, response of voltage control object plant is barely affected by the cross terms, which are also under inner closed current loop control. Slight modification of magnitude and

phase response is observed at a high frequency range (relative to designated voltage loop cross-over frequency $f < 120Hz/5$).

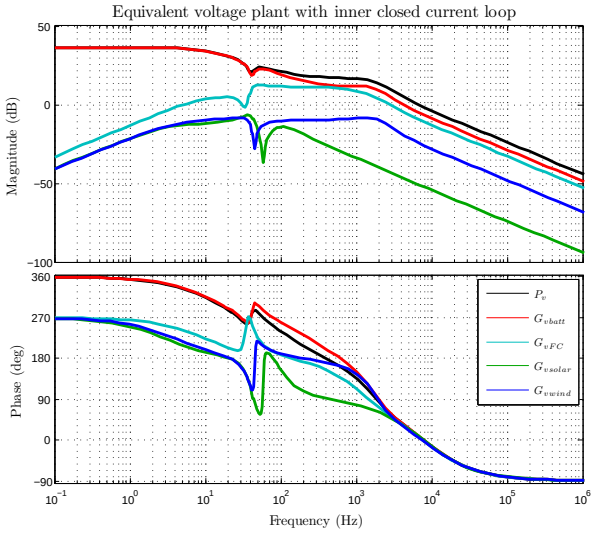

Figure 4.17. Frequency response of equivalent voltage control object and cross terms.

A classical PI controller is chosen for the voltage loop of MPEI, the cross-over is picked at lower frequency than single source case due to practical considerations of disturbance injection from other ports. The controller parameter is shown in Equation 4.17. As indicated in Figure 4.18, the cross-over frequency is picked up at $1.89Hz$, the gain margin of $48.8dB$ and phase margin of $81.3°$ are achieved.

$$C_v = \frac{0.025s + 10}{s} \tag{4.17}$$

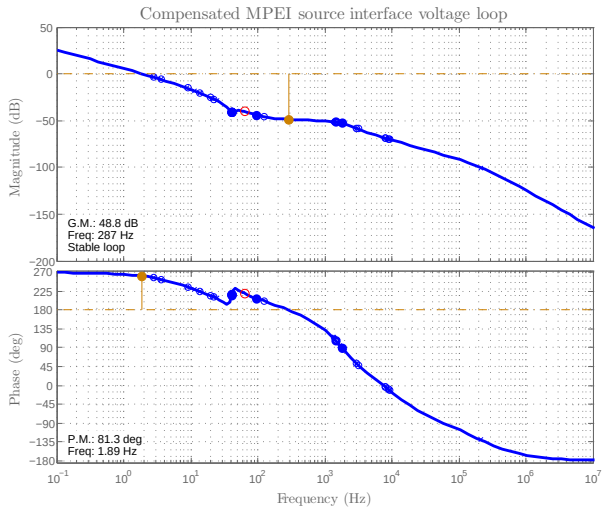

Figure 4.18. Compensated MPEI source interface voltage loop.

4.2 Local Power Management System

4.2.1 Photovoltaic and Wind Energy Harvesting

The power harvesting is realized by current control of photovoltaic and wind turbine interface. The maximum power point tracking technique is extensively studied during the past decades. Different micro-controller based methods [74][75] have been proposed, for example: Incremental Inductance method [76], analytical method[77], perturbation & observation method [78], hill-climbing method [79], open circuit voltage & short-circuit current method [80] and loss-free resistor method [81] etc. P&O method is chosen as the power tracking method in this paper due to its compatibility to existing control structure. Under the small step current perturbation, variation in power is acquired and compared with previous value, hence tracking of maximum power can be achieved. The detailed program flow is shown in Figure 4.19. To better understand the operation of power tracking, four typical operation points (point $1 \sim 4$) and power curve under full sun irradiation are used as in Figure 4.20.

At the beginning of the Maximum Power Point Tracking (MPPT) routine, current readings of solar cell current and voltage are retrieved, and output power are calculated as $P(n)$ to compared with previous value $P(n-1)$. In the case of power increase, there are two possibilities as indicated by Figure 4.20(a): on left hand side of power curve as $P_1 = P(n) > P(n-1) = P_3$ or on the right hand of power curve as $P_4 = P(n) > P(n-1) = P_2$. If solar cell voltage is increased with respect to the previous value, the variation of power is taking place on the left hand side of curve. Therefore, in order to pump more power from solar cell, the operating point has to be shifted to the right, which translates to a reduction of current in order to increase voltage. On the other hand, negative voltage variation indicates operating point on the right hand side of power curve, and the current reference has to be increased in order to decrease operation voltage. Similar method can be applied to the case of decrease in power output. If power output happens to be the same, which is indicated by the blue dashed line with intersection points P_1 and P_2 on the curve. Voltage information is also used to determine the relative location of two operating points; if V_1 is the current voltage reading, a decrease in current reference is desired to move the operating point toward peak power point, otherwise an increment of current reference should be applied.

Solar panel output presents a constant current source characteristics over a long operation range, the start of MPPT routine is preferred at the left hand side of $I-V$ curve; as indicated in Figure 4.20(b), the solar output voltage is more susceptible near the knee point of current curve: give the same step size of current, voltage variation will be more obvious and start of tracking will be more effective.

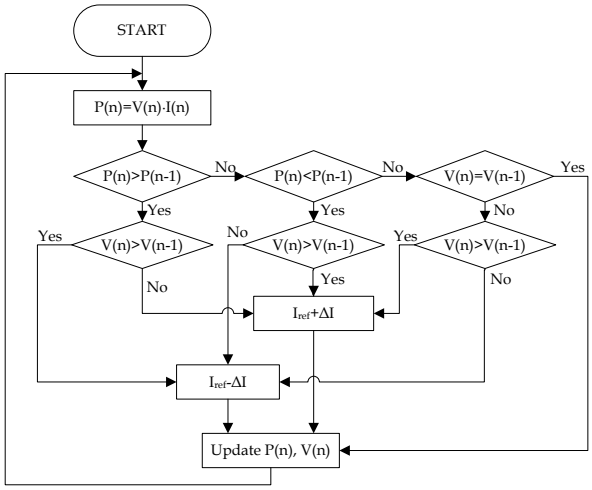

Figure 4.19. Perturbation and observation method for power tracking.

4.2.2 Power Flow Control

The polarization curve of fuel cell is provided in Figure 4.21; according to manufacture's specifications [47][48], the entire operation range is divided into three parts: light load region, normal load region and over load region. Fuel cell is more efficient and sustainable when operating in the normal load region. There are two ways to maintain the fuel cell operating point within the desired region. First approach is to apply proper amount of load to the system such that the power provided by the fuel cell is located in the normal load region on the polarization curve. The first approach is entirely load-dependent and nearly not applicable in a dynamic situation. The second approach is to properly control current of either fuel cell or secondary power source so that fuel cell operation point is forced or naturally falls into the normal load region on the polarization curve. Direct and indirect control of fuel cell current can achieve better system efficiency and longer life time of fuel cell.

With CQCS technique proposed in the dissertation, the operation point of fuel cell can be easily shifted by changing fuel cell output current (switching cell input current). For direct control, the control element L_x in fuel cell current control loop

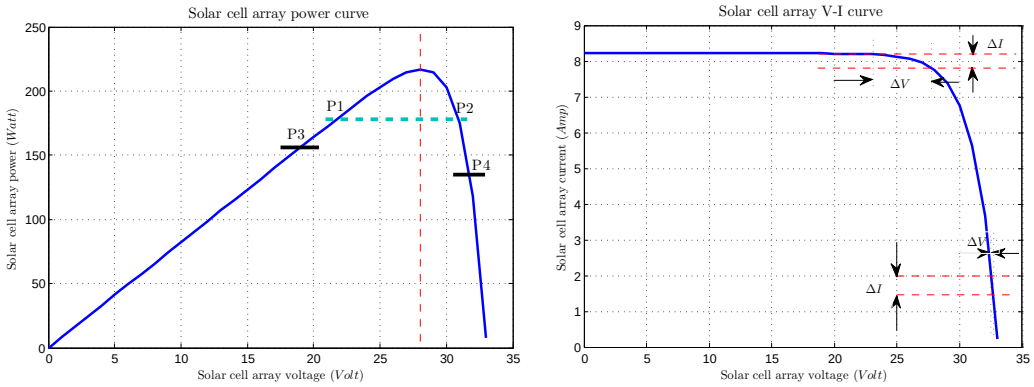

Figure 4.20. Solar cell array characteristics: (a) P-V curve, (b) I-V curve.

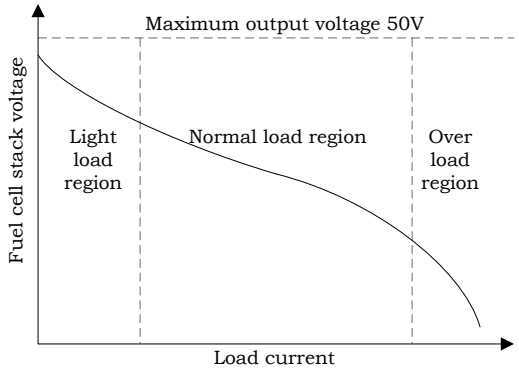

Figure 4.21. Polarization curve of PEM Fuel cell.

can be programmed such that fuel cell can work on desired power point; in the case of indirect control, fuel cell channel works under ACM control and the current reference is programmed for the rest of conversion channels, the fuel cell current is controlled indirectly.

The power flow is controlled by means of port variable regulation, given the power flow P_L on dc-link and ideal switching conversion, the power flow equation is expressed in (4.18). Optimal harvesting can be achieved by tracking the maximum power from solar and wind energy using P&O method. Since the power harvested

from solar and wind sources are known, power flow from fuel cell and battery can be managed by controlling the current drawn.

$$P_L = V_{PV} I_{PV} + V_{Wind} I_{Wind} + V_{FuelCell} I_{FuelCell} + V_{Batt} I_{Batt} \tag{4.18}$$

4.3 System Controller Design

The system controller is proposed and designed based on the modes of sustainable operation in section 2.3. The transition between operational modes and internal states are based on prescribed events. In the generation mode, the ambient power is harvested whenever available and sent to grid with limited support from battery; during the period of no ambient input ($P_{solar} + P_{wind} < P_{MIN}$), the battery will generate to grid given economical electricity price and sufficient SOC. Therefore, three events are dominating the generation mode: ambient resources, battery SOC and real time electricity price.

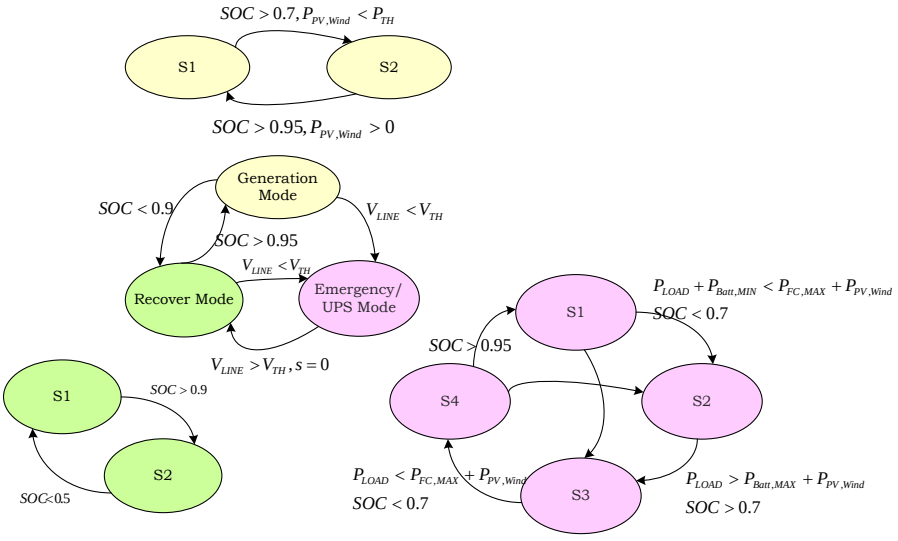

Figure 4.22. System state flow.

Emergency mode of operation is called upon the detection of line voltage collapse ($V_{line} > V_{TH}$).To start the emergency mode, battery is used as the primary source with ACM control, with solar and wind power providing the maximum power possible under current control, while fuel cell undergoes warm-up process during this state of operation. The system operation will transit to recover state ($S2$) if load demand is relieved ($P_L < P_{FC} + P_{wind} + P_{solar}$); fuel cell, solar and wind source are supplying the load and charging battery as well if SOC needs recovery. Power peak state is active when the load demand is higher than the summation of rated battery and ambient power ($P_{load} > P_{Batt} + P_{solar} + P_{wind}$), and battery SOC is higher than the threshold. To accommodate continuous demand from load side, energy storage can be exhausted ($SOC < 0.7$), and fuel cell and ambient source have to supply the load without the battery; in State S4, fuel cell inevitably takes over the load transient alone or shares with the ambient sources. The event for state transitions in emergency mode is illustrated in Figure 4.22 and one need to note that the states are bidirectional with counter trigger events, as listed in the figure.

The state transition in recovery mode depends on battery SOC. In heavy recovery mode ($SOC < 0.7$), all possible resources are used to charge the battery, however if battery state of charge is sufficient ($SOC > 0.9$), it is demanding and economical to use utility and fuel cell to recover the charge, while wind and solar are used to supplement the rest of the charge or float charge.

CHAPTER 5

HARDWARE IMPLEMENTATION AND EXPERIMENTAL RESULTS

5.1 Hardware Implementation

5.1.1 Power Stage Design

Three versions of power stages have been constructed in the design process. Initially the power stage is implemented entirely with wire and bus bar connection. Nevertheless, the parasitic inductance is relatively large and connection capacitance is difficult to predict. Thermal clad is a good choice for high power density design, and circuit parasitics can be minimized. Therefore, it is suitable for the finalized design. For design process with a number of iterations, the PCB version is favored due to controlled parasitics and easy assembly; the power stage is constructed on a bared trace PCB with via for heat dissipation and conduction trace is thickened properly by applying solder on the surface for high current. The PCB prototype is shown in Figure 5.1, with semiconductor switches vertically mounted and heat dissipated through the heat sink.

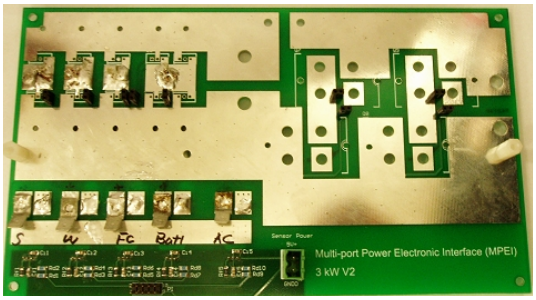

Figure 5.1. Power stage PCB.

For the phase-leg topology, non-isolated low cost driver is one of the most reliable and simple solutions. IR2210 is used in the bi-directional buck-boost switching cell and inverter phase legs, which can sustain up to 500V offset voltage in floating drive application and provide up to $2A$ of driving current. The experiment will be conducted with $42V$ battery pack and $100V \sim 120V$ dc-link voltage condition, therefore, IR2110 is sufficient in this case. Low impedance high current MIC4422 is used as low-side MOSFET drive for other three uni-directional boost cells. Figure 5.2 shows the PCB of the gate driver for six phase-legs in MPEI.

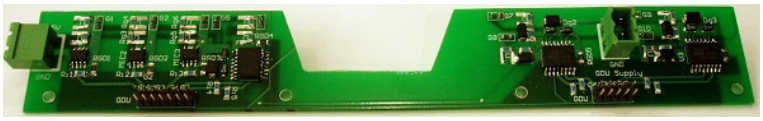

Figure 5.2. Gate driver PCB.

As a relative current intensive system, low voltage MOSFET is chosen to bring down the system cost; therefore voltage stress on the switching device must be taken care of. The parasitic inductance L_p (mainly trace inductance and MOSFET internal inductance) and capacitance C_p (mainly MOSFET/diode output capacitance and mounting capacitance) form a closed resonant loop and induce significant overshoot at switch turn-off instant with a very high resonant frequency. The ringing at the switching node can become destructive to switching device and strongly affect the adjacent sensitive electronic device (such as DSP controller used in the testbed) [82]. As indicated in Figure 5.3(a), the main switch for battery conversion channel has $146V$ as overshoot voltage and resonant frequency about $58MHz$. Due to the physical layout of the PCB board, the resonant peak for fuel cell switching cell MOSFET is $205V$ with resonant frequency about $63MHz$, which already exceeds maximum MOSFET drain-source voltage, as illustrated in Figure 5.3(b).

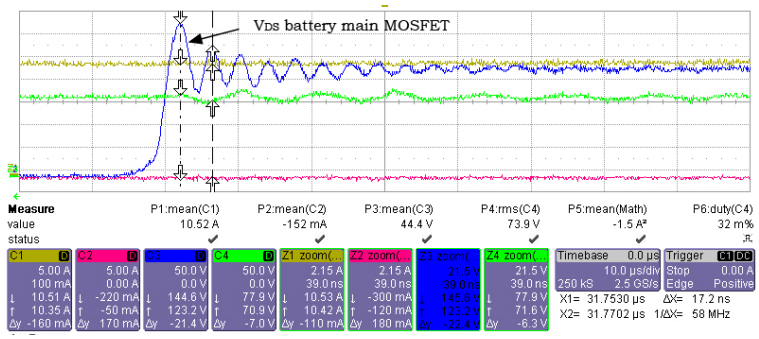

(a)

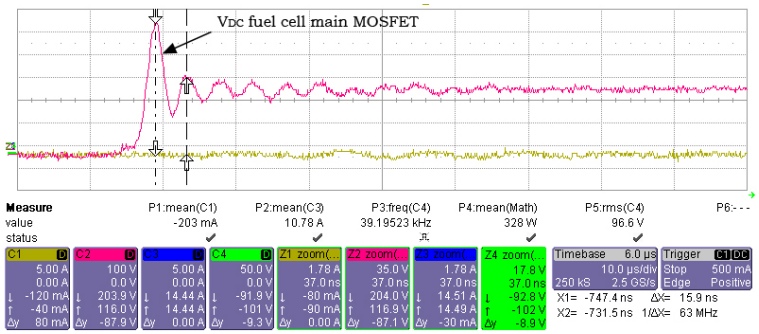

(b)

Figure 5.3. Voltage across drain and source of main switching MOSFET without snubber: (a) battery MOSFET, (b) fuel cell MOSFET.

RC snubber is selected to damping the overshoot for its simple implementation and low cost. The choice of snubber parameter is approached experimentally, which is described below.

- Parallel an external capacitor C_{EX} between MOSFET drain and source, still the resonant frequency has been damped to half of the original measured value according to Equation (5.1) $C_{EX} = 3C_p$
- Calculate parasitic inductance value with Equation (5.1); add the resistor R_{EX} in series with C_{EX}; select the resistance value close to characteristic impedance value of original circuit referring to Equation (5.2).

- Calculate the power consumption of the resistor with Equation (5.3) and select the component with correct power rating, where f_{sw} is the switching frequency and V_{DC} is the dc-link voltage.

$$f_r = \frac{1}{2\pi\sqrt{L_p \cdot C_p}} = 2 \cdot \frac{1}{2\pi\sqrt{L_p \cdot (C_{EX} + C_p)}} \tag{5.1}$$

$$R_{EX} = \sqrt{\frac{L_p}{C_p}} \tag{5.2}$$

$$P_{loss} = f_{sw} C_{EX} V_{DC}^2 \tag{5.3}$$

Figure 5.4. RC snubber implementation.

Snubber capacitor is chosen as $4700pF$ to provide a significant damping in oscillation frequency and 5Ω, $1W$ resistor is selected to provide damping to voltage overshoot. A low-profile circuit implementation is shown in Figure 5.4. The drain-source voltage of MOSFET with snubber is shown in Figure 5.5(a) for battery switching cell, as indicated in the figure, the oscillation frequency has been reduced and overshoot voltage is suppressed from $146V$ to $114V$ peak. The fuel cell switching node resonant peak voltage has been reduced from $205V$ to $122V$. In the mean time, the switch-off transient is not affected by snubber circuit, no switch-off delay is observed in Figure 5.5 comparing with the voltage rise time in Figure 5.3.

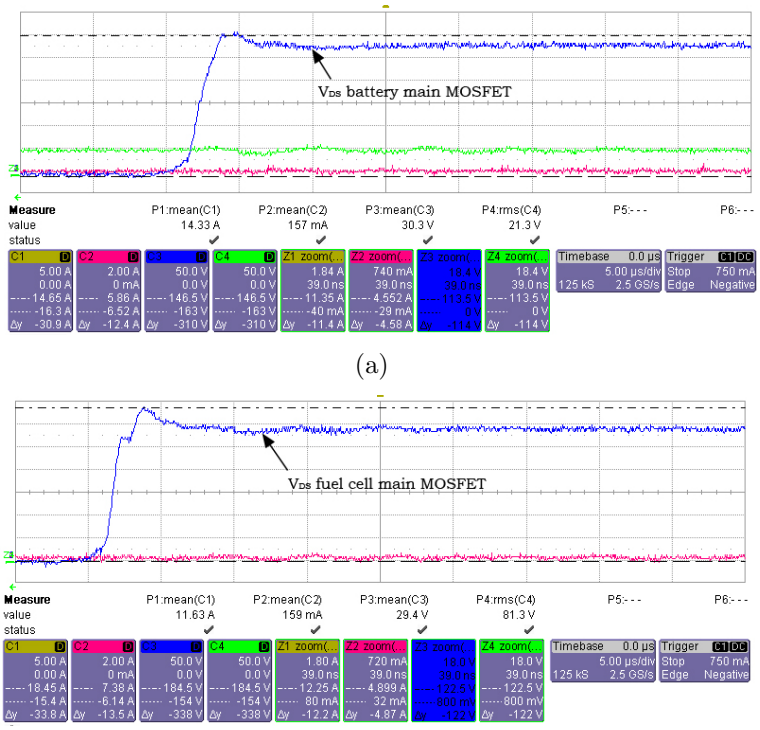

Figure 5.5. Voltage across drain and source of main switching MOSFET with snubber: (a) battery MOSFET, (b) fuel cell MOSFET.

5.1.2 Sensor and Conditioning Circuit

Open loop hall-effect sensor is chosen for current sensing due to low cost, compactness and low mounting-profile. Automotive grade high bandwidth current sensor ACS756 from Allegro MicroSystems [83] is selected as MPEI current sensor. Calibration is done to evaluated the static performance of the sensor, which is plotted in Figure 5.6. The Volt-to-Amp function can be easily obtained with line fitting method. The I-V function for 50A and 100A rated sensor are expressed in Equation 5.4 and 5.5. The PCB prototype for current sensing circuit is presented in Figure 5.7.

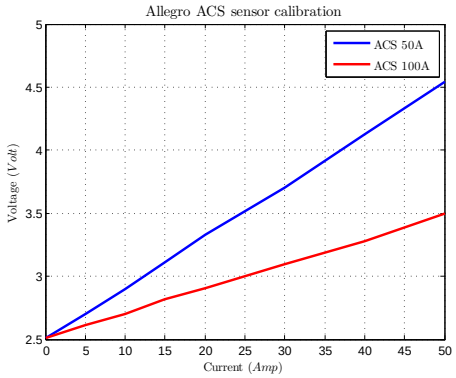

Figure 5.6. Current sensor calibration.

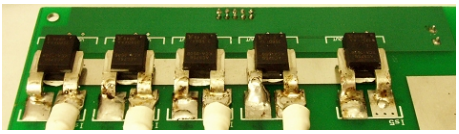

Figure 5.7. Current sensor PCB.

$$V_{50A} = 0.0407 \cdot I_{50A} + 2.5008 \tag{5.4}$$

$$V_{100A} = 0.0195 \cdot I_{100A} + 2.5135 \tag{5.5}$$

Hall-effect voltage transducer LV-20P from LEM [84] is used to sense dc-link and port voltages. For dc port and dc-link sensing, the sampling resistor is used directly with zener diode protection as indicated in Figure 5.8. Since ADC of DSP does not take negative voltages, ac signal must be conditioned before being sampled by ADC. Figure 5.9 and 5.10 show the voltage transducer board and signal conditioning circuit respectively; and single chip quad-op amp LF347 is used for conditioning purposes.

The sampled ac voltage signal from voltage transducer board is first fed into a buffer stage and inversely compressed in the second stage to half the amplitude; the third stage inverses the signal and provides a $1.5V$ dc voltage biasing for proper ADC reading; the fourth stage is a second order active filter for noise suppression.

The signal conditioning PCB is shown in Figure 5.11, which can offer conditioning for five channel of signals.

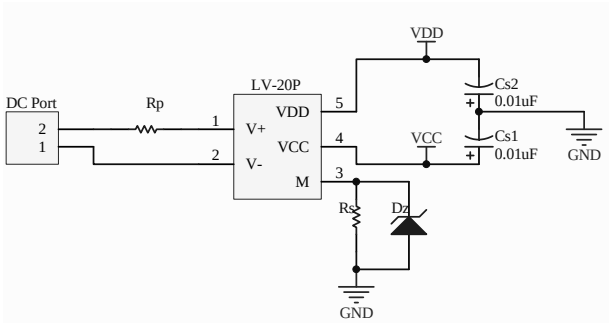

Figure 5.8. Voltage sensing schematics.

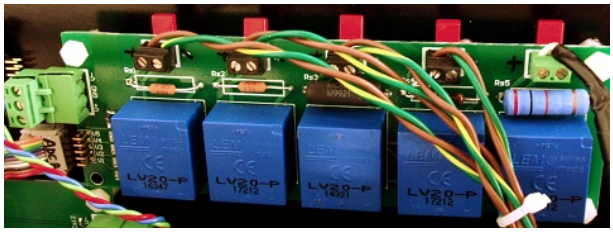

Figure 5.9. Voltage sensor PCB.

5.1.3 DSP Interface

TMS320F2812 DSP is used as the core processor in MPEI. System resources are allocated for different tasks: system timing, switching and sampling. A docking interface is created to group the DSP I/O for MPEI operation. The interface designed for DSP docking offers external power supply input, on-board voltage regulation, PWM outputs, ADC input, LCD I/O and system peripheral outputs/inputs. A finished interface board with DSP connected is presented in Figure 5.12.

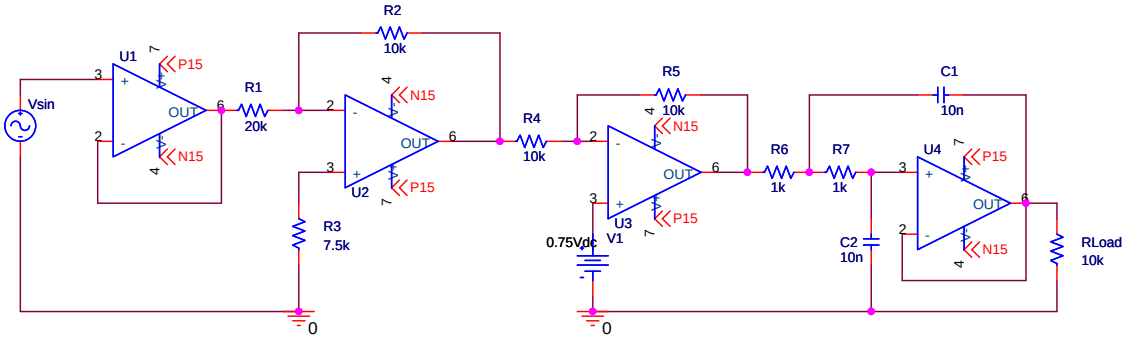

Figure 5.10. Voltage signal conditioning circuit.

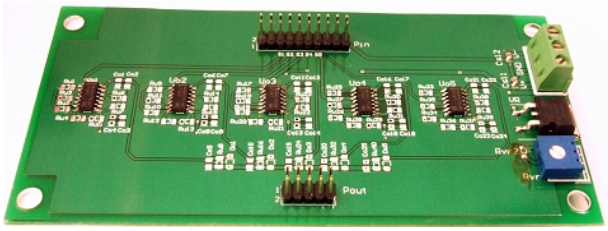

Figure 5.11. Signal conditioning PCB.

5.2 Experimental Results

5.2.1 Maximum Solar and Wind Power Harvesting

Maximum power point tracking for solar panel is implemented in the DSP, the current loop cut-off frequency is placed at $1.07kHz$ for a fast response. The maximum power tracking function is called very $20ms$ to offer several decades of separation in time constants. The initial experimental results is shown in Figure 5.13(a), a low frequency oscillation around $6.6Hz$ is reflected in the experimental waveform, which apparently does not relate to the current loop resonant frequency or circuit parameters. However, under direct current control, $120Hz$ ripple is found at terminal voltage of solar panel output; considering the fact that only the most recent sampled voltage value before MPPT routine is used for power point calculation, misplacement of sampling instants might have some influence on current reference decision. Also by observing the current loop performance in time domain, a overshot over 10% is

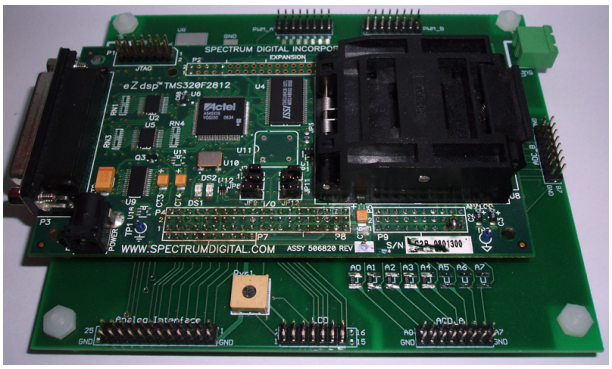

Figure 5.12. DSP docking interface.

found in step response as illustrated in Figure 5.13(b), which is normally tolerable in battery and fuel cell control loop; however, solar panel presents constant current source chacteristics in a wide load region and the terminal voltage will be subjected to large variation if overshoot of current exists. Based on the facts mentioned, several modifications are proposed:

- Synchronize MPPT function call time to inverter fundamental frequency to minimize voltage and current disturbances caused by inverter operation.
- Modify current controllers for lower overshot.
- Reduce the current step command to further reduce the current overshoot.
- Limit duty cycle slew rate for smoother current loop response.

The current control loop is redesigned in Figure 5.14 for lower overshoot. The modified bandwidth of current controller is set at $651Hz$ for a significant reduction of system overshoot as shown in Figure 5.14(b). The results with improvement is presented in Figure 5.15(a) and 5.15(b) at two different time of the day, which offers stable maximum power point tracking and reduced oscillation.

Test in Figure 5.15(a) and 5.15(b) are conducted under single switching cell plus inverter configuration, and the output voltage is not controllable in this configuration since only input current is regulated. This configuration is not desirable in MPEI

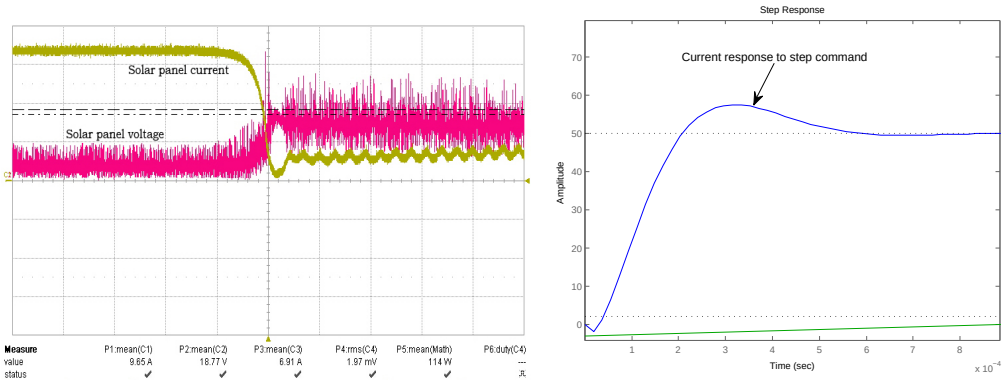

(a) (b)

Figure 5.13. Solar power tracking: (a) tracking with low frequency fluctuation, (b) step response.

operation since dc-link voltage is subjected to unpredictable fluctuation. Under the frame of operation modes as proposed in section 2.3, solar power harvesting operation can take place in two configurations:

- Deliver maximum power while working parallel with other switching cells.
- Deliver maximum power to energy storage alone.

The first option can be implemented with direct current control of solar/wind switching cell, while other paralleled switching cell(s) can be operated with ACM control; the input power variation due to MPPT process and load transients will be handled by ACM controlled switching cells; the control structure in Figure 5.16(a) can be well applied to this MPPT+load sharing process. The second option is more difficult for maximum power transfer since the power extracted from solar panel does not guarantee to be consumed by battery if charging current reference is not adjusted in time; imbalanced power flow will either induce voltage surge or drop on dc-link capacitor, rendering poor performance or semiconductor over-voltage failure. To accommodate this special scenario, a control structure is proposed in this dissertation and applied to synchronously switched cells, which is presented in Figure 5.16(b)

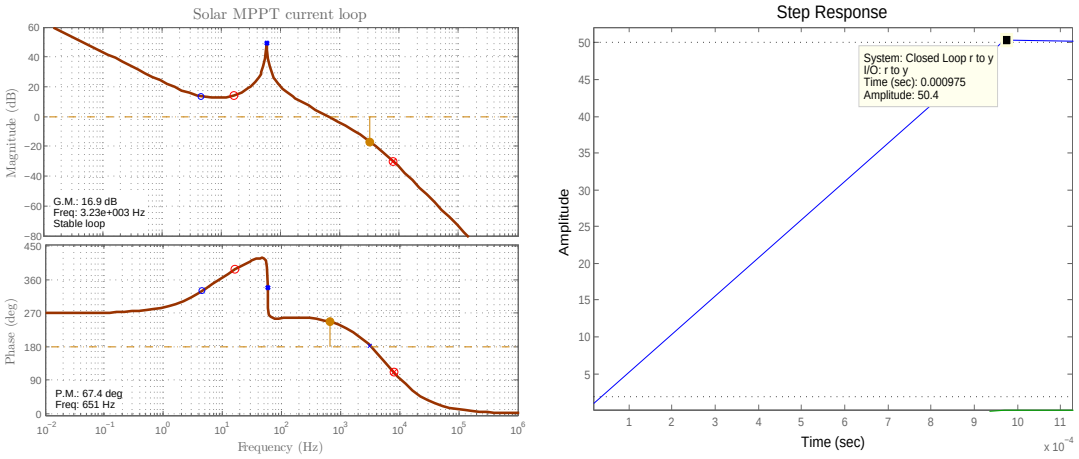

(a) (b)

Figure 5.14. Modified current control loop: (a) solar current loop design, (b) step response.

as Current Mode Maximum Power Transfer (CMMPT) method. To avoid power imbalance issue, the control structure offers a direct link between output and input power. As illustrated in the figure, the charging current is sensed and compared with the current reference generated by solar MPPT routine; charging current error is amplified by current controller $C_1(s)$ and fed into current controller $C_2(s)$ as an internal reference, hereinafter, forming a current-mode control loop. The boost and buck cells are switched synchronously to make sure power flow is balanced at two sides of dc-link capacitor, furthermore large signal and small signal stability can be achieved for intermediate dc-link voltage.

Figure 5.17 shows the experimental results for MPT of solar power to the load/storage, where CH1 (yellow, 2A/div) is solar panel current, CH2 (red, 5A/div) is battery current, CH3 (blue, 20V/div) is solar panel voltage and CH4 (green, 50V/div) is ac output voltage in 5.17(a) and dc-link voltage in 5.17(b). Figure 5.17(a) demonstrates the steady state of load share operation when solar switching cell is under MPPT current control and battery switching cell is under ACM control. CMMPT is

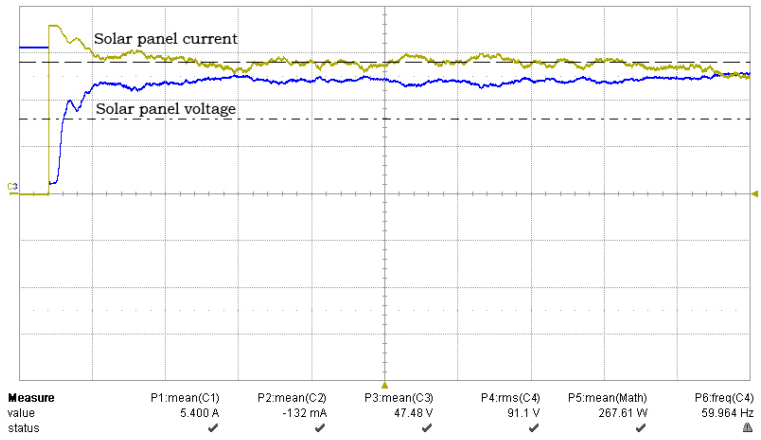

(a)

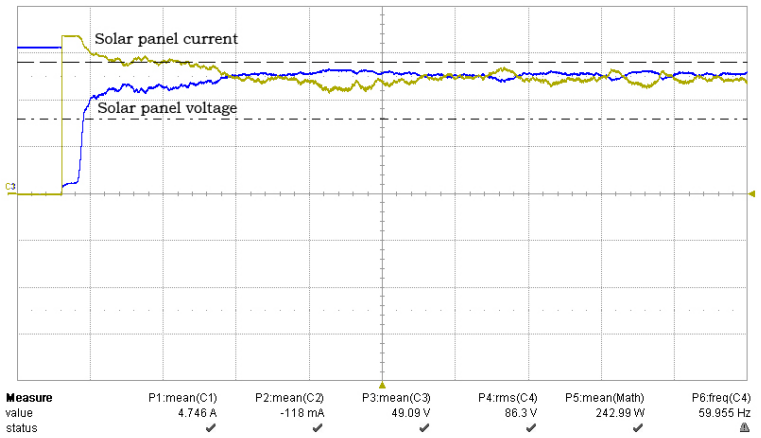

(b)

Figure 5.15. Solar maximum power tracking (20V/div, 2A/div): (a) solar power output at 2:30PM, (b) solar power output at 3:00PM.

implemented in the scenario that no load/generation demand comes from ac side and solar cell transfers the maximum power to energy storage. As illustrated in Figure 5.17(b), at two close time instants of the day (11:00AM) with very close sun irradiation intensity, two configuration successfully deliver very close amount of power to down-stream converters ($239W$ and $235W$ respectively).

MPPT for wind energy channel adopts the similar P&O technique with slight modifications. Since wind turbine output current is not the monofonic function of turbine voltage, there is no one-to-one decision on current reference variation by only

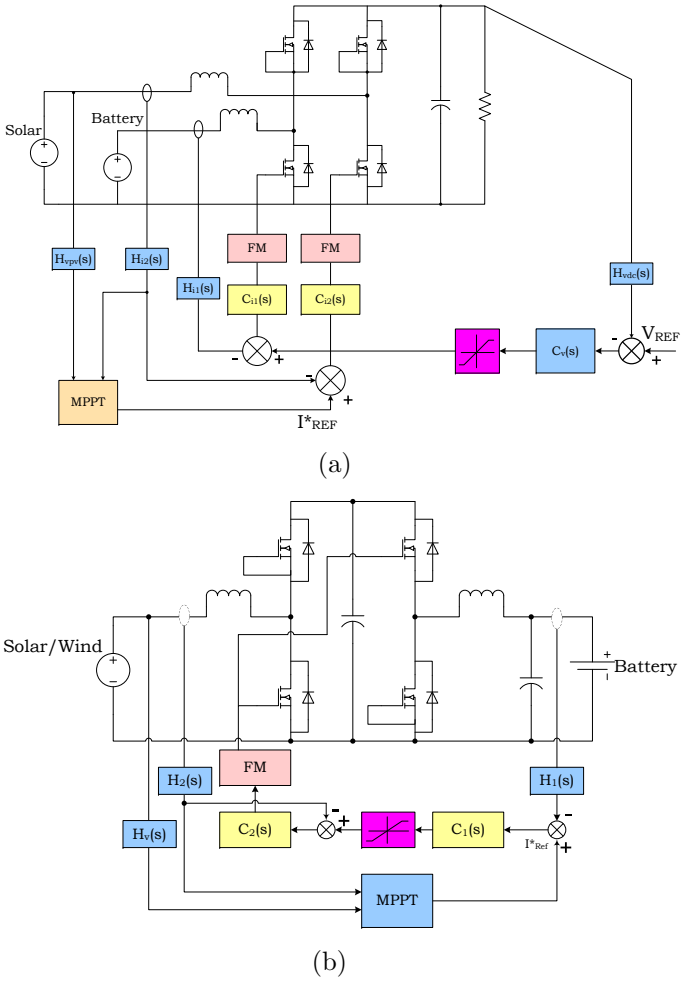

Figure 5.16. Solar/Wind maximum power transfer control schemes: (a) load share method, (b) Current Mode Maximum Power Transfer method.

inspecting power input and terminal voltage. As indicated in Figure 5.18, the $I-V$ curve shares the similar shape as $I-P$ curve, though with shifted peak values; the peak current current point will shift to the left of maximum power point as the wind speed decreases. In addition to MPPT routine used in solar energy conversion, the slope of $I-V$ curve will be taken into consideration when the operating point is located on the left side of the power curve. Figure 5.19 exhibits the tracking of both solar and wind power at steady state.

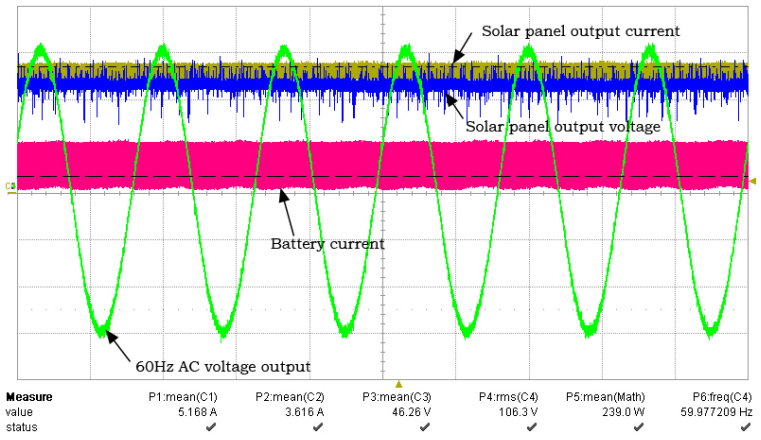

(a)

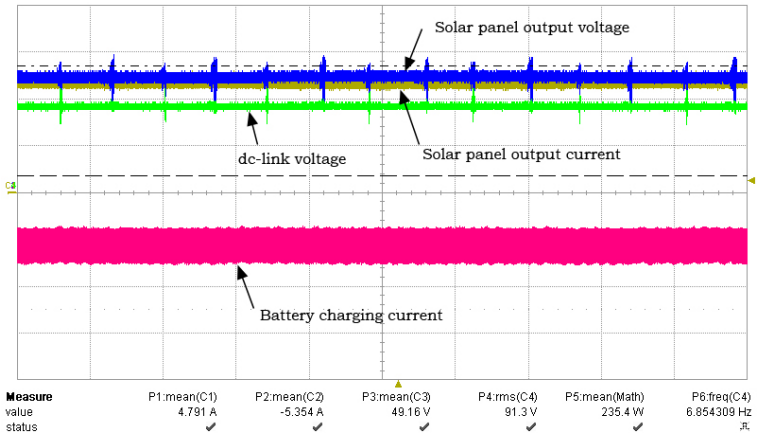

(b)

Figure 5.17. Solar maximum power transfer tests: (a) MPT by load share, (b) MPT by CMMPT control.

5.2.2 Active Current Ripple Mitigation for Fuel Cell

The effort of control loop design is demonstrated with fuel cell as the only source in MPEI. As elaborated in section 4.1.3, current and voltage control loops have been carefully designed in order to mitigate the $120Hz$ ripple propagated from inverter side; Figure 4.10 and 4.15 indicated more than half a decade separation from $120Hz$ for fuel cell current and voltage loop. The inductor input current under fixed duty cycle modulation is shown in Figure 5.20(a); the $120Hz$ ripple drawn from fuel cell is obvious under open loop operation. With proposed current and voltage controller

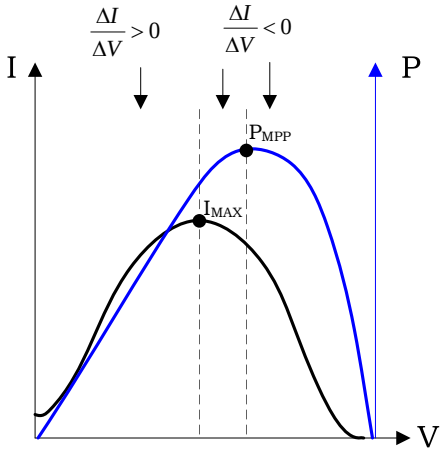

Figure 5.18. Wind turbine I-V and I-P curve.

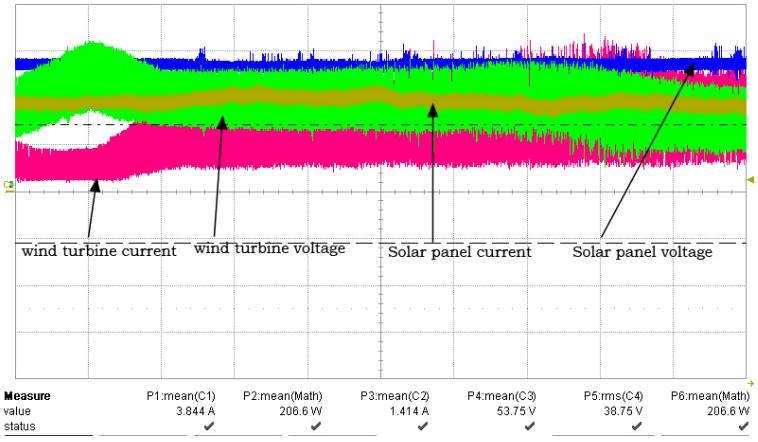

Figure 5.19. Maximum power tracking of solar and wind sources.

in section 4.1.3, the steady state output voltage and input current waveforms are obtained in Figure 5.20(b); amplitude reduction of $120Hz$ current ripple envelop is observed, but small amount of low frequency ripple still exists.

A further reduction of voltage control bandwidth is implemented by pushing voltage loop cross-over frequency down to $1.89Hz$ using the controller designed for MPEI voltage loop. Compared with previous controller design, the attenuation for $120Hz$ components is increased from $-30dB$ to $-50dB$; the improved phase and gain margin are $82.5°$ and $54.6dB$ respectively, as indicated in Figure 5.21(a). The

experimental results in Figure 5.21(b) indicate that under the modified controller, the $120Hz$ current ripple is further reduced to very low level and the methodology of controller loop tuning is effective.

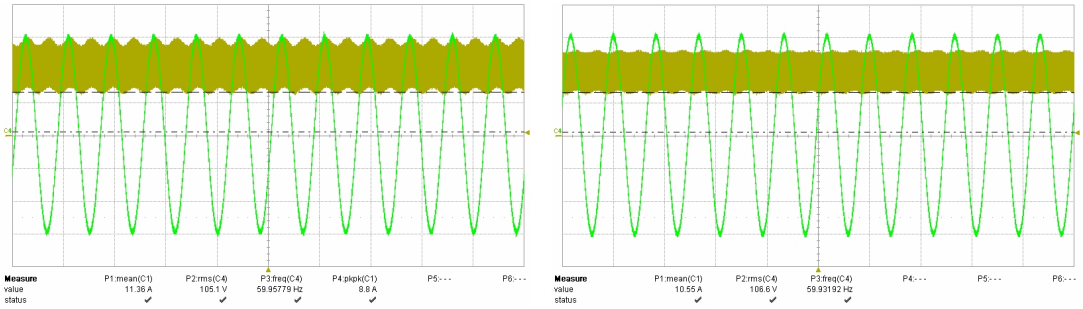

(a) (b)

Figure 5.20. Fuel cell current ripple mitigation (50V/div, 5A/div): (a) switching cell with open loop, (b) switching cell with ACM control, cross-over frequency $\omega_c = 5.41Hz$.

5.2.3 Dynamic and Steady State Test in UPS Mode

In emergency/UPS mode of operation, MPEI harvests the ambient resources as much as possible; thereupon solar and wind switching cells are working under perturbed current control. Fuel cell and battery work as the main sources in the system. As defined in section 2.3, if line voltage collapse is detected, MPEI goes into UPS mode of operation. Figure 5.22(a) presents the four-state-transition in UPS mode. In State I (first segment on the left), battery kicks in as the only source in the system, during this period, fuel cell is in start-up state and not involved in power generation. In State II, fuel cell chamber is warmed up to proper temperature for reaction, MPEI is able to provide power peaking for end-customer; the second segment on the left in Figure 5.22(a) indicates the power peaking state of operation in which fuel cell and battery provide an equal amount of current for the load. In

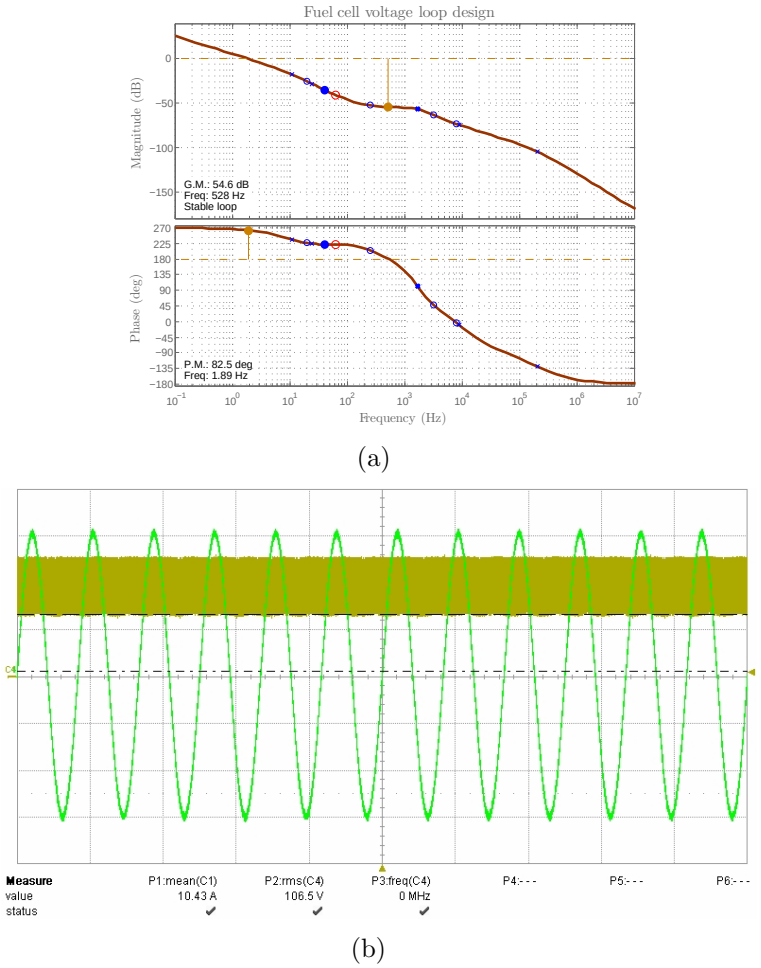

Figure 5.21. Improved current ripple mitigation: (a) refined fuel cell voltage loop with cross-over frequency $\omega_c = 1.89Hz$, (b) further reduced current ripple (50V/div, 5A/div).

even current sharing operation, since the programmed current reference is the same for each inner current loop, fuel cell and battery current controller will track the same current command with different speed. The battery SOC will gradually drop as the loading processing continues, at certain threshold SOC, system goes into State III for battery charge recovery: fuel cell supplies the load as well as charges the battery. However, if the load demand is still stringent during low battery SOC, only fuel cell

will supply the load as indicated in the first segment on the right in Figure 5.22(a). Figure 5.22(b)-5.22(d) shows the transients between different states.

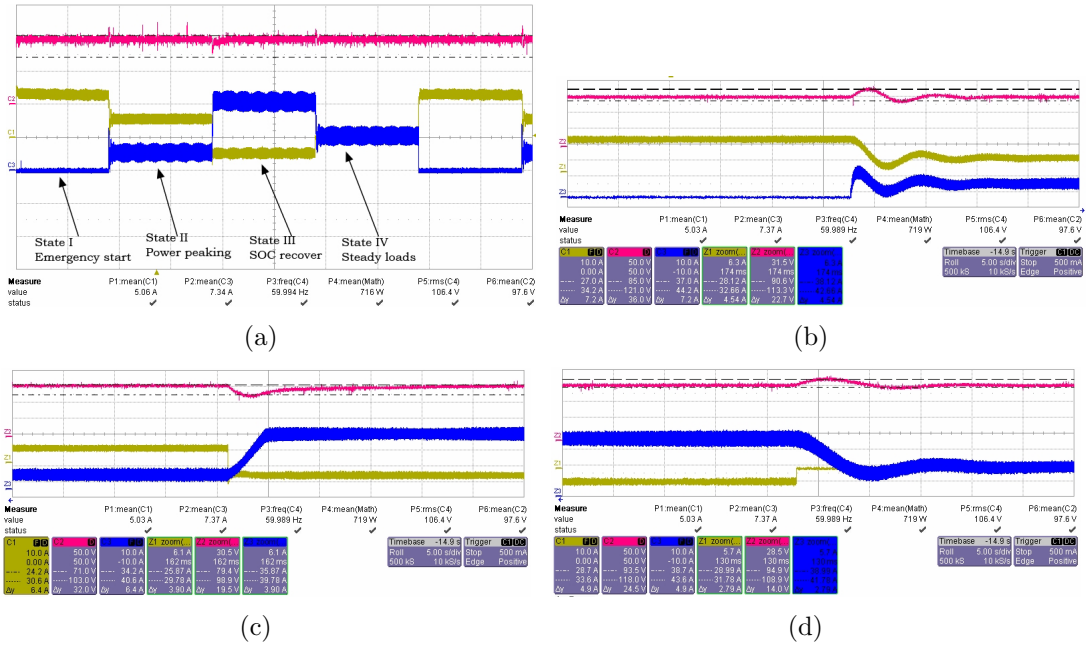

Figure 5.22. Emergency mode of operation (CH1 yellow: battery current; CH2 red: dc-link voltage; CH3 blue: fuel cell current): (a) four modes operation, (b) battery supply to load share transient, (c) load share to battery charging transient, (d) battery charging to fuel cell supply.

Loop response is tested with a dynamic load under dual and triple port supply. Figure 5.23 shows the current drawn from solar panel (red) and battery (yellow); as indicated, since solar channel is under direct current control, the pulse load ($300W$) has negligible effect on MPPT operation on solar source, and most load dynamics are taken by battery control loop(s). Figure 5.24 is the step load test with solar panel, wind turbine, and battery in load sharing mode, in which solar and wind source are under direct current control and battery is under ACM control. As expected, the battery provides the step of current during the step load dynamics and solar and

wind channel current is not effected by the load change due to direct current control.

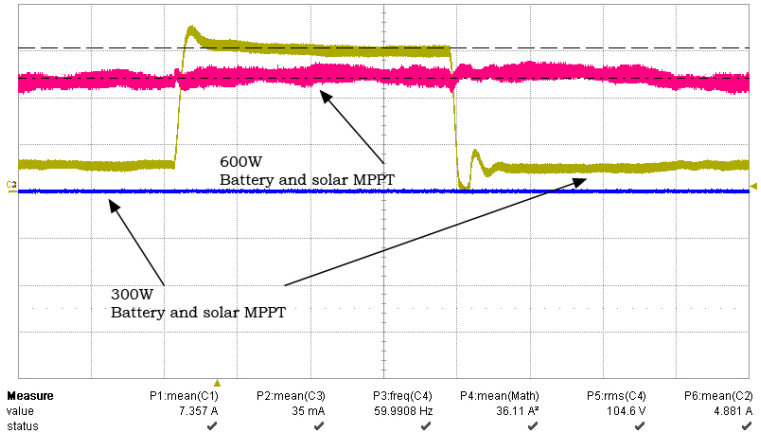

Figure 5.23. Pulse load test with solar and battery power sharing.

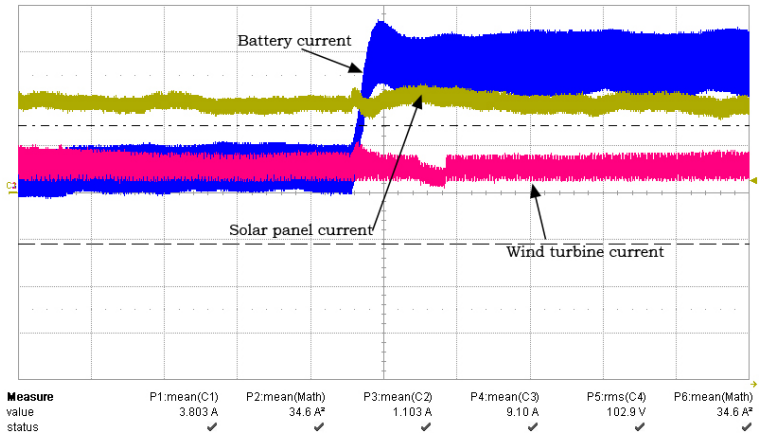

Figure 5.24. Step load test with solar, wind turbine and battery power sharing.

MPPT in solar/wind energy harvesting provides a boundary condition on optimal energy harvesting, therefore, power dispatching problem is reduced to proper allocation of power drawn from two sources: battery and fuel cell. As explained in section 4.1.2 and 4.2.2, better fuel cell efficiency and protection of battery can be

achieved by proper management current drawn from each source. This can be implemented by adjusting the control vector $\vec{\boldsymbol{L}}$ based on Equation (4.2) and (4.3). Figure 5.25 indicates the steady state load sharing with the same and different current programmed reference. The change of control vector is triggered on a timely basis, as shown in Figure 5.25, the control vector for battery and fuel cell current is configured as $[\frac{1}{3}, 1]$, $[1, 1]$, $[1, \frac{1}{2}]$, $[\frac{1}{2}, 1]$ respectively for the segment from left to right in the figure. By modifying the control vector, the current drawn from each source can be precisely controlled for power dispatching and efficiency optimization purposes.

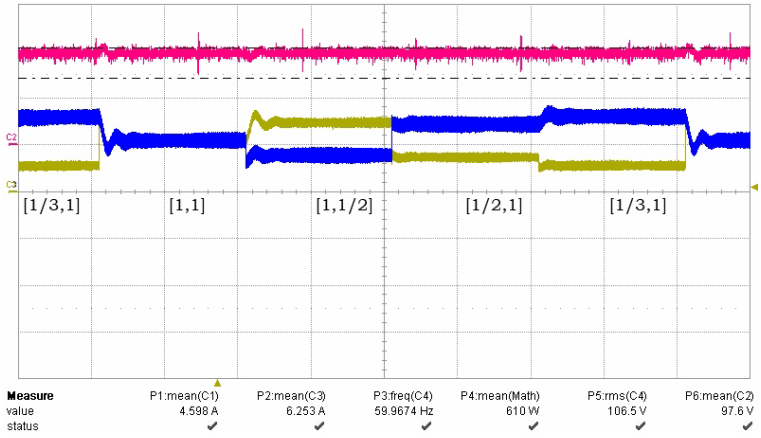

Figure 5.25. Steady state power peaking state with different current share.

Pulse load is also applied to the system with CQCS controlled current loop. Figure 5.26 presents the current in fuel cell and battery under pulse load test. Current loop response is shown in Figure 5.26(a) under even current share; as can be observed, both current loops track the same profile which is given by the outer voltage controller and share the same load dynamics.

For better protection of fuel cell system and relief the stress on membrane, load dynamics would prefer being decoupled or at least reduced on fuel cell channel. However, in case of large load demand with only fuel cell and battery available, fuel

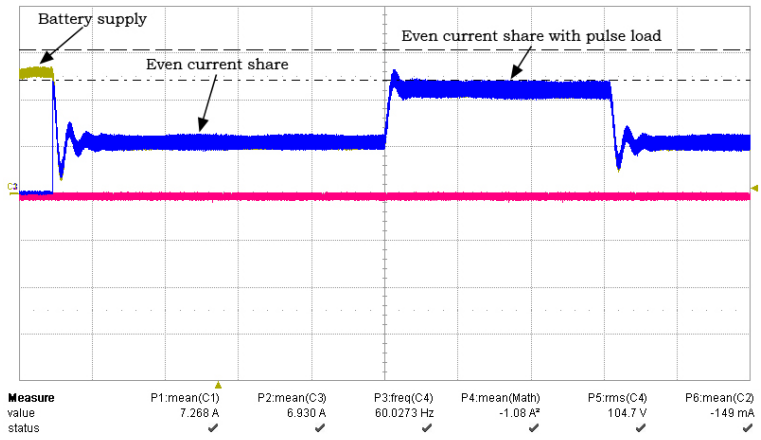

(a)

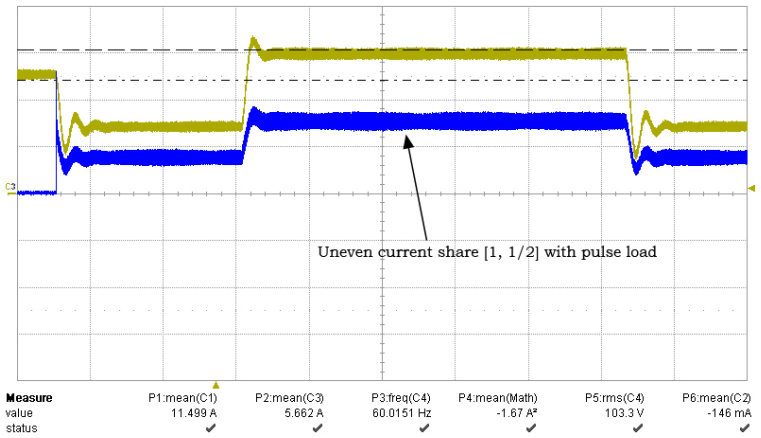

(b)

Figure 5.26. Pulse load response of current sharing operation: (a) even current sharing, (b) uneven current sharing.

cell must be engaged into dynamic current sharing. Based on SOC of battery and state of fuel cell, different portion of current can be programmed for inner current loops; Figure 5.26(b) shows the fuel cell and battery current response in presence of pulsed load. As indicated in the figure, control vector $[1, \frac{1}{2}]$ is configured for battery and fuel cell current loop respectively, which indicates a share of $\frac{1}{3}$ load dynamics by fuel cell channel. Similarly, the CQCS method can also be applied to the battery channel if battery SOC and State of Health (SOH) are not at desirable levels.

The design effort of inner current loop can be observed from rise time of each current under step current command. Figure 5.27(a) and 5.27(b) show the fuel cell and battery current loop response to an increment and decrement of current reference. The rise time of the current ($5A$ to $10A$) is found as $350\mu s$ and $500\mu s$ respectively for battery and fuel cell current loop. The out voltage loop response to step input voltage is shown in Figure 5.28. As indicated in the figure, the start up of MPEI with single battery source requires $500ms$ for dc-link voltage to reach steady state.

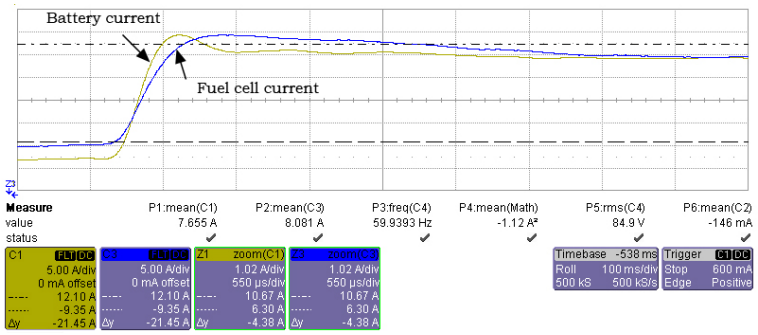

(a)

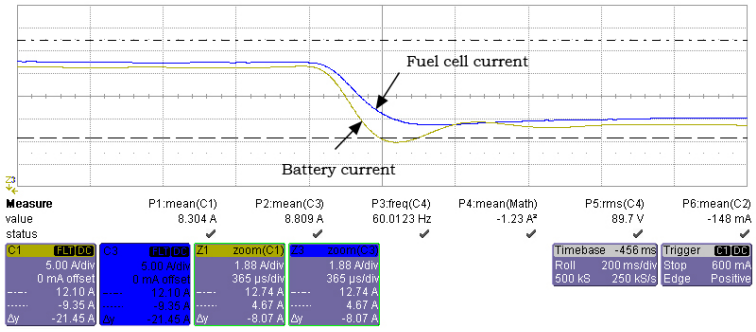

(b)

Figure 5.27. Inner current loop test: (a) with step-up current reference, (b) with step-down current reference.

Figure 5.29 shows the steady state power peaking operation with solar, wind and battery sources involved.

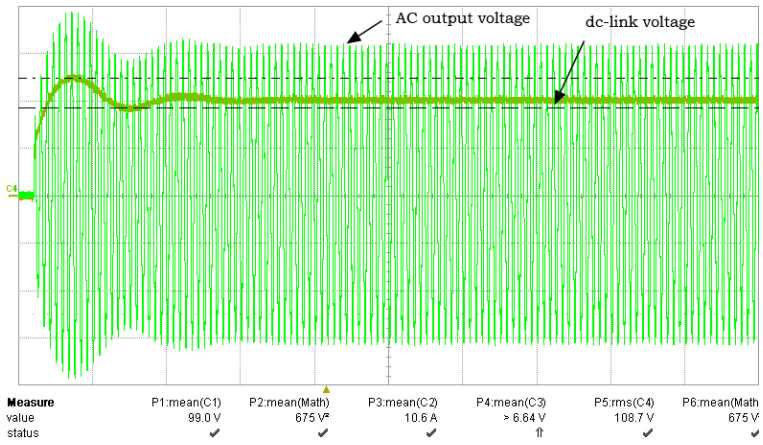

Figure 5.28. DC-link and ac output voltage transient with step input.

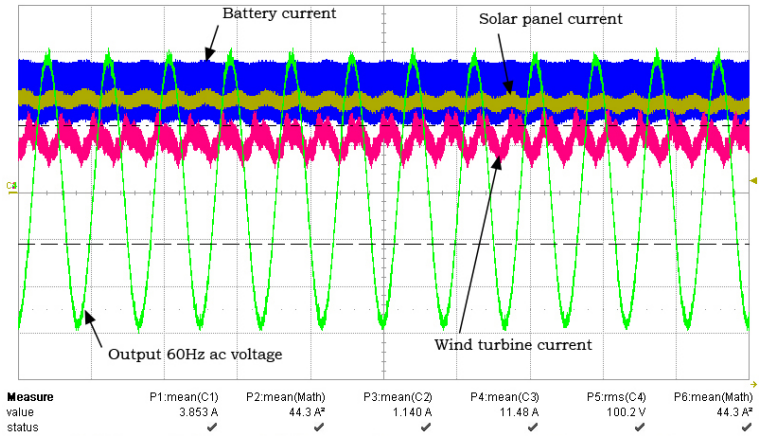

Figure 5.29. Steady state operation of three different sources.

5.2.4 Recovery Mode

Different sources are involved in recovery mode operation. In case of low battery SOC, all possible sources can be used to recover the charge of battery; however, economical operation naturally limits the usage of fuel cell and utility power. The priority of different usable sources from high to low is given as: solar/wind, utility grid, fuel cell.

The maximum power transfer from solar to battery pack has been studied and verified in Figure 5.17(b). Power transfer from fuel cell to battery is verified in the

four-state transition study in section 5.2.3 Figure 5.22(a). If no solar or wind power available, utility grid is the source of battery charge recovery; Figure 5.30 indicates the scenario of uncontrolled off-line battery charging, as indicated in the figure, during uncontrolled rectification (diode rectifier without power factor correction), off-line charge has poor power factor and injects abundant harmonics into the utility grid.

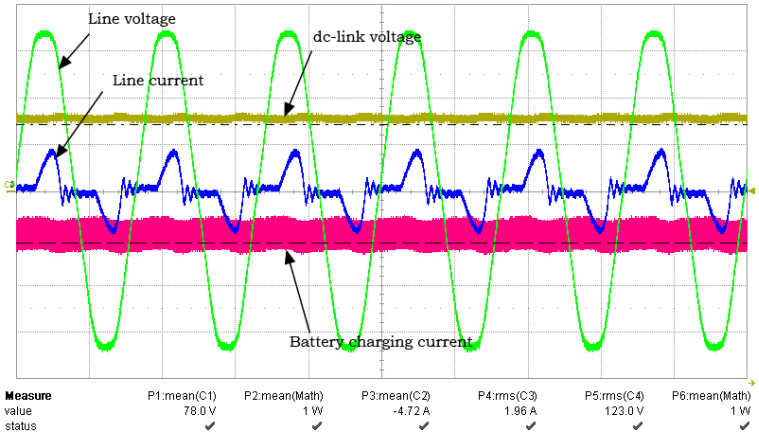

Figure 5.30. Off-line charging without power factor correction.

5.2.5 Generation Mode

As significant part of power dispatch and generation, generation mode of MPEI shed light into active line interaction for future smart grid. Different options are made based on the availability of renewable sources and real-time electricity prices. Figure 5.31 illustrates the configuration for grid-tie operation; since the dc-link is stabilized by the front-end converter, the inverter can be controlled independently. The output of inverter is connected to a L-C-L filter and to grid via an isolation step-up transformer. During the operation, the inverter is under current control to track the synchronous signal from grid. A dump load is used to match the output voltage to line voltage before grid-tie.

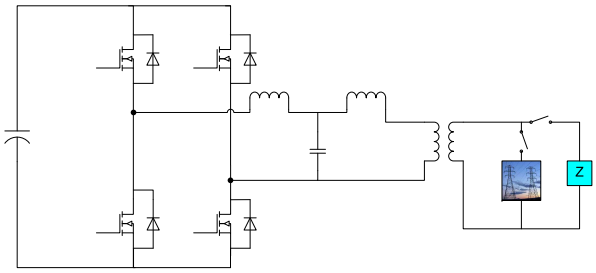

Figure 5.31. Grid-tie mode configuration.

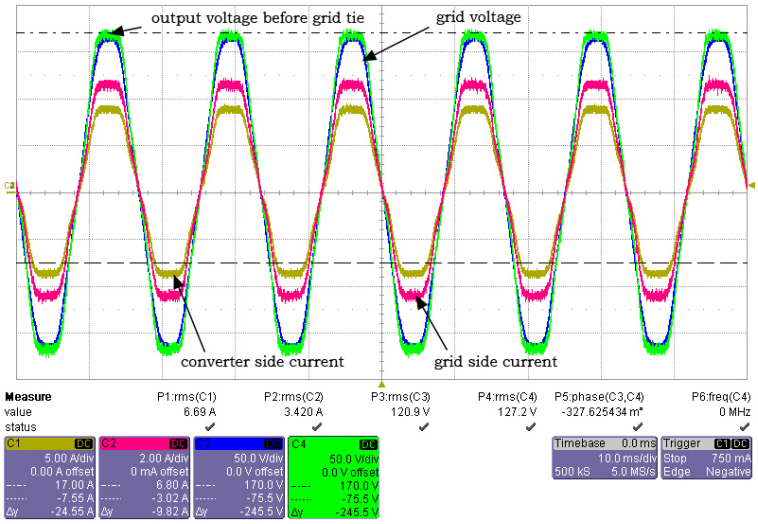

Figure 5.32. Terminal voltage with dump load before grid-tie.

Figure 5.32 shows the ac interface output terminal voltage before grid-tie operation, the phase error controlled under 1° to minimized the inrush current during the grid-tie transient. Figure 5.33 is the waveform on ac interface during the grid-tie and dc interface to the battery. As indicated in the figure, the battery is generating 461W active power to the utility; stabilized dc-link voltage and $120Hz$ ripple-free battery current are indicated in Figure 5.33(b).

Multi-source generation offers more advantages than conventional single source generation. As the solar converter is under current control with periodically perturbed current reference, any additional perturbation introduced by the load would

deteriorate the performance of MPPT; in fact such additional perturbation does exists as mentioned in [78], which is $120Hz$ oscillation introduced by inverter operation. In the case of multi-source configuration, interactions in one-source generation scenario can be compensated by the second/other conversion channel, which adopts the control structure proposed in Figure 5.16(a). Figure 5.34(a) shows the co-generation with solar and battery source. As indicated in the figure, solar power conversion is under direct current control and maximum power point is tracked during the entire generation process, and the battery channel is under ACM control to supply the rest of power and handle possible dynamics.

Fuel cell will be incorporated in grid-tie generation in case of higher real-time price than generation cost. The relative independence between source interface and load interface and enables power sharing between different sources without affecting grid-tie generation. Figure 5.34(b) is the experimental result of grid-tie co-generation between fuel cell and battery; the source current is programmed by control vector such that fuel cell and battery share $8A$ and $6.28A$ of current respectively.

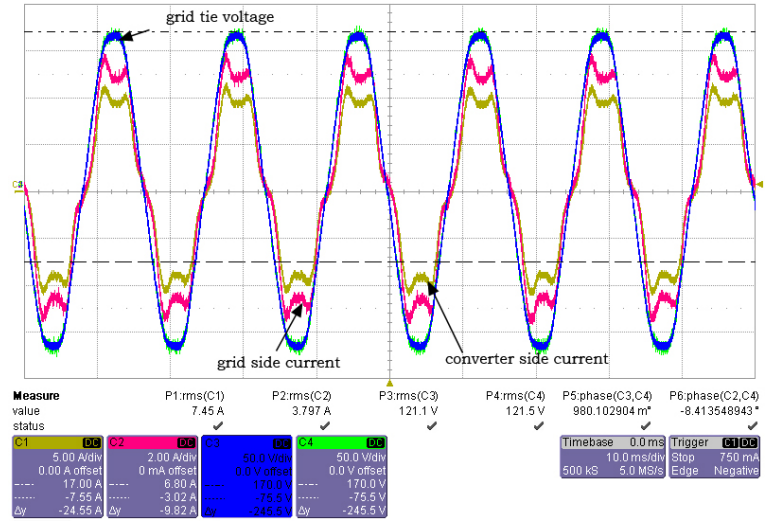

(a)

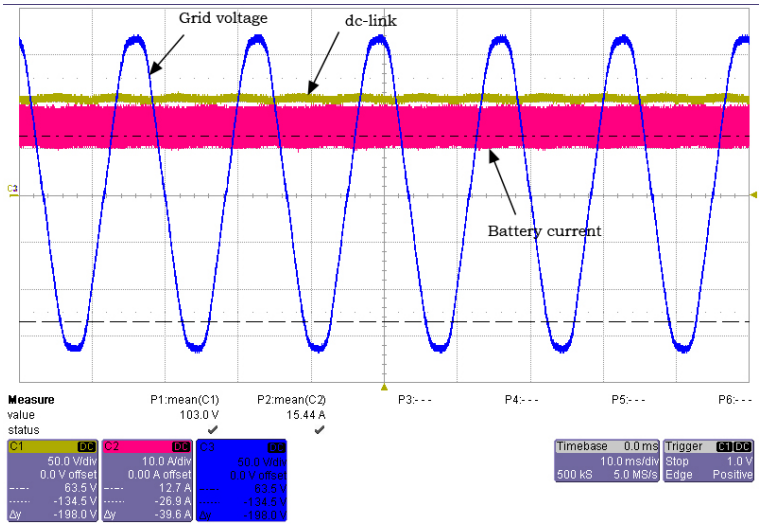

(b)

Figure 5.33. Grid-tie with battery: (a) ac side waveforms, (b) dc side waveforms.

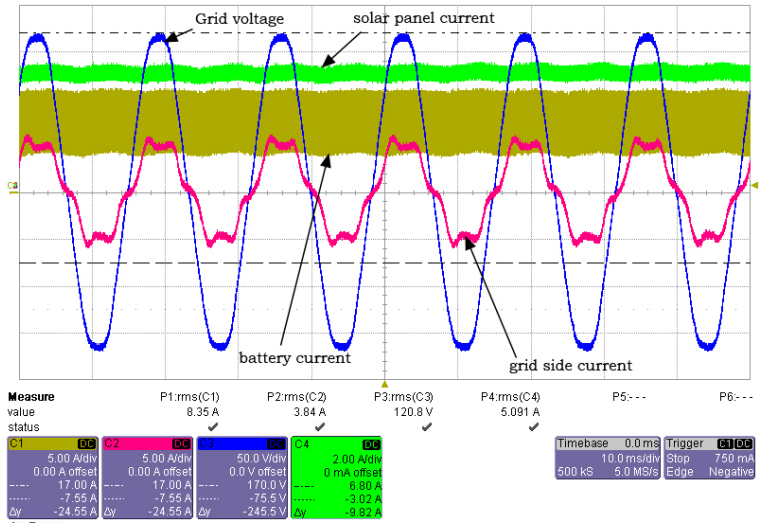

(a)

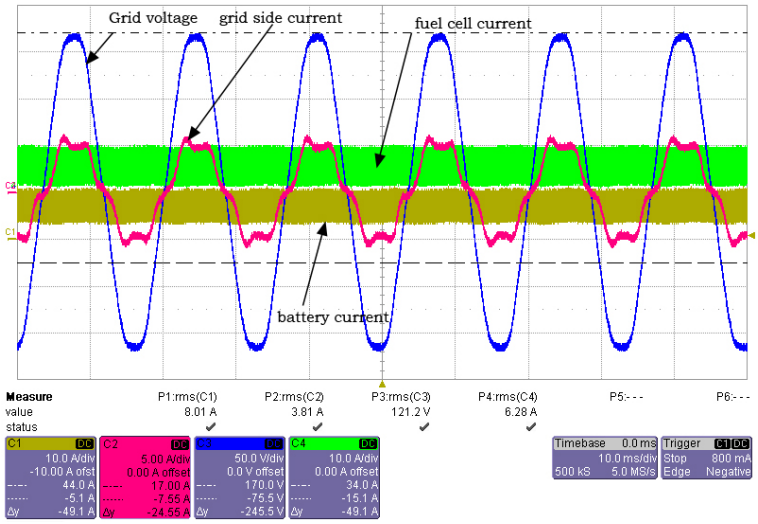

(b)

Figure 5.34. Grid-tie co-generation: (a) solar and battery, (b) fuel cell and battery.

CHAPTER 6

CONCLUSIONS AND FUTURE WORK

6.1 Conclusion

Localized power harvesting, generation and distribution offer an potential solution to future smart grid system. Incorporating different renewable sources and storages in such local stationary and motional power systems has become a definite trend due to increasing electricity power demand. To provide a better understanding of multiple source system and a generic solution to the existing hybrid power system, the concept of Multi-port Power Electronic Interface (MPEI) is proposed in this dissertation and a six-phase-leg topology is adopted as the object of study. Detailed system level as well as small signal level analysis are conducted for better profiling the dynamics of such a system. Novel control structures are proposed for MPEI in different scenarios to achieve:

- Integrated control structure.
- Power/current sharing in source interface for better efficiency.
- Load transient/dynamics sharing in source interface to protect power source.
- Integration of P&O routine with battery charging algorithm for more efficient solar power transfer.

Different modes of operation are defined for system sustainability, the transition of which are based on pre-defined events for present research. The proposed system are tested with hardware prototype; control system and pre-programmed modes of operation are implemented in a single digital signal processor. The critical modes of operation are tested and demonstrated.

6.2 Future Work

MPEI is proposed as an intelligent power and information exchange interface rather than a complicated power converter system. Agenda on future research will be focused on expansion of the functionality of MPEI toward future power grid and vehicular power systems, which involves the following research objectives:

- Versatile energy conversion and communication interface, as shown in Figure 6.1.
  - To develop more general interface type for renewable sources, such as ac wind turbine/motor and ultra-capacitor.
  - To develop generic grid interface: split single phase and three phase systems; offer active/reactive power generation and active load balancing [1] capability.
  - To integrate power electronic interface of fuel reforming and electrolysis functions.
  - To develop communication and human-machine interface.
- System design improvement
  - To develop event-driven control system for better local power management.
  - To develop advanced data processing system for economical generation and trading.
  - To evaluate and implement super-node integration of MPEI for microgrid.
- Low cost implementation for H2G application, as illustrated in Figure 6.2
- MPEI on a chip (MPEIOC)[2] for portable electronics and communication power applications.

[1] See Appendix C.1

[2] See Appendix D.1

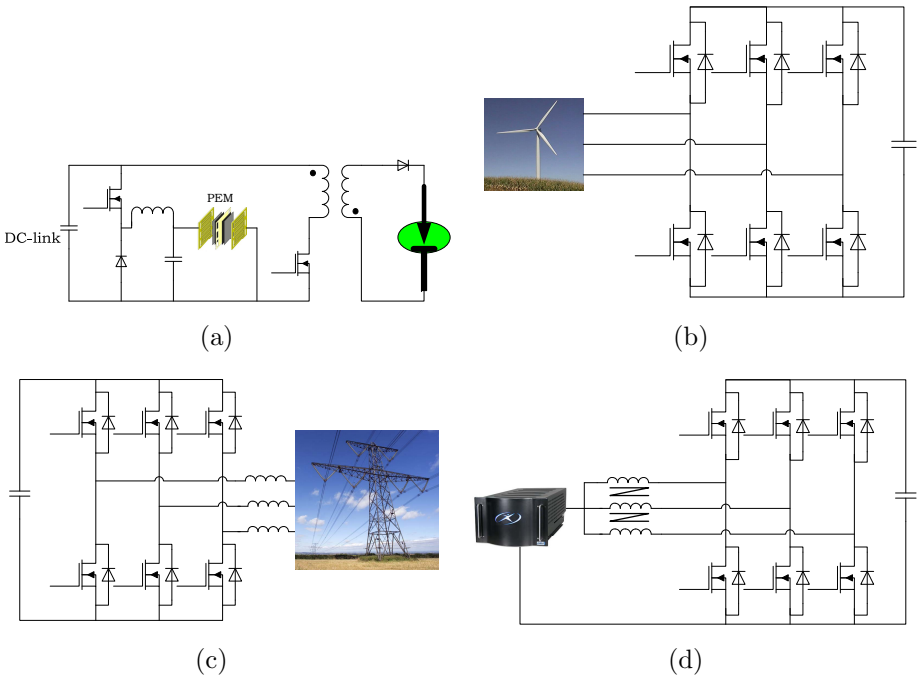

Figure 6.1. MPEI function expansion: (a) reformer and electrolyzer, (b) multi-phase turbine or motor, (c) generic grid interface, (d) multi-phase converter.

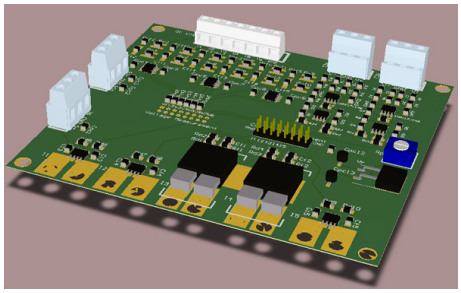

Figure 6.2. Low cost sensor & conditioning board.

APPENDIX A

MPEI TESTBED

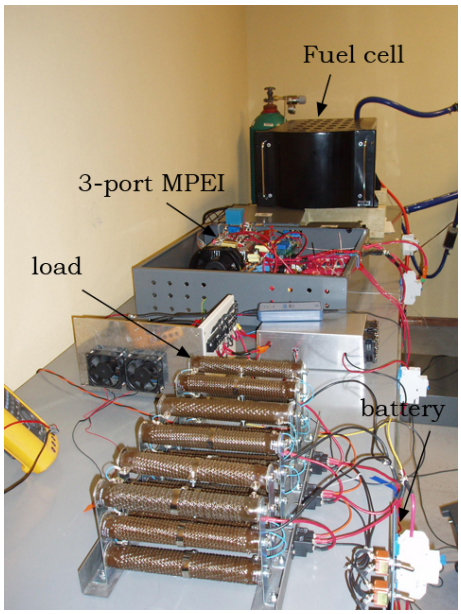

Figure A.1. Three-port MPEI testbed.

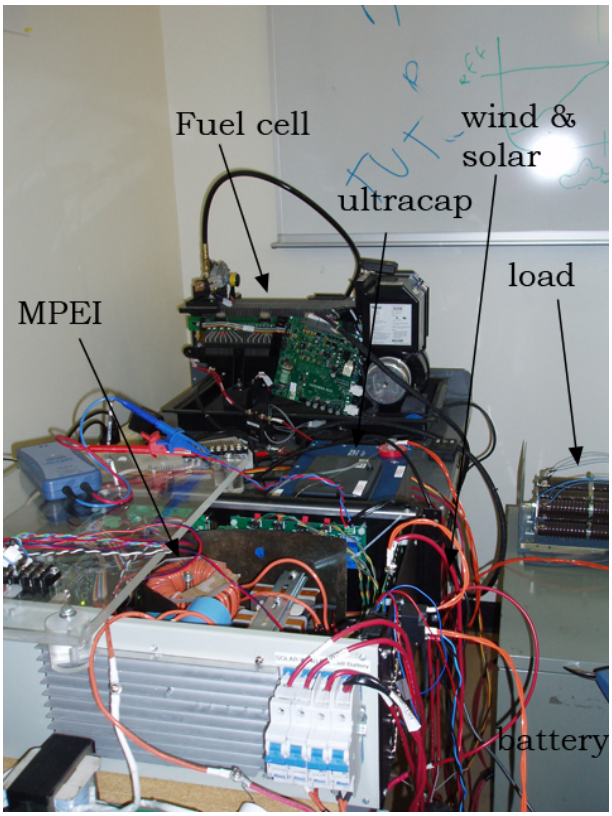

Figure A.2. Five-port MPEI testbed.

APPENDIX B

SCHEMATICS FOR SYSTEM COMPONENT

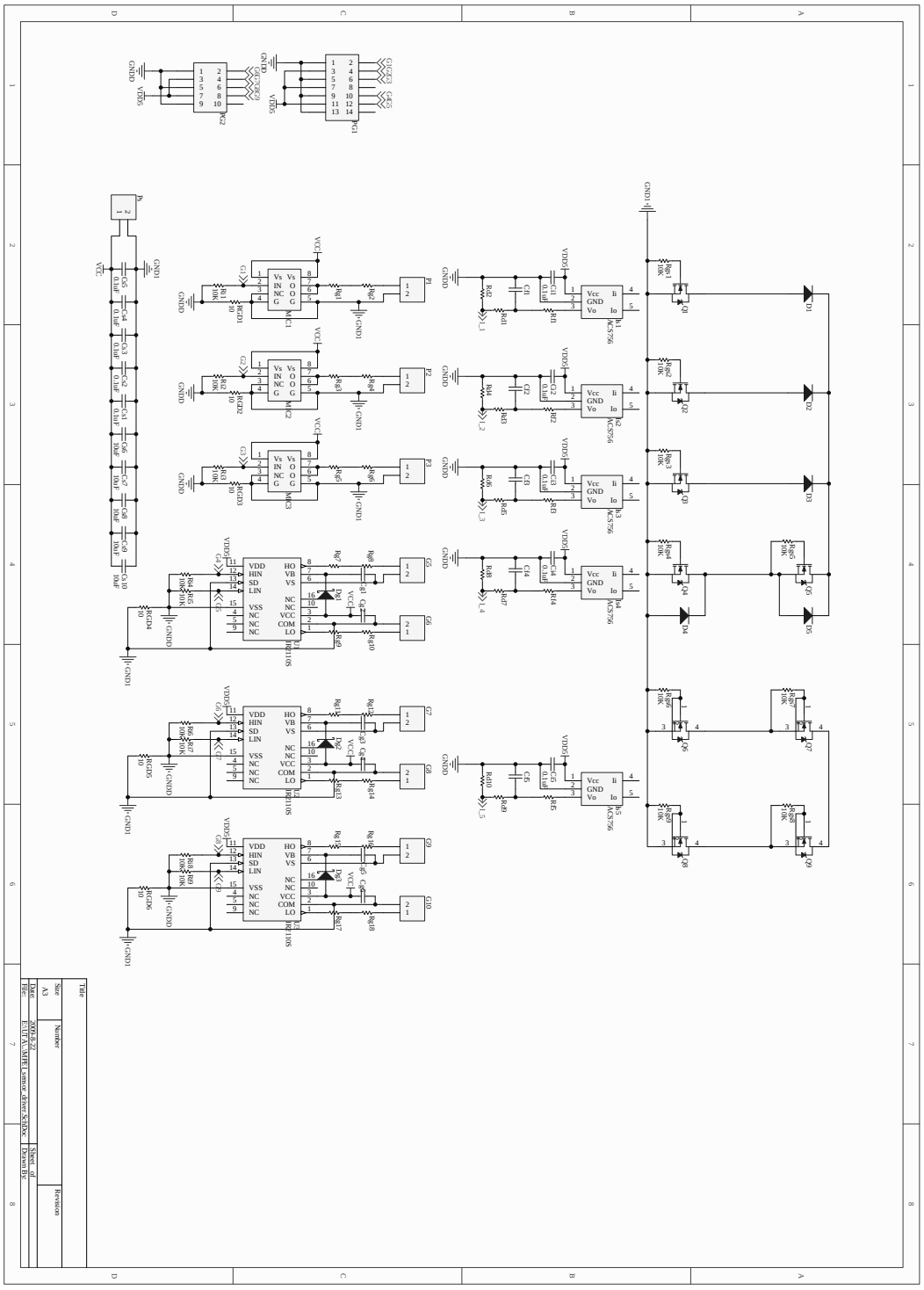

Figure B.1. Five-port MPEI with integrated current sensor and MOSFET driver.

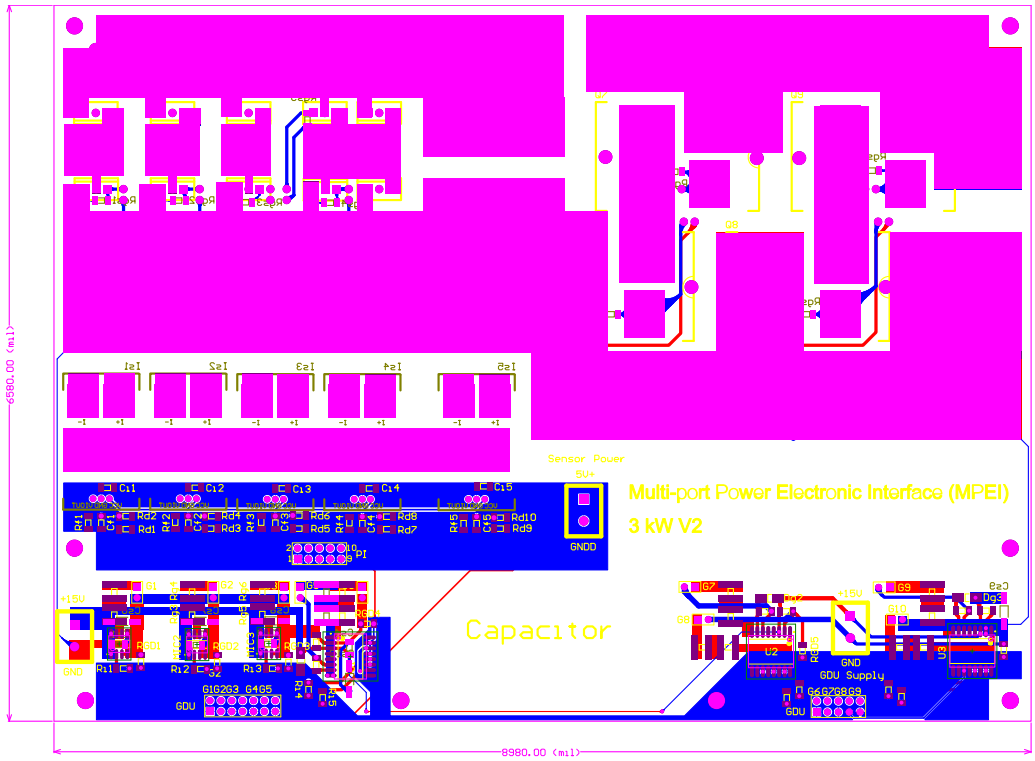

Figure B.2. Five-port MPEI power stage CAM file.

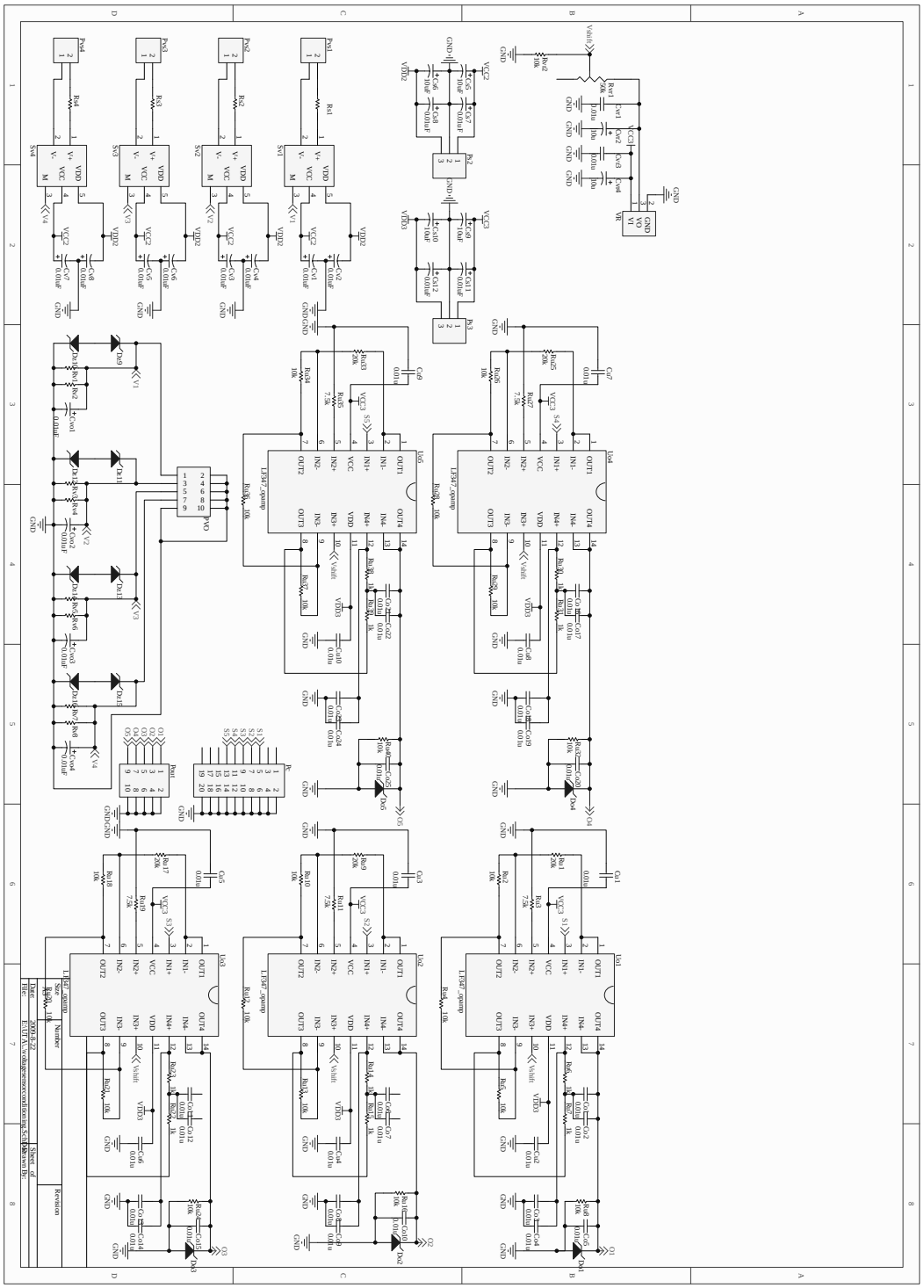

Figure B.3. Voltage sensing and conditioning circuit.

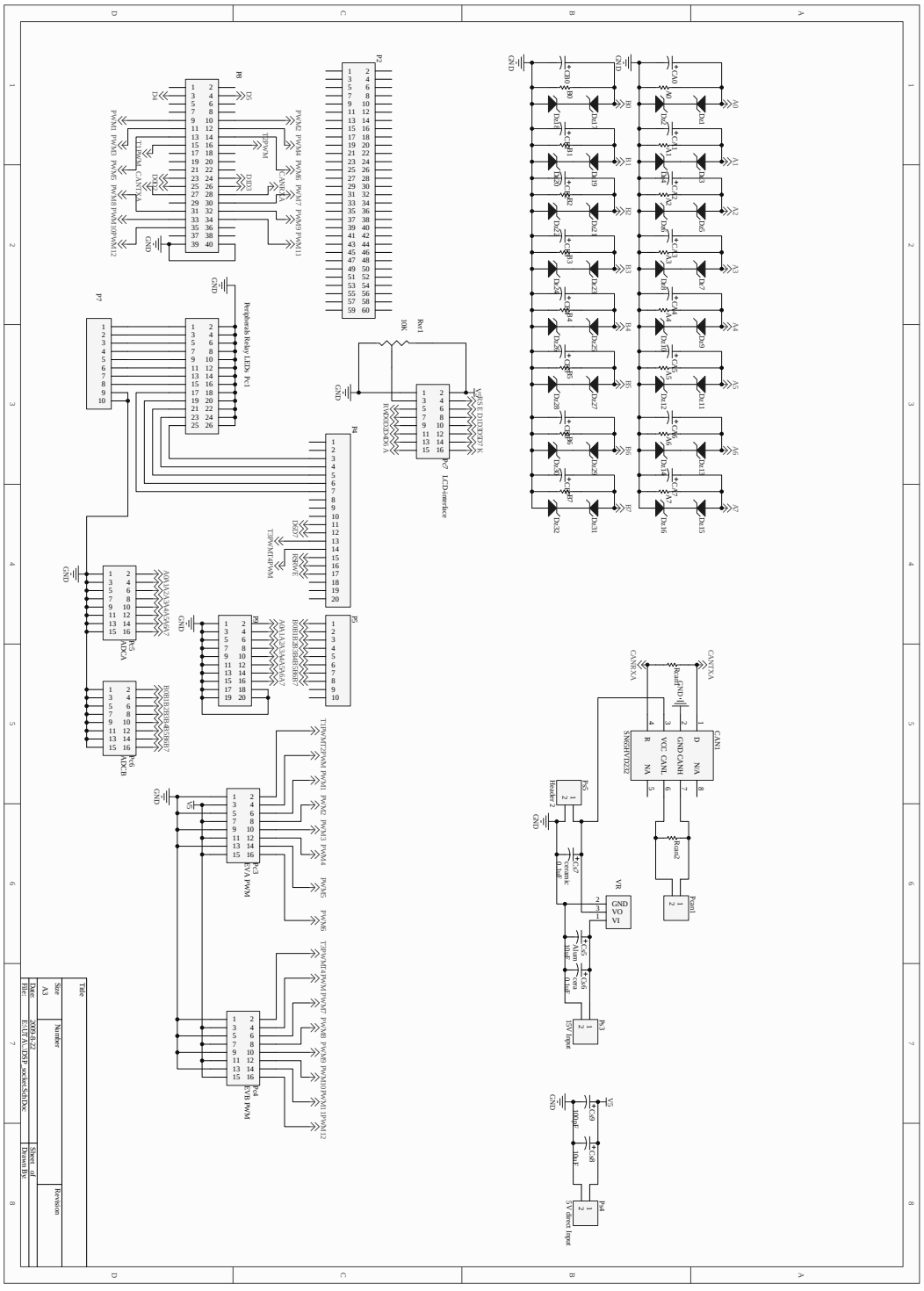

Figure B.4. DSP docking PCB.

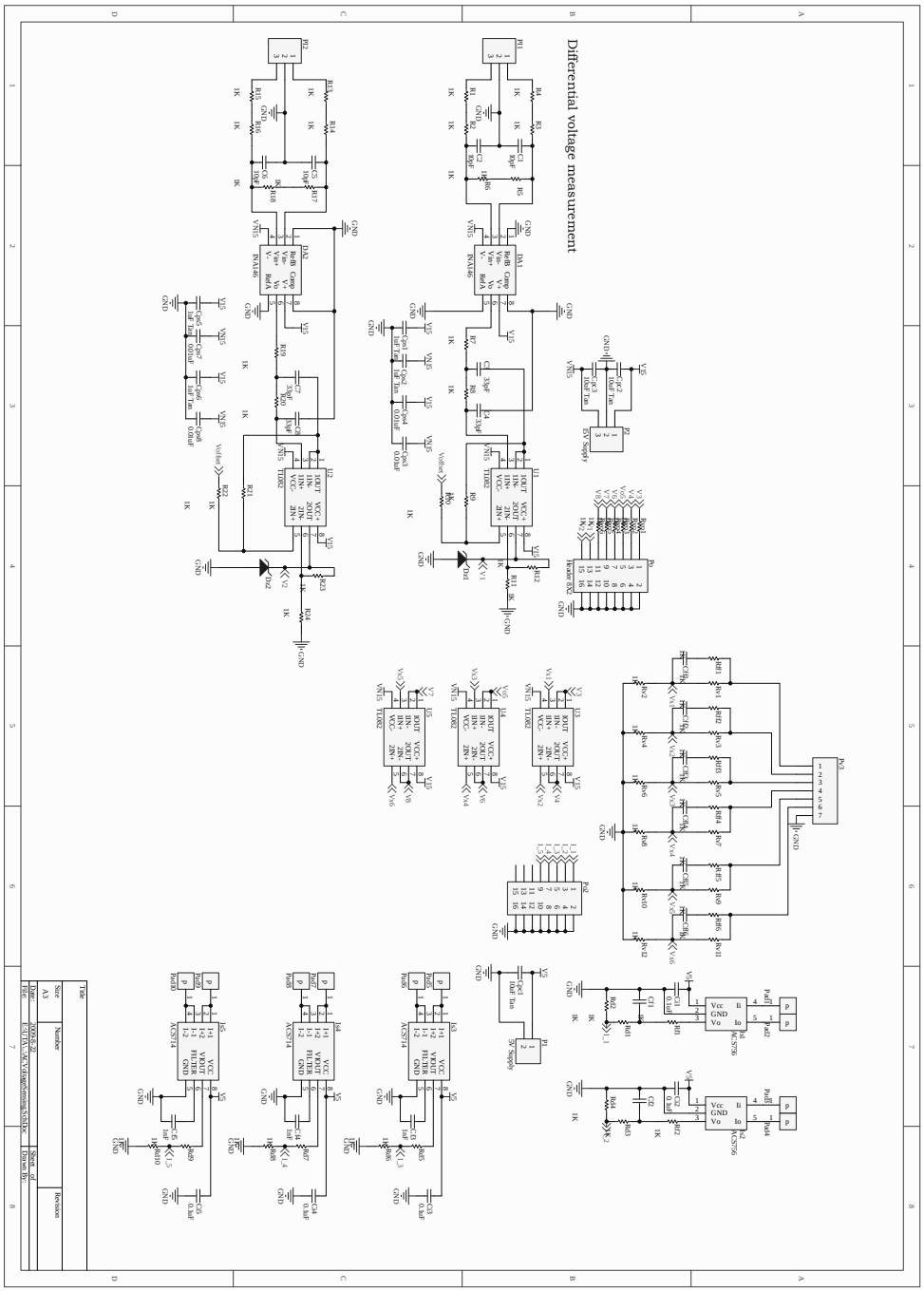

Figure B.5. Low cost sensor & conditioning board.

APPENDIX C

ACTIVE PHASE BALANCER

C.1 Background

The extension of MPEI concept can be applied to local power network since MPEI can offer generic interface for both single phase and three phase applications. The following paragraphs will explain the application of MPEI as phase balancer in distribution networks.

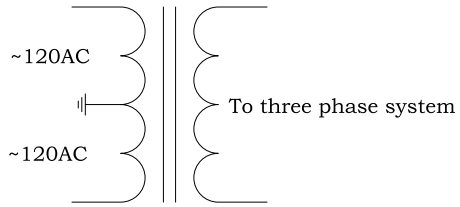

Figure C.1. Local single phase distribution transformer.

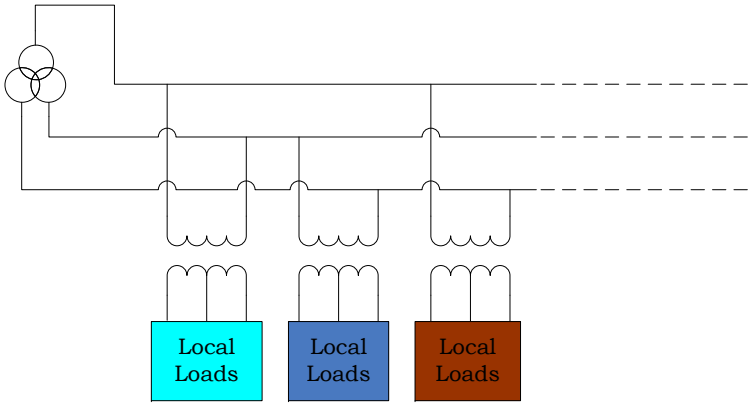

Figure C.2. Organization of single phase distribution transformer for three phase load balance.

The local power network for residential and business users are commonly fed by three phase power lines. Single phase users take power from a single phase transformer which in connected to two phases of three phase system; the output of the single phase transformer offers 120V/240V with center tap grounded, which is shown

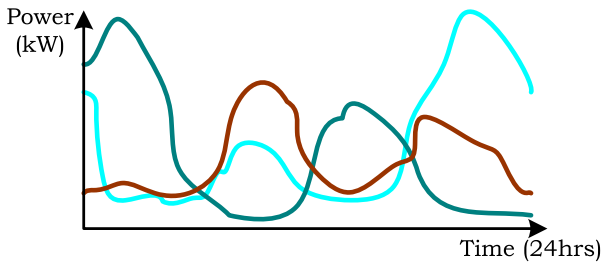

Figure C.3. Power consumption daily profile for different customers.

in Figure C.1. Since the entire power consumption can not be provided by only one phase of three-phase system, the loads should be distributed evenly for each phase for a balanced operation, which is indicated in Figure C.2. Although the allocation of distribution transformer can be made equal in space and number, the power consumption of each end-customer is however incidental. FigureC.3 shows the power consumption pattern of different households which take power from different single phase distribution transformers. Average power consumption of different customer can be statistically equal for local users, however, the instantaneous power consumption is quite different as can be seen from the figure. Difference in instantaneous power consumption leads to unbalanced operation of three phase system and hence extra losses in different phases.

C.2 Active Phase Balancer

MPEI proposed in this dissertation can be used as an Active Phase Balancer (APB) to solve this problem. The role of MPEI in local distribution system is the active load: since MPEI can interface with different energy storages, once unbalance in three phase lines are detected by MPEI control system, the phase-leg which interfaces to energy storage (eg. battery) can work as a buck converter to storage energy into battery. The value of charging current/power can be determined by examining the

difference between MPEI input current and the currents of the other phases. The installation of MPEI in a local distribution system is shown in Figure C.4, where each distribution transformer is connected to MPEI, which interfaces to both energy storage and end-customer.

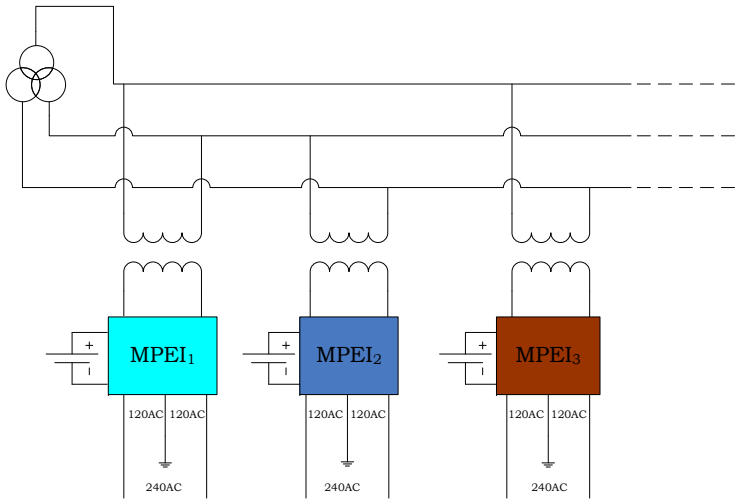

Figure C.4. MPEI as active load balancer in local distribution networks.

The topology implementation of active phase balancer is presented in Figure C.5. Single phase ac interface is connected to isolation transformer and take power from the grid with unity power factor and low harmonics; the rectified ac voltage is properly controlled as a solid voltage dc-link; a phase-leg which enables buck and boost operation is connected to battery pack; on the customer-end, a three wire single phase inverter is used to provide split 120VAC as well as 240VAC.

Two operation modes is defined in the active phase balancer application: active balancing mode and generation mode. In active balancing mode, as indicated in Figure C.6, the power flow is from the grid to battery as well as end-customer, the tri-port MPEI is actively balancing the three-phase line currents; in generation mode,

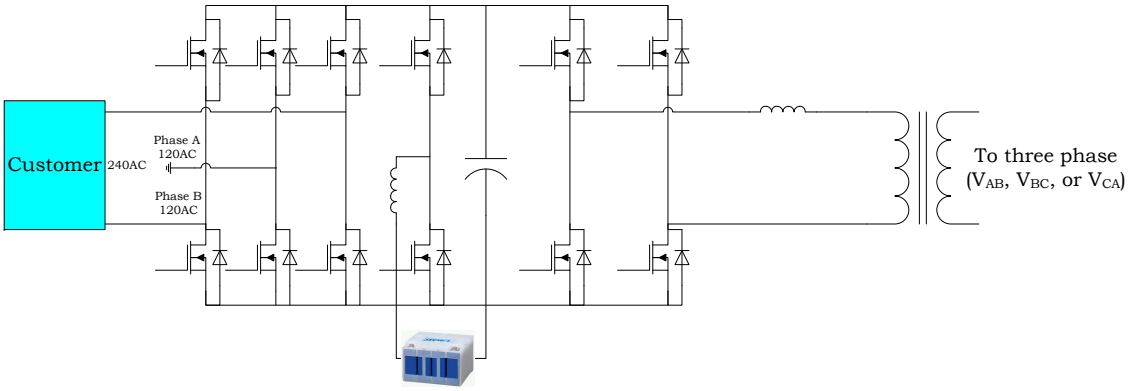

Figure C.5. Active Phase Balancer Principle.

three phase line current is naturally balanced and the battery is discharged with boost operation of the phase-leg, the power delivered to the end-customer is shared with utility grid.

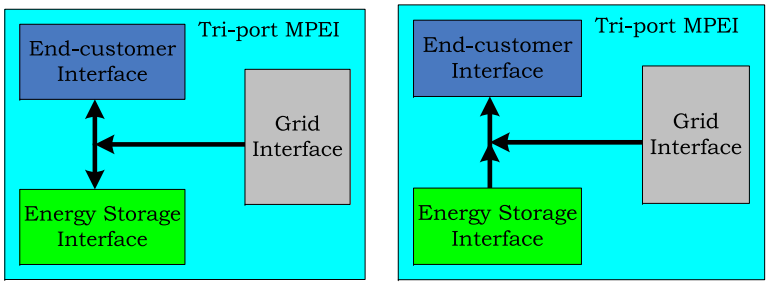

(a) (b)

Figure C.6. Converter under close loop control (a) voltage control, (b) current control.

APPENDIX D

MPEI ON A CHIP

D.1 MPEI on a Chip (MPEIOC)

In portable electronics and communication power applications, the power demand is much less than residential application, usually in mW range. MPEI can be a very attractive candidate for those type of applications due to its capability of interfacing to different very low power sources and energy buffers. There are several qualifying features that MPEI need to have,

- Competitive in size
- Low cost
- Operation frequency at HF/VHF level

The phase-leg structure can be used in mW power conversion, which can be organized in boost switching cells, buck switching cells or mixed buck boost switching cells. The silicon packaging of switching components, drivers, sensing peripherals and control circuits can be easily implemented at chip level. However, the integration of inductor is the main challenge since conventional ferrite and powder iron cores are too space-occupying. In order to implement MPEI on the chip level, air core inductor and strap inductor should be used together with very high switching frequency.

Since MPEIOC is used to process power at milliwatt level, the relation among switching frequency, inductor value and mode of operation have to be reexamined. In order to sink inductor size further, discontinuous current mode (DCM) of operation is recommended for MPEIOC. From this perspective, the small signal model for high-bandwidth controller design has to be re-evaluated also.

There are more options for power sources at milliwatt level. Radio-Frequency (RF) waves and piezoelectric vibrators are the popular candidates as external power source, which MPEIOC can harvest with no extra cost. However, RF sources are of high frequency and low input amplitude, and piezoelectric devices deliver power at

wide spectrum of frequencies. The precondition of low amplitude, uncertain-frequency power signals can not be done by the buck/boost switching cells in present MPEI, and extra circuit is required for MPEIOC. For the external signals with ac in nature, the multi-stage rectifier can be used as preconditioner to amplify small ac power signal to a high level dc which is readily to be used by MPEIOC. Figure D.1(a) and D.1(b) indicate the implementation of multi-stage rectifier: the input power is of 0.2V in amplitude, which is harvested directly or from far/near field coupling; the multistage rectifier can rectify the ac power signal and offer a $2.5V$ dc signal for the downstream switching cells.

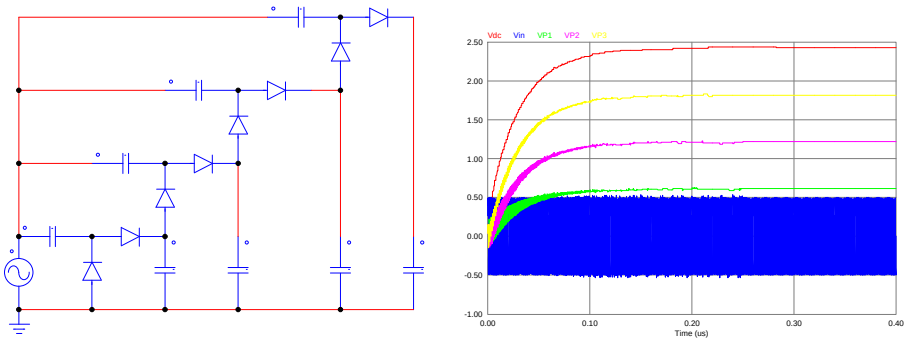

(a) (b)

Figure D.1. Recommended front stage for MPEI (a) Multi-stage rectifier, (b) Rectifier output voltage.

REFERENCES

[1] Energy Information Administration, "Internal energy outlook 2009," Office of Integrated Analysis and Forecasting, Tech. Rep. DOE/EIA-0484(2009), 2009.

[2] J. W. Tester, E. M. Drake, M. J. Driscoll, M. W. Golay, and W. A. Peters, *Sustainable Energy: Choosing Among Options*. Cambridge, MA: The MIT Press, 2005.

[3] DOE, "The smart grid: A introduction," Office of Electricity Delivery and Energy Reliability, Tech. Rep. DE-AC26-04NT41817, 2008.

[4] W.-J. Lee, "The opportunities and challenges of microgrid development," Energy Systems Research Center, University of Texas at Arlington, Arlington, TX, Tech. Rep., Jun. 2008.

[5] R. Strzelecki and G. Benysek, *Power Electronics in Smart Electrical Energy Networks*. London, UK: Springer-Verlag, 2008.

[6] L. Wang, H. Cheung, A. Hamlyn, C. Yang, and R. Cheung, "Network-integrated protection and control strategy for power distribution systems," *Large Engineering Systems Conference on Power Engineering*, pp. 39–43, Oct. 2007.

[7] M. Ehsani, Y. Gao, S. Gay, and A. Emadi, *Modern Electric, Hybrid Electric, and Fuel Cell Vehicles: Fundamentals, Theory, and Design*. Boca Raton, FL: CRC Press, 2004.

[8] DOE, "Grid 2030 a national vision for electricity's second 100 years," Office of Electric Transmission and Distribution, Tech. Rep., 2003.

[9] R. H. Lasseter, "Microgrids and distributed generation," *Journal of Energy Engineering*, vol. 133, no. 3, pp. 144–149, Sep. 2007.

[10] J. Lagorse, M. G. Simoes, and A. Miraoui, "A multi-agent fuzzy logic based energy management of hybrid systems," *IEEE Industry Applications Society Annual Meeting*, Oct. 2008.

[11] Z. Jiang, "Agent based power sharing scheme for active hybrid power sources," *Journal of Power Sources*, vol. 177, no. 1, Feb. 2008.

[12] B. H. Cho and F. C. Lee, "Modeling and analysis of spacecraft power systems," *IEEE Trans. Power Electron.*, vol. 3, no. 1, pp. 44–54, Jan. 1988.

[13] B. Choi, B. H. Cho, F. C. Lee, and R. B. Ridley, "The stacked power system: a new power conditioning architecture for mainframe computer systems," *IEEE Trans. Power Electron.*, vol. 9, no. 6, pp. 616–623, Nov. 1994.

[14] Y. Panov, J. Rajagopalan, and F. C. Lee, "Analysis and design of n paralleled dc-dc converters with master-slave current-sharing control," 12^{th} *Annual IEEE Applied Power Electronics Conference and Exposition*, vol. 1, pp. 436–442, Feb. 1997.

[15] C. Byungcho, B. H. Cho, and H. Sung-Soo, "Dynamics and control of dc-to-dc converters driving other converters downstream," *IEEE Trans. Circuits Syst. I*, vol. 46, no. 10, pp. 1240–1248, Oct. 1999.

[16] A. Khaligh, A. M. Rahimi, Y.-J. Lee, J. Cao, A. Emadi, S. D. Andrews, C. Robinson, and C. Finnerty, "Digital control of an isolated active hybrid fuel cell/li-ion battery power supply," *IEEE Trans. Veh. Technol.*, vol. 56, no. 6, pp. 3709–3721, Nov. 2007.

[17] H. Matsuo, W. Lin, F. Kurokawa, T. Shigemizu, and N. Watanabe, "Characteristics of the multiple-input dc-dc converter," 24^{th} *Annual IEEE Power Electronics Specialists Conference*, vol. 51, no. 3, pp. 625–631, Jun. 2004.

[18] Y.-M. Chen, Y.-C. Liu, and F.-Y. Wu, "Multi-input dc/dc converter based on the multiwinding transformer for renewable energy application," *IEEE Trans. Ind. Appl.*, vol. 38, no. 4, pp. 1096–1104, Jul. 2002.

[19] H. Tao, J. L. Duarte, and M. A. M. Hendrix, "Three-port triple-half-bridge bidirectional converter with zero-voltage switching," *IEEE Trans. Power Electron.*, vol. 23, no. 2, pp. 782–792, Mar. 2008.

[20] H. Matsuo, T. Shigemizu, F. Kurokawa, and N. Watanabe, "Characteristics of the multiple-input dc-dc converter," 24^{th} *Annual IEEE Power Electronics Specialists Conference*, pp. 115–120, Jun. 1993.

[21] H.-J. Chiu, H.-M. Huang, L.-W. Lin, and M.-H. Tseng, "A multiple-input dc/dc converter for renewable energy systems," *IEEE International Conference on Industrial Technology*, pp. 1304–1308, Dec. 2005.

[22] A. S. W. Leung, H. S. H. Chung, and T. Chan, "A zcs isolated full-bridge boost converter with multiple inputs," 38^{th} *IEEE Power Electronics Specialists Conference*, pp. 2542–2548, Jun. 2007.

[23] R. W. DeDoncker, D. M. Divan, and M. H. Kheraluwala, "A three-phase soft-switched high-power-density dc/dc converter for high power applications," *IEEE Trans. Ind. Appl.*, vol. 27, no. 1, pp. 63–71, Jan. 1991.

[24] F. Z. Peng, H. Li, G.-J. Su, and J. S. Lawler, "A new zvs bidirectional dc-dc converter for fuel cell and battery application," *IEEE Trans. Power Electron.*, vol. 19, no. 1, pp. 54–65, Jan. 2004.

[25] M. Michon, J. L. Duarte, M. Hendrix, and M. G. Simoes, "A three-port bidirectional converter for hybrid fuel cell systems," 35^{th} *Annual IEEE Power Electronics Specialists Conference*, vol. 6, pp. 4736–4742, Jun. 2004.

[26] Y. Zhongming, J. Praveen, and S. Paresh, "Control of series parallel resonant converter with two different input voltage sources," 37^{th} *Annual IEEE Power Electronics Specialists Conference*, pp. 1–7, Jun. 2006.

[27] D. Liu and H. Li, "A zvs bi-directional dc-dc converter for multiple energy storage elements," *IEEE Trans. Power Electron.*, vol. 21, no. 5, pp. 1513–1517, Sep. 2006.

[28] J. L. Duarte, M. Hendrix, and M. G. Simoes, "Three-port bidirectional converter for hybrid fuel cell systems," *IEEE Trans. Power Electron.*, vol. 22, no. 2, pp. 480–487, Mar. 2007.

[29] H. Tao, A. Kotsopoulos, J. Duarte, and M. A. M. Hendrix, "Family of multiport bidirectional dc-dc converters," *IEE Proceedings Electric Power Applications*, vol. 153, no. 3, pp. 451–458, May 2006.

[30] A. M. McLandrich, "Sensorless control of a bidirectional boost converter for a fuel cell energy management system," Master's thesis, Virginia Polytechnic Institute and State University, Blacksburg, VA, 2003.

[31] M. Marchesoni and C. Vacca, "New dc-dc converter for energy storage system interfacing in fuel cell hybrid electric vehicles," *IEEE Trans. Power Electron.*, vol. 22, no. 1, pp. 301–308, Jan. 2007.

[32] B. Ozpineci, L. Tolbert, and Z. Du, "Multiple input converters for fuel cells," 39^{th} *Industry Applications Conference*, vol. 2, pp. 791–797, Oct. 2004.

[33] N. Benavides and P. L. Chapman, "Power budgeting of a multiple-input buck-boost converter," *IEEE Trans. Power Electron.*, vol. 20, no. 6, pp. 1303–1309, Nov. 2005.

[34] A. Kwasinski and P. T. Krein, "Multiple-input dc-dc converters to enhance local availability in grids using distributed generation resources," 22^{th} *Annual IEEE Applied Power Electronics Conference*, pp. 1657–1663, Feb. 2007.

[35] R. Wai, C. Lin, L. Liu, and Y. Chang, "High-efficiency single-stage bidirectional converter with multi-input power sources," *Electric Power Applications*, vol. 1, no. 5, pp. 763–777, Sep. 2007.

[36] Y.-M. Chen, Y.-C. Liu, S.-C. Hung, and C.-S. Cheng, "Multi-input inverter for grid-connected hybrid pv/wind power system," *IEEE Trans. Power Electron.*, vol. 22, no. 3, pp. 1070–1077, May 2007.

[37] A. D. Napoli, F. Crescimbini, L. Solero, F. Caricchi, and F. G. Capponi, "Multiple-input dc-dc power converter for power-flow management in hybrid vehicles," 37^{th} *Annual IEEE Industry Applications Conference*, vol. 3, pp. 1578–1585, Oct. 2002.

[38] L. Solero, A. Lidozzi, and J. A. Pomilio, "Design of multiple-input power converter to hybrid vehicles," *IEEE Trans. Power Electron.*, vol. 20, no. 5, pp. 1007–1016, Sep. 2005.

[39] R. Rizzo and P. Tricoli, "Power flow control strategy for electric vehicles with renewable energy sources," *IEEE International Power and Energy Conference*, pp. 34–39, Nov. 2006.

[40] W. Jiang, J. Brunet, and B. Fahimi, "Application of active current sharing control in fuel cell-battery off-line ups system," 39^{th} *Annual IEEE Power Electronics Specialists Conference*, pp. 796–801, Jun. 2008.

[41] W. Jiang and B. Fahimi, "Multi-port power electronic interface for renewable energy sources," 24^{th} *Annual IEEE Applied Power Electronics Conference and Exposition*, pp. 347–352, Feb. 2009.

[42] H. Al-Atrash, F. Tian, and I. Batarseh, "Tri-modal half-bridge converter topology for three-port interface," *IEEE Trans. Power Electron.*, vol. 22, no. 1, pp. 341–345, Jan. 2007.

[43] R. Venkataramanan, "Sliding mode control of power converters," Ph.D. dissertation, California Institute of Technology, Pasadena,CA, May 1986.

[44] B. Fahimi and W. Jiang, "Methods and apparatus for design and control of multi-port power electronic interface for renewable energy sources," U.S. Patent 09-04, 2008.

[45] J. Hamelin, K. Agbossou, A. Laperriere, F. Laurencelle, and T. K. Bose, "Dynamic behavior of a pem fuel cell stack for stationary applications," *International Journal of Hydrogen Energy*, vol. 26, no. 6, pp. 625–629, Oct. 2001.

[46] M. W. Ellis, M. R. V. Spakovsky, and D. J. Nelson, "Fuel cell systems: Efficient, flexible energy conversion for 21^{st} century," *Proceedings of the IEEE*, vol. 89, no. 12, pp. 1808–1818, Nov. 2001.

[47] *Ballard $Nexa^{TM}$ Power Module Users Manual*, Ballard Power Systems Inc., 2003.

[48] J. L. Dicks, *Fuel cell system explained, 2nd edition.* John Wiley & Sons, 2003.

[49] S. M. Lukic, J. Cao, R. C. Bansal, F. Rodriguez, and A. Emadi, "Energy storage systems for automotive applications," *IEEE Trans. Ind. Electron.*, vol. 55, no. 6, pp. 2258–2267, Jun. 2008.

[50] K. C. Divya and J. Oestergaard, "Battery energy storage technology for power systemsan overview," *Electric Power Systems Research*, vol. 79, no. 4, pp. 511–520, Apr. 2009.

[51] J. Wang, F. Z. Peng, J. Anderson, A. Joseph, and R. Buffenbarger, "Low cost fuel cell converter system for residential power generation," *IEEE Trans. Power Electron.*, vol. 19, no. 5, pp. 1315–1322, Sep. 2004.

[52] A. Emadi, A. Nasiri, and S. B. Bekiarov, *Uninterruptible Power Supplies and Active Filters.* Boca Raton, FL: CRC, 2004.

[53] D. Franzoni, E. Santi, A. Monti, F. Ponci, D. Patterson, and N. Barry, "An active filter for fuel cell applications," 36^{th} *Annual IEEE Power Electronics Specialists Conference*, pp. 1607–1613, Jun. 2005.

[54] L. Gao, Z. Jiang, and R. A. Dougal, "Evaluation of active hybrid fuel cell/battery power sources," *IEEE Trans. Aerosp. Electron. Syst.*, vol. 41, no. 1, pp. 346–355, Jan. 2005.

[55] C. Liu, A. Johnson, and J.-S. Lai, "A novel three-phase high-power soft-switched dc/dc converter for low-voltage fuel cell applications," *IEEE Trans. Ind. Appl.*, vol. 41, no. 6, pp. 1691–1697, Dec. 2005.

[56] D. C. Hamill, "Generalized small-signal dynamical modeling of multi-port dc-dc converters," 28^{th} *Annual IEEE Power Electronics Specialists Conference*, vol. 1, pp. 421–427, Jun. 1997.

[57] R. D. Middlebrook, "Input filter considerations in design and application of switching regulators," *Advances in Switched-Mode Power Conversion*, vol. 1, no. 7, 1983.

[58] G. W. Wester and R. D. Middlebrook, "Low-frequency characterization of switched dc-dc converters," *IEEE Trans. Aerosp. Electron. Syst.*, vol. 11, no. 1, pp. 376–385, May 1973.

[59] R. D. Middlebrook and S. Cuk, "A general unified approach to modeling switching-converter power stages," *IEEE Power Electronics Specialists Con. Rec.*, pp. 18–34, 1976.

[60] P. T. Krein, J. Bentsman, R. M. Bass, and B. L. Lesieutre, "On the use of averaging for the analysis of power electronic systems," *IEEE Trans. Power Electron.*, vol. 5, no. 2, pp. 182–190, Apr. 1990.

[61] S. R. Sanders, J. M. Noworolski, X. Z. Liu, and G. C. Verghese, "Generalized averaging method for power conversion circuits," *IEEE Trans. Power Electron.*, vol. 6, no. 2, pp. 251–259, Apr. 1991.

[62] A. Emadi, "Modeling of power electronic loads in ac distribution systems using the generalized state-space averaging method," *IEEE Trans. Ind. Electron.*, vol. 51, no. 5, pp. 992–1000, Oct. 2004.

[63] A. S. Kislovski, R. Redl, and N. O. Sokal, *Dynamic Analysis of Switching-mode DC/DC Converters.* New York: Van Nostrand Reinhold, 1991.

[64] V. Vorperian, "Simplified analysis of pwm converters using model of pwm switch part i: Continuous conduction mode," *IEEE Trans. Aerosp. Electron. Syst.*, vol. 26, no. 3, pp. 490–496, May 1990.

[65] B. Lehma and R. M. Bass, "Switching frequency dependent averaged models for pwm dc-dc converters," *IEEE Trans. Power Electron.*, vol. 11, no. 1, pp. 89–98, Jan. 1996.

[66] R. D. Middlebrook, "Small-signal modeling of pulse-width modulated switched-mode power converters," *Proc. IEEE*, vol. 76, no. 4, pp. 343–354, Apr. 1988.

[67] R. W. Erickson and D. Maksimovic, *Fundamentals of Power Electronics, 2nd edition.* Boston, MA: Kluwer, 2000.

[68] R. D. Middlebrook, "Topics in multiple-loop regulators and current-mode programming," *IEEE Trans. Power Electron.*, vol. PE-2, no. 2, pp. 109–124, Apr. 1987.

[69] L. Dixon, "Average current mode control of switching power supplies," Unitrode Power Supply Design Seminar Manual, SEM-700, Tech. Rep., 1990.

[70] W. Tang, F. C. Lee, and R. B. Ridley, "Small-signal modeling of average current-mode control," *IEEE Trans. Power Electron.*, vol. 8, no. 2, pp. 112–119, Apr. 1993.

[71] M. E. Schenck, L. Jih-Sheng, and K. Stanton, "Fuel cell and power conditioning system interactions," 20^{th} *Annual IEEE Applied Power Electronics Conference and Exposition*, vol. 1, pp. 114–120, Mar. 2005.

[72] S. Wang, M. Krishnamurthy, R. Jayabalan, and B. Fahimi, "Low-cost quasi-resonant dc-dc converter for fuel cells with enhanced efficiency," 21^{th} *Annual IEEE Applied Power Electronics Conference and Exposition APEC*, pp. 1280–1285, Mar. 2006.

[73] W. Choi, P. N. Enjeti, and J. W. Howze, "Development of an equivalent circuit model for a fuel cell stack to evaluate the effects of inverter ripple current," *Journal of Power Sources*, vol. 158, no. 2, pp. 1324–1332, Aug. 2006.

[74] B. K. Bose, P. M. Szczesny, and R. L. Steigerwald, "Microcomputer control of a residential photovoltaic power conditioning system," *IEEE Trans. Ind. Appl.*, vol. 21, no. 5, pp. 1182–1191, Sep. 1985.

[75] C. Hua, J. Lin, and C. Shen, "Implementation of a dsp-controlled photovoltaic system with peak power tracking," *IEEE Trans. Ind. Electron.*, vol. 45, no. 1, pp. 99–107, Feb. 1998.

[76] K. H. Hussein, I. Muta, T. Hoshino, and M. Osakada, "Maximum photovoltaic power tracking: an algorithm for rapidly changing atmospheric conditions," *IEE Proc. Generation, Transmission and Distribution*, vol. 142, no. 1, pp. 1350–2360, Jan. 1995.

[77] E. I. Ortiz-Rivera and F. Z. Peng, "Analytical model for a photovoltaic module using the electrical characteristics provided by the manufacturer data sheet," 36^{th} *IEEE Power Electronics Specialists Conference*, pp. 2087–2091, Jun. 2005.

[78] N. Femia, G. Petrone, G. Spagnuolo, and M. Vitelli, "Optimization of perturb and observe maximum power point tracking method," *IEEE Trans. Power Electron.*, vol. 20, no. 4, pp. 963 – 973, Jul. 2005.

[79] T. Esram and P. L. Chapman, "Comparison of photovoltaic array maximum power point tracking techniques," *IEEE Trans. Energy Convers.*, vol. 22, no. 2, pp. 439–449, Jun. 2007.

[80] M. A. S. Masoum, H. Dehbonei, and E. F. Fuchs, "Theoretical and experimental analyses of photovoltaic systems with voltage and current-based maximum power-point tracking," *IEEE Trans. Energy Convers.*, vol. 17, no. 4, pp. 514–522, Dec. 2002.

[81] N. Femia, G. Petrone, G. Spagnuolo, and M. Vitelli, "A pure realization of loss-free resistor," *IEEE Trans. Circuits Syst.*, vol. 51, no. 8, pp. 1639–1647, Aug. 2004.

[82] P. C. Todd, "Snubber circuits: theory, design and application," Unitrode Power Supply Design Seminar Manual, SEM-900, Tech. Rep., 1993.

[83] "ACS756 data sheet rev. 2," Allegro MicroSystems, Inc., Mar. 2009.

[84] "LV-20P data sheet," LEM, Feb. 2008.

BIOGRAPHICAL STATEMENT

Wei Jiang was born in Yangzhou, China in 1980. He received B.S. degree from Southwest Jiaotong University, Chengdu, China and M.S. degree in University of Texas at Arlington (UTA), Arlington, Texas, USA both in electrical engineering. He is currently a Ph.D. candidate in area of sustainable energy systems at UTA. From 2003 to 2004 he worked as an electrical engineer in Bombardier CPC Propulsion System Co. Ltd. and Zhejiang Windey Engineering Co. Ltd. in China. He was a senior design engineer in EF Technologies L.L.C. Arlington, TX in 2007, leading the R&D of renewable-interface power converters. His research interests include digital power electronics in hybrid power systems and optimal design of electromechanical energy converters. He has published more than 10 referred journal and peer reviewed conference papers and has two patents pending in related research fields. Mr. Wei Jiang is a student member of IEEE as well as SAE.